FLORIDA INTERNATIONAL UNIVERSITY

A Resource for the State of Florida

HURRICANE LOSS REDUCTION

FOR

HOUSING IN FLORIDA:

Full-scale External and Internal Pressure Measurements for a Low-rise Building

A Research Project Funded by
The State of Florida Division of Emergency Management

Submitted by:

Dr. Girma T. Bitsuamlak, PEng, Assistant Professor

Amanuel S. Tecle, Graduate Research Assistant

In Partnership with:

The International Hurricane Research Center

Florida International University

September 2009

EXCUTIVE SUMMARY

In this project, a wind induced internal and external pressure in typical low-rise building models is investigated primarily by using a full-scale wind testing facility generically named Wall of Wind (WoW). Effect of different dominant openings (representing open door and window conditions or breaching of a building envelope by wind-borne debris), vents (gable end, goose neck, turbine, and soffit) and background leakage under different wind angle of attack is carried out. Prior to performing the full-scale analysis, a three tier approach comprising (i) a less expensive computer simulation and (ii) small-scale WoW (1:8 replica of the full-scale WoW) followed by (iii) a confirmatory test using the full-scale WoW is adopted to assess effect of blockage and proximity to the WoW flow simulator. Computer model of various size are first simulated to assess the blockage effect and additional simulations are done to assess the proximity effect by placing a model at different distance from the wall of wind. For the computer simulation, a commercially available software FLUENT (version 6.2) is utilized. In order to verify and ascertain the results of the computer simulations, a less expensive small scale physical experiment was carried out by designing three small WoW model cubes (i.e., scale 1:8 with 5ft, 7ft, and 9.5ft side lengths). The outcomes of the small scale WoW analysis was compared with the results of the numerical computation (i.e., CFD) and previously carried out researches from literature. Both the numerical and small scale WoW test results indicated the importance of blockage and proximity effect and the need for further study at full-scale. Thus, a confirmatory blockage was carried out using a full-scale WoW. These blockage and proximity effect studies resulted in the selection of an optimal low-rise building test model dimensions (i.e. 9ft L by 7ft

W and 7 ft H) and testing location (i.e. the test model placed at 12 ft from the WoW) that provides aerodynamically sound data.

A low-rise building model with interchangeable gable and hip roofs was designed and fabricated. Detailed multiple dominant openings (doors with secondary openings and windows), ventilation openings (soffit, goose neck, turbine and soffits), vertical (ceiling) and horizontal (partition wall) compartments are fabricated. These details have enabled to study (i) the impact of the fluctuation of external pressure over the internal pressure, (i) the intensity of critical internal pressure that build up as a consequence of compartmentalization and various opening sizes of dominant openings (iii) the influence of ventilation openings in dampening the internal pressure excitation and (iv) the net roof design wind load that generates as a result of coupling of attic internal pressure and roof external pressure. It is shown that the fluctuation in external pressure is highly correlated to of the fluctuation in the internal pressure. It is also noticed that partitioning of the building has a significant impact in the variation of the intensity of internal pressure and hence the net envelope design wind load. Moreover, the size of dominant openings (i.e., door and window porosity ratio with respect to windward wall) influences the level of internal pressure that develops both in the attic and living room of a low-rise building. From the present study it is concluded that to reduce a potential probability building failure during strong storms, not only windows and doors needs to be covered with shutters, but also vents (soffit) and ceiling hatches needs to be covered.

Table of Contents

List of figures

List of tables

1. **Introduction**

Design wind loads on building envelope (roofs, windows, doors, and walls), are a combination of external and internal pressure. Internal pressure can contributes a significant portion to the total design wind load (Irwin and Sifton 1998) depending on the opening size and location, shape of the building and other aerodynamic factors. Particularly if wind-borne debris breaches a building envelope it will lead to development of high internal pressure. Although significant work has been done in boundary layer wind tunnels (BLWT) to assess the *external* pressure by different researchers, relatively limited research is carried out to assess *internal* pressures limited to few building opening scenarios. Internal pressure coefficients in buildings with openings in one wall received a lot of attention starting in the 70's mainly for structural applications. Aynsley et al. (1977) investigated the impact of wall porosity on internal pressures. Stathopoulos et al. (1979) carried out BLWT experiments in order to investigate the impact of various opening configurations on internal pressures for different background leakage values, wall openings and exposures. State of the art review was reported by Oh et al. (2007). Recently Karava (2008) studied internal pressure at model scale for a dominant opening for natural ventilation purposes.

The present study will focus on internal and external pressure studies for low rise buildings. According to ASCE 7-05, low rise-buildings (housing, small commercial and industrial buildings) are defined as enclosed or partially enclosed buildings with mean roof height (h) less or equal to 60 ft or roof height (h) not exceeding the least horizontal dimension. The assessment of wind loads on low-rise buildings involves several factors such geometrical (aerodynamic), construction method, surrounding buildings, upstream terrain, and geographical (hurricane prone regions, coastal regions, main land etc). These factors can influence the development of internal and external pressure on the building. The combined effect of internal and external pressure can

cause minor to major building envelope failures such as roof, walls, shingle or other claddings and/or structural failures (Holmes 1979; Stathopoulos et al. 1979; Liu and Saathoff 1981; Liu and Saathoff 1983; Vickery 1986; Oh et al. 2007). The design wind pressure on each envelope component (whether main wind resisting structural system or cladding and components) depends on the sum of external and internal pressure that is generated over each component. According to ASCE 7-05 (Section 6.5.12.1.2), the values of the external and internal pressures are algebraically combined in order to determine the most critical load. The local peak wind loads developing at building (roof, wall, soffit corners) and other "hot-spots" usually lead to the initiation of failure unless properly evaluated by considering both external and internal pressures into account and subsequently considered during the design process.

Compared to tall buildings, low rise-buildings are immersed within the layer of aerodynamic roughness on the earth's surface where the turbulence intensities are high (Holmes, 2001). These kinds of complexities in aerodynamic conditions that characterize low rise-buildings are often difficult to analyze due to the extreme fluctuation of wind pressure that develop within the atmospheric boundary layer. The fluctuations in wind pressure are mainly attributed to two sources, turbulent velocity fluctuations inducing internal to external pressure variation and local vortex shedding in the separated flow regions near sharp corners, roof eaves and ridges causing the formation of unsteady pressure.

Internal pressure: Internal pressure is the pressure that buildup inside a building due to openings in the building envelope and in response to wind induced external pressure fluctuations. The change in internal pressure results basically due to the infiltration or exfiltration of air from the exterior of a building into its interior and vice versa due to the porosity of a building. The porosity can, often, be due to cracks around doors, windows; openings at soffits, utility ducts and

vents; or wind-borne breach of a building envelope. The inflow of wind through broken doors or windows commonly leads to over pressurization of the internal dwellings unless otherwise there is an equivalent opening in the leeward side to compensate the pressure development. Previously carried out studies have indicated that the contribution of internal pressure to the total load is very significant (Holmes 1979; Stathopoulos 1979; Irwin and Sifton 1998; Sharma et al. 2003 & 2005). Understanding the basic principles of internal pressure and knowing how it behaves with different aerodynamic factors involved becomes essential to properly design the main frame resisting structures, and claddings and components (Davenport and Slurry, 1984), as well as the computation of infiltration/exfiltration of building systems and the migration of water (moisture) through building envelopes.

A number of wind engineering tools are available to study wind induced pressure (both external and internal). These include experimental boundary-layer wind tunnel studies; numerical modeling based on computational fluid dynamics and other analytical approaches and very limited full scale field measurements. Several factors affect the internal pressure in a complex manner making analytical approaches very challenging and approximate. Wind tunnel experiments and full scale tests on the other hand provide the industry with widely accepted measurements. Compared to external pressure measurements, internal pressure measurements are more complex (Liu 1990). Some of the major factors that influence the magnitude of internal pressure generated in the interior of a building are: a) the fluctuations of external pressure impacting the building, b) the size and position of dominant openings including background porosity, c) the distribution of external pressure over the perimeter of the dominant opening, d) wind direction and turbulence intensity, e) internal volume and compartmentalization, and f) flexibility of the structure (Holmes 1979; Stathopoulos et al. 1979; Liu & Saathoff 1981, 1983;

Vickery 1986; Vickery and Bloxham 1992; Oh et al. 2007). Simultaneous interactions of aerodynamic, micro-meteorological, construction details and structural factors play a key role in generating internal pressure fluctuations in response to the variation in the external pressure.

All of the above studies are based on single internal volume at model-scale, and limited opening locations. In addition, proper method to convert model-scale data to a full-scale building needs to be developed. Compartmentalized volume and various opening locations and scale issues require further investigation using full-scale experiments. There are also inherent scale issues related to the internal volume, background leakage etc that need to be addressed while studying internal pressure in a BLWT experiments using small-scale models (1:200, 1:300 scales). These scale issues are better addressed by using a new-state of the art full-scale testing facility, the Wall of Wind (WoW) at the IHRC.

2. Methodology

2.1 Wind tunnel versus WoW

Traditionally, experimental investigations of wind/building interactions are performed using low wind speed boundary layer wind tunnel testing methodology which is widely accepted by the construction industry. Wind tunnel simulations are carried out on scaled building models that are commonly scaled to 1:100, 1:200 and 1:400 in order to fit into the win d tunnel test section without causing blockage. Although wind tunnels are the basis for most of the existing knowledge, building code and standard provisions there are still some documented shortcomings. For example, testing wind speeds and test building specimens are small compared to design wind speeds and the actual building respectively thus violating Reynolds number similarity criteria. There are additional constraints in wind tunnel while conducting tests for internal pressure

measurement such as internal volume scaling, porosity modeling (for background leakage), and compartmentalization effects. Furthermore, buildings are composed of various types of building constructional materials with different wind performance capabilities. It is the interaction of all such components within the building as a whole system that determines the performance of the building under the actions of wind. As a result, a number of assumptions are made while conducting wind tunnel testing.

The present study attempts to address some of these limitations by conducting external and internal pressure studies on an actual large-scale low-rise building constructed following prevalent Florida Construction methods. The test building is subjected to mean wind speed 45.26 mph using the full scale testing facility WoW as shown in Figure 1. FIU IHRC's WoW is located at Engineering Center is composed of six fans. It can generate a 24 ft wide and 16 ft high wind field with a mean wind speed of 125 mph and can engulf a small size full-scale low–rise building. This capability of the current WoW allowed conducting fundamental studies on internal pressure studies on a low rise building structure built with real construction materials. The major objective of the study is to evaluate the distribution of pressure fields over the surface of the building's envelope (on the gable and hip type roofing), both internally and externally, and to identify the magnitude and direction of critical wind loads that instigate failure of envelope components in the presence of various opening scenarios. Since the pre-fabricated model consists of different background porosities, vents[1] (gable end vents, soffit vents, roof vents such as turbine and goose neck type), partitioning at ceiling level separating ground and attic floor, it provides realistic opportunities to simulate and evaluate hurricane induced pressures on low -rise

[1] Wind loads on the vents and water intrusion through them was the subject of another parallel study by Chowdhury et al. (2009).

buildings and thus obtain valuable data to mitigate hurricane forces and emphasize on some pressure preparedness measures such as covering windows, vents during hurricane etc.

Figure 1: Low-rise building with gable roof in front of WoW in a testing position

Figure 2: Hip roof building model in front of WoW apparatus ready for test

2.2 WoW test building specimen design, construction and detailing

Based on the study of blockage and proximity effect discussed in section 3.1.3 optimum size of the test building specimen was identified. Thus, a 9ft W x 7ft L x 7ft H wooden fabricated model with shingle roof, proper soffit and goose neck and turbine vents was designed and fabricated. The building has two interchangeable roofing, gable and hip roof types as shown in Figure 1 and Figure 2. The doors and the windows were designed to provide several dominant openings for example by designing a secondary opening inside a door as shown in Figure 3d. Figure 3 describes the design in 3D SolidWorks rendering and 2D AutoCAD working drawings. Each component of the building is designed and laid out in accordance with locally prevailing construction methods and was detailed carefully to replicate realistic construction details. Moreover, since the effect of external pressure in generating fluctuating internal pressure is highly related to the dominant openings on the walls, properly designed windows and doors were provided. In order to investigate the impact of dominant opening porosities, three door opening areas were selected and fabricated accordingly (D1=3.24ft x 1.50ft, D2=2.16ft x 1.50ft and D3=2.70ft x 0.75ft) as shown in Figure 3 d and Figure 6 a. Besides providing various sizes of dominant openings, compartmentalization of the internal part of the building was another factor that was given due consideration. In the design and fabrication process, the building model was partitioned both vertically and horizontally (Figure 4 and Figure 6). The building was divided into living room and attic by a ceiling and a folding wall was designed to divide the living room into two halves along the wider length of the building as shown in Figure 6. A hatch opening which is a common practice in low rise housing was provided on the ceiling in order to investigate the transfer of wind load within the living room and the attic in the presence of ceiling opening as shown in Figure 7. Another opening that was considered in the preparation of

the model was the ventilation mechanism inside the attic floor. Vent openings are aimed at keeping the attic dry and cool. However they also adversely cause high internal pressure to develop inside the attic. In order to investigate the impact of vent openings, calculated areas of openings were provided over the soffit, gable end, ridge and roof surface for both the gable and hip roof building models (Figure 8 a and b). For both Gable and Hip roofs a representative roof 4:12 slope was selected (i.e. the roof pitch is taken to be 18.8°). Finally the roof envelope was properly covered with underlayment and shingles. The laying and nailing of the underlayment and shingles were done in accordance with the guides given by the Florida Building Code of practice as shown in Figure 9.

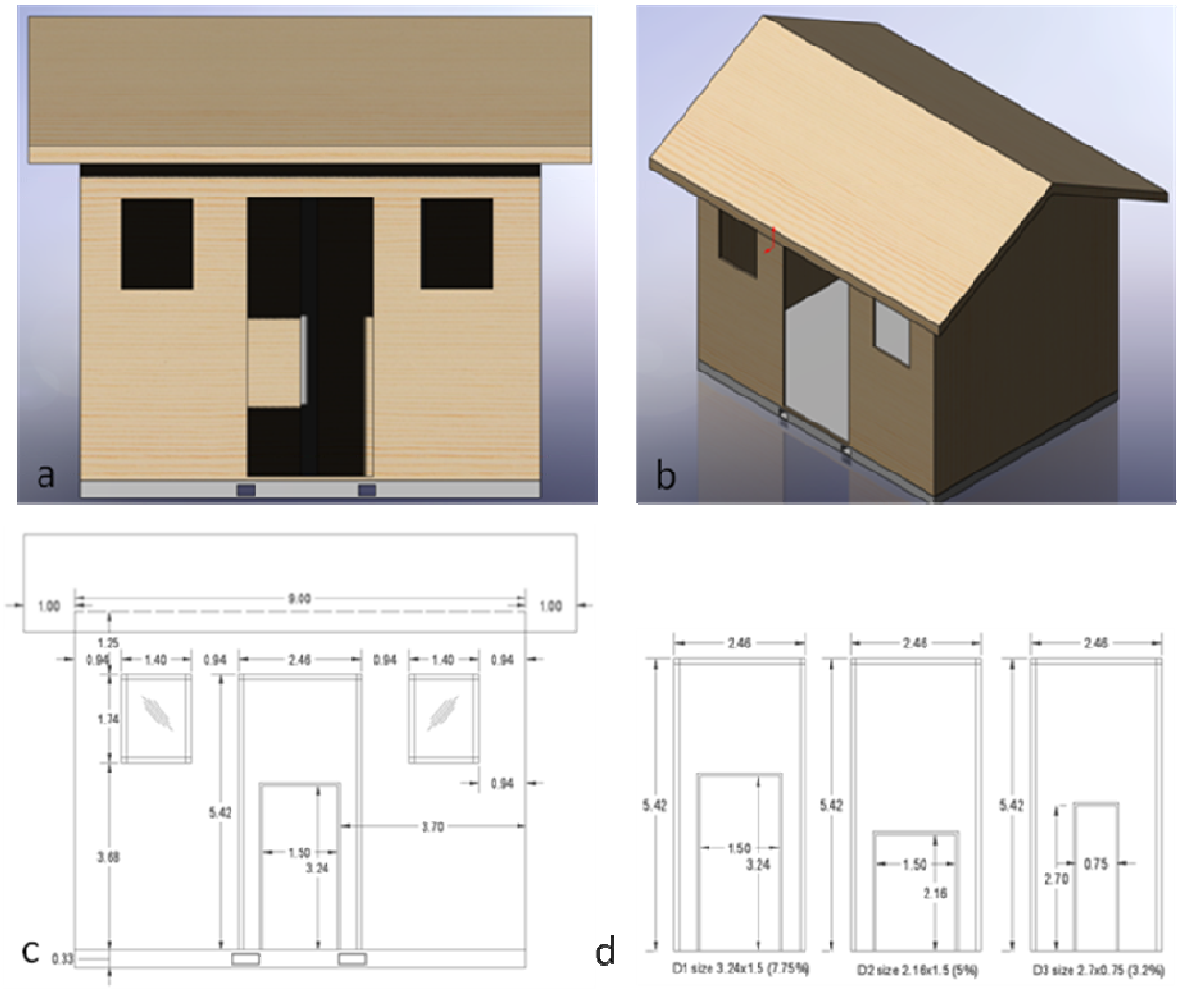

Figure 3: Conceptual model design; a & b) 3D model of gable building using SolidWorks, c & d) details using AutoCAD (dimension in ft)

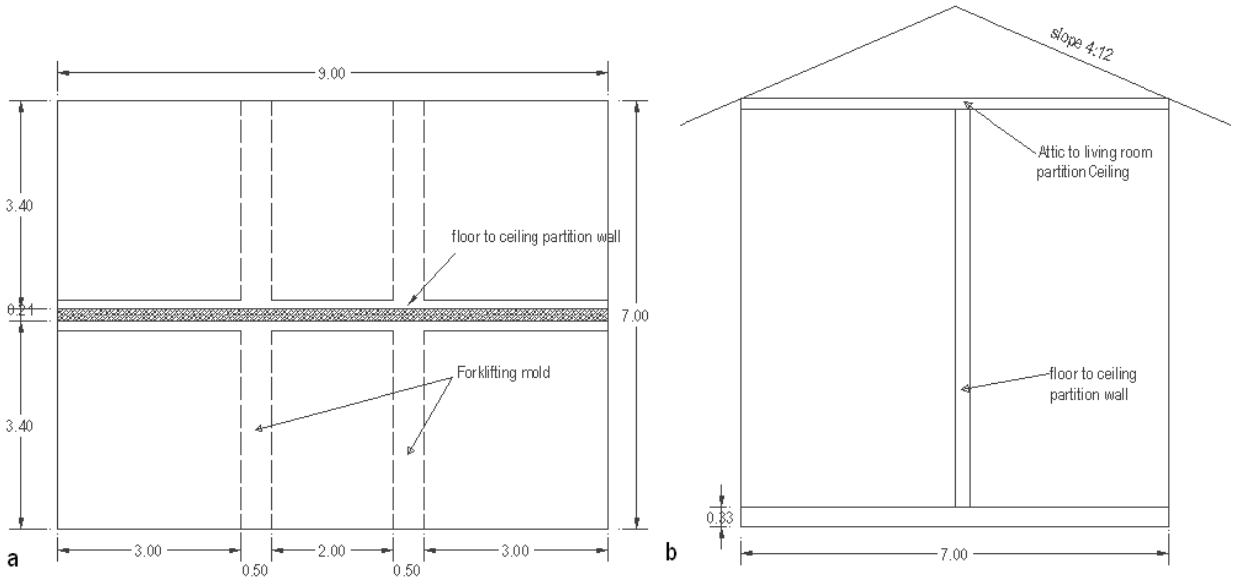
9.00
3.40
floor to ceiling partition wall
0.21
7.00
Forklifting mold
3.40
a
3.00
0.50
2.00
0.50
3.00
slope 4:12
Attic to living room partition Ceiling
floor to ceiling partition wall
0.33
b
7.00

:al and


a
b
c
d


a
b

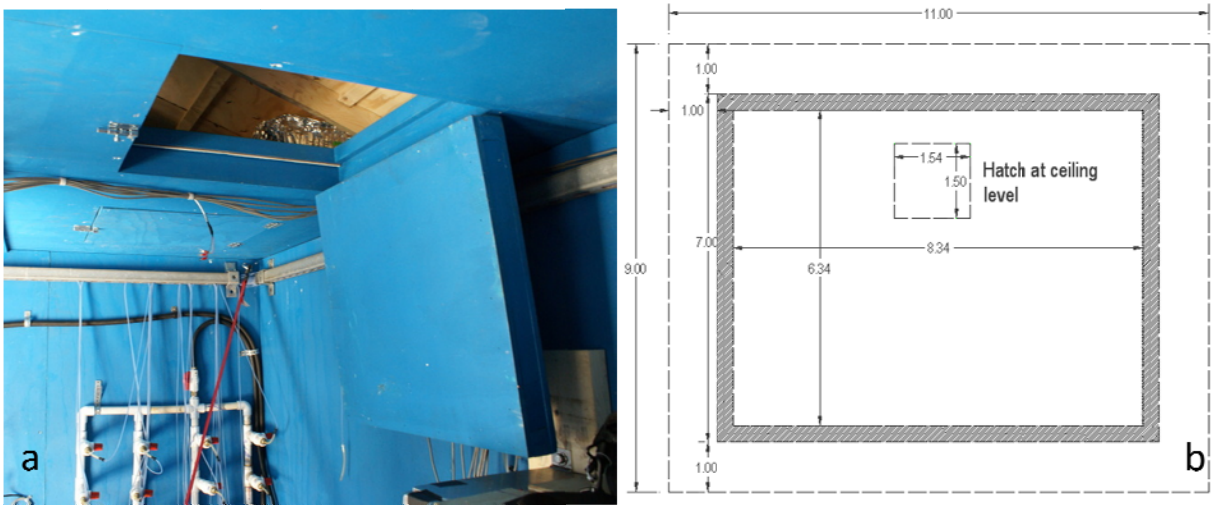
a
11.00
1.00
1.00
1.54
1.50
Hatch at ceiling level
7.00
8.34
6.34
9.00
1.00
b

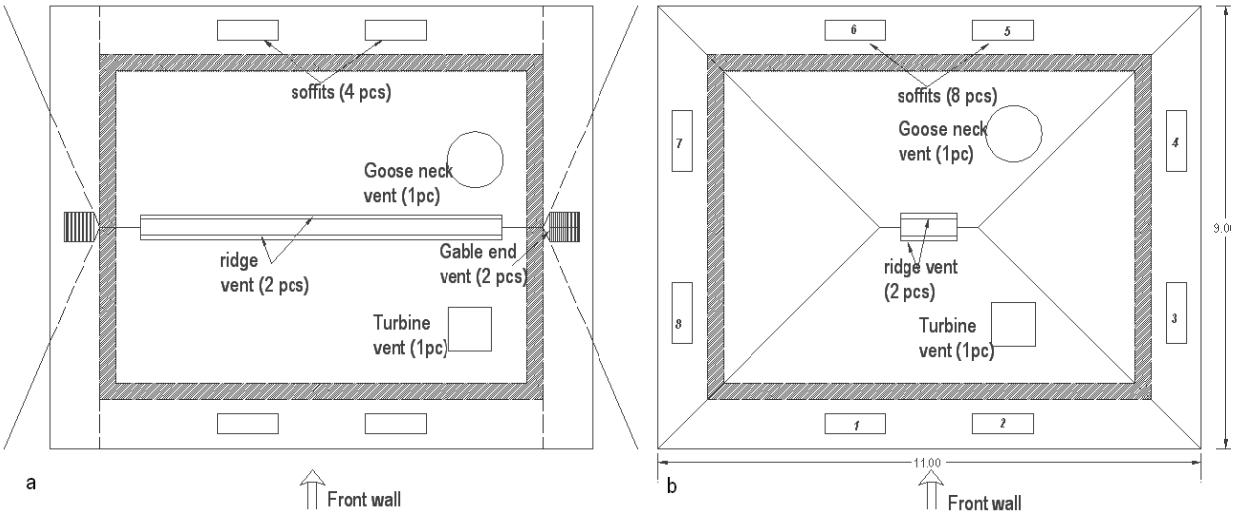
soffits (4 pcs)
Goose neck
vent (1pc)
ridge
vent (2 pcs)
Gable end
vent (2 pcs)
Turbine
vent (1pc)
a
Front wall
6
5
soffits (8 pcs)
Goose neck
vent (1pc)
7
4
ridge vent
(2 pcs)
8
3
Turbine
vent (1pc)
1
2
9.00
11.00
b
Front wall

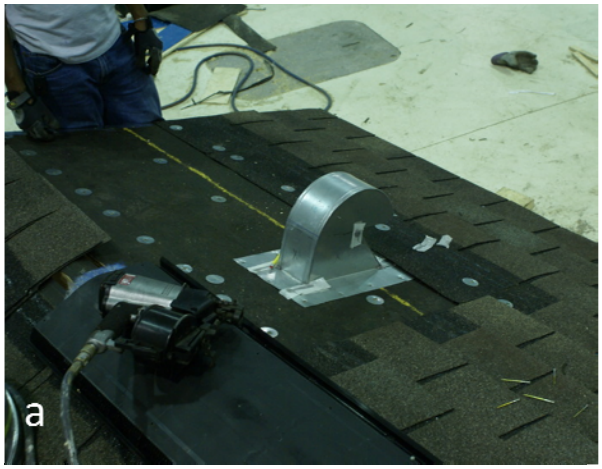
a


b

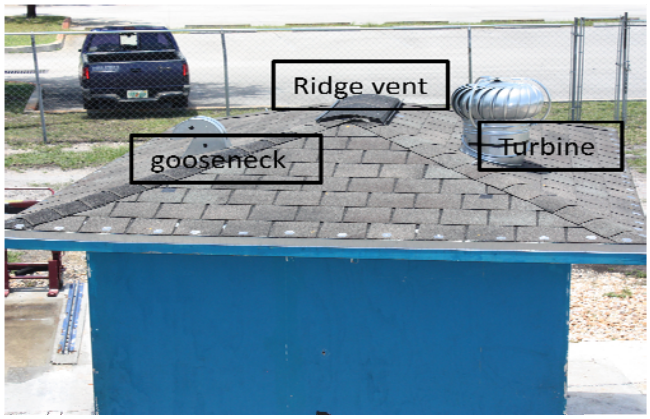
Ridge vent
gooseneck
Turbine


Soffit

and


a


b

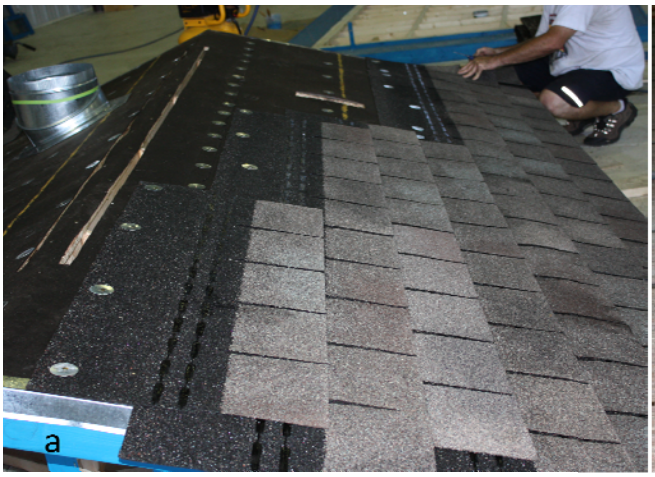
a

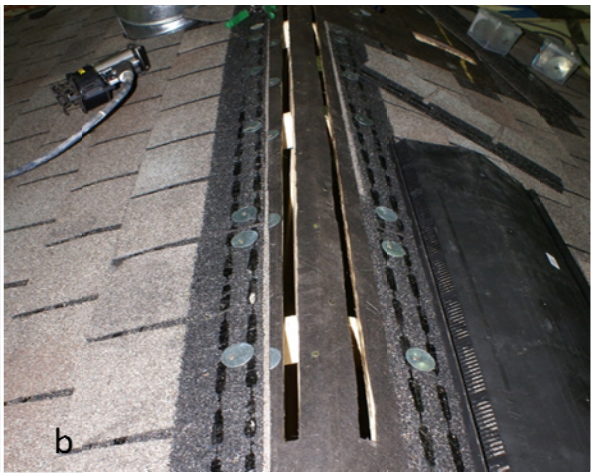
b

2.3 Equivalent analytical equation approximation for internal pressure

Theoretical models for a rigid full scale building is provided by Holmes (1979), Liu and Saathoff (1981) and Vickery (1992). Generally the factors involved in the propagation of internal pressure equivalently can be explained by the non linear analytical formulation founded on mass-spring analysis. Wind dynamic response of a simple mass-spring damper system can be represented by the following differential equation.

$$M\ddot{X} + B\dot{X} + KX = F(t) \qquad [1]$$

The first term in the mass-spring equation (eqn. 1) describes the inertia of the air jet that flows through an opening, while the second term describes the damping which accounts for the energy losses through the opening. The third term is the spring stiffness-resistance of internal pressure to displacement of air slug. According to Holmes (1979), the differential equation of motion of slug of air (eqn. 1) represented by the spring system can be rewritten by breaking the three terms into their respective unique formulations (Figure 13). Thus, the mass-spring equation becomes:

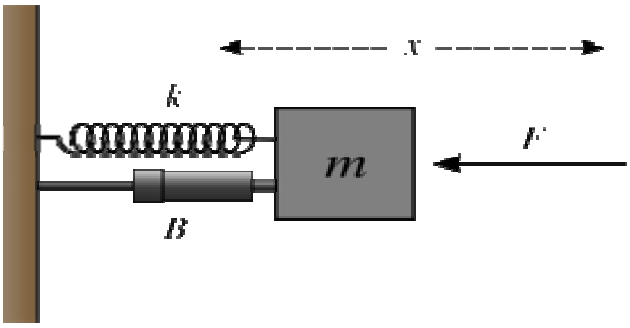

Figure 13: Pneumatic spring-mass-damper system (Nskape Curtesy of Illmari Karonen, 1992)

$$\rho_a A L_e \ddot{X} + \frac{\rho_a A}{2(k)^2} |\dot{X}| \dot{X} + \frac{\gamma p_o}{V_o} X = A \Delta p_e(t) \quad [2]$$

It is assumed that a slug of air, of length *Le*, moves in and out of the opening due to the compression and expansion of air during external and internal pressure interaction at an opening. The variable *X* is, thus, the displacement of the slug of air from its initial or static equilibrium position.

Helmholtz oscillation and its influence on internal pressure: The study undertaken by Holmes (1979) on the building model investigated the relation between internal pressure and Helmholtz resonance. Experimental studies undertaken by Holmes (1979) and Liu and Saathoff (1981) on wind tunnel models with variable single dominant openings have shown that excitation of peak internal pressure occurs close to the undamped Helmholtz frequency.

Helmholtz resonance equation derived by Helmholtz is given in eqn. (3) as:

$$f_H = \frac{1}{2\pi} \sqrt{\frac{nAP_o}{\rho L_e V_{ie}}} \quad [3]$$

Where f_H represents the Helmholtz frequency; A is the area of the opening; n is the polytropic exponent (equal to 1.4 for adiabatic air); P_o is the reference pressure; ρ is the density of air and V_{ie} is the internal volume of the room. Holmes (1979) reported that a building with a single room and single dominant opening behaves like a Helmholtz resonator and the compressibility of the air in the room causes fluctuation of internal pressure (Figure 14).

Taking the second derivative of the coefficient of internal pressure with respect to the displacement given in eqn. (2), according to Holmes (1979) and Vickery (1986), the mass-spring formulation can be expressed in terms of the coefficient of pressure as:

$$\frac{\rho L_e V}{Anp_a}\ddot{C_{pi}} + \frac{\rho q V^2}{2(kAnp_a)^2}\left|\dot{C}_{pi}\right|\dot{C}_{pi} + C_{pi} = C_{pe} \qquad [4]$$

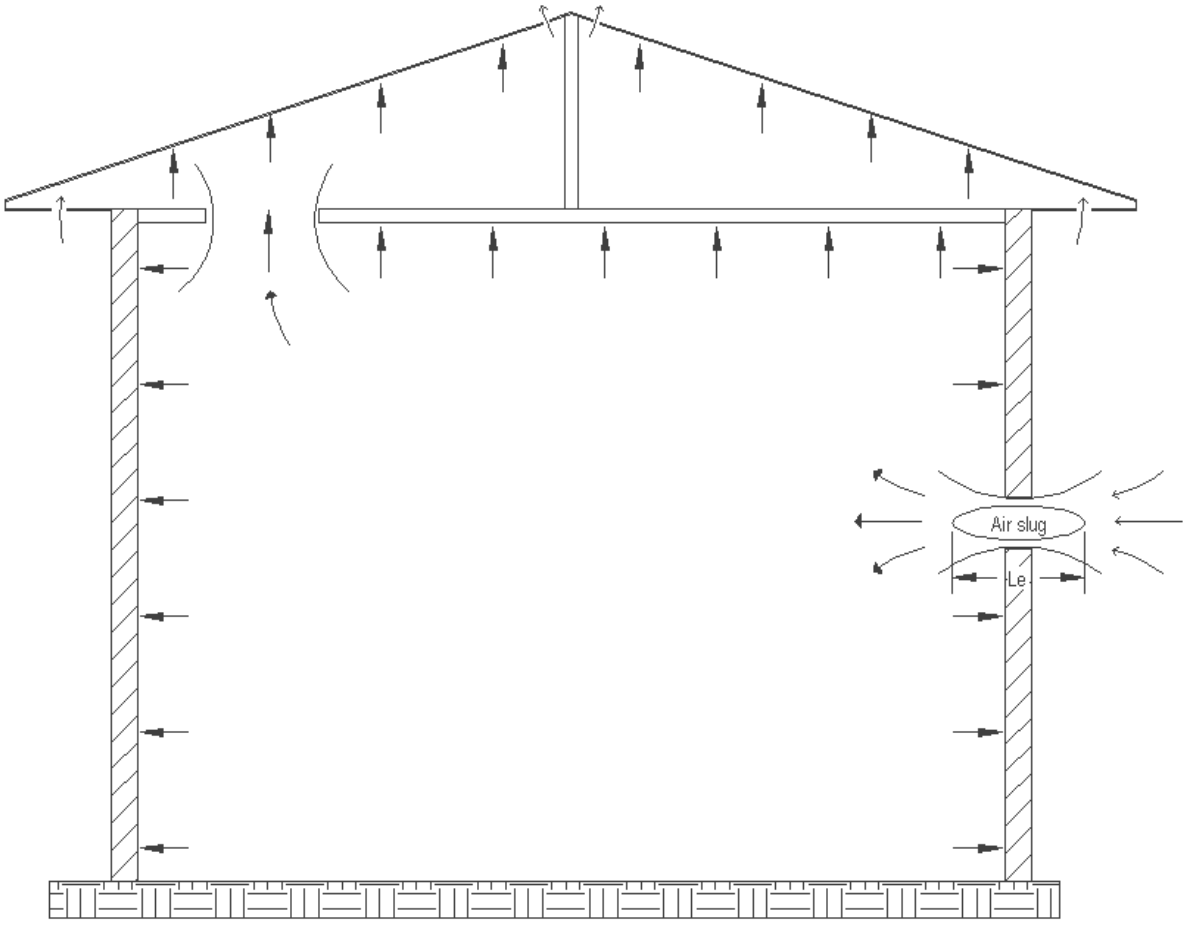

Figure 14: Air Slug Movement through an Opening and its Impression on the Building Envelope

Where q is the dynamic pressure; k is the orifice coefficient of the opening and Le is the length of the air Slug at the opening; C_{pi} and C_{pe} represent the coefficient of internal and external pressure respectively. By employing special form of Bernoulli equation, Liu and Saathoff (1981) introduced a rigorous derivation of the internal pressure variation as shown in eqn. (5)

$$\frac{\rho L_e V}{kAnp_a}\ddot{C_{pi}} + \frac{\rho q V^2}{2(kAnp_a)^2}\left|\dot{C_{pi}}\right|\dot{C_{pi}} + C_{pi} = C_{pe} \qquad [5]$$

The only difference between eqn. 4 and 5 is the presence of orifice contraction coefficient in the inertia term of eqn. 5. Moreover, when damping and inertia terms of eqn. (5) are set to zero, it turns to the original Helmholtz equation with the introduction of k as shown in eqn. (6).

$$f_H = \frac{A^{1/4}}{\pi^{5/4}}\sqrt{\frac{knRT}{2V}} \qquad [6]$$

Liu and Rhee (1986) undertaken a thorough investigation to compare eqns. (3) and (6) and ascertain the validity of each by using different flows with varying velocity profiles and turbulence characteristics. Test was carried out in a boundary layer wind tunnel and the experimental building model tested was a single room, block type, flat roof with internal dimensions of 140 mm L x 140 mm D x 290 mm H. Variable sized square window openings (0,10,20,30 and 40 mm L) were introduced on the windward and leeward walls. The spectral analysis of the internal pressure fluctuations showed that the value of k varies between 0.75 and 0.99, with the average being 0.88. Unlike the previous experiments performed by (Holmes (1979), Liu & Saathoff (1981)), in which case, the polytropic exponent was kept fluctuating in order a fit in the system, an adiabatic condition (n=1.4) was considered during the analysis.

The outcome of the analysis proved that both eqns. (3 and 6) give satisfactory results. However, comparably, the experiment demonstrated eqn. (5) to be more reasonable since it keeps the factor n=1.4 for a case of adiabatic process rather than fluctuating it in order to fit into the system as used by eqn.(1) and that used by Holmes (1979). The experiment also revealed that the Helmholtz peak resonance gets to be large as the size of the openings increase.

Even though the investigation was thorough, the experiment was performed while the model was completely sealed in such a case the impact of background leakage to maximize the damping effect at the Helmholtz peak was undermined. Thus, a further study should be performed to verify if the results hold for a real building with its inherent porosity.

2.4 .Blockage and proximity effect

Testing larger test specimens within the finite WoW wind field, either to achieve Reynolds number similarity or to assess performance of full-scale building components under wind, wind-driven rain, and debris impact resistance, may entail blockage issues. The blockage effect discussed in the present study is concerned with the size of the test specimen compared to the finite size of the wind field generated at the inlet. The need to keep the test specimen as close as possible to the wind simulator in order to subject the test model to strong wind before it diffuses and loses its strength may also affect the quality of the aerodynamic data. The objectives of this study are, therefore, to assess computationally (i) the blockage effect as a function of the size of the test specimens, and develop correction strategies for those cases where those effects are significant, and (ii) the wind simulator proximity effect for various distances between the wind simulator and the test building, and develop proper test guidelines to ensure that this effect is acceptably small.

In the present study, relatively less expensive numerical wind flow simulations around parallelepipeds of various sizes, and located at various distances from the wind simulator and engulfed inside the numerical WoW and Atmospheric Boundary Layer (ABL) model have been carried out. Based on the observations from the numerical confirmatory blockage and proximity effect experiments were carried out by using the 1:8 scale small WoW replicas in conjunction with the full-scale WoW. Previous computational blockage assessments for wind tunnels include studies by Okajima (1997) pertaining to the effect of tunnel walls on various aerodynamic features as mentioned earlier. In the present blockage and wind simulator proximity effect study, however, the focus is on the effect of the size of the test buildings with respect to the finite size of WoW wind field and test building's proximity to the wind simulator. The WoW wind field can for practical purpose be considered to be a wind jet generated by an array of fans with controlled wind-profile characteristics. In the following sections the methodology adopted to assess the blockage and proximity effects.

2.4.1 Numerical assessment for blockage and proximity effect

Numerical modeling

The commercial software FLUENT 6.2 was utilized for the present numerical simulation, and the governing equations employed were the Reynolds Averaged Navier-Stokes (RANS) equations, together with the Renormalization Group (RNG) k-ε turbulence model. For blockage assessment studies, the upstream (U/S) , top, downstream (D/S), and two sides of the computational domain (CD) were set to 3.5H, 7H, 10.5H, and 5.5H from the center of the base of the parallelepiped, respectively, as shown in Figure 15, where H is the parallelepiped height under investigation, as shown in Fig. 4. For wind simulator proximity assessments, cubical

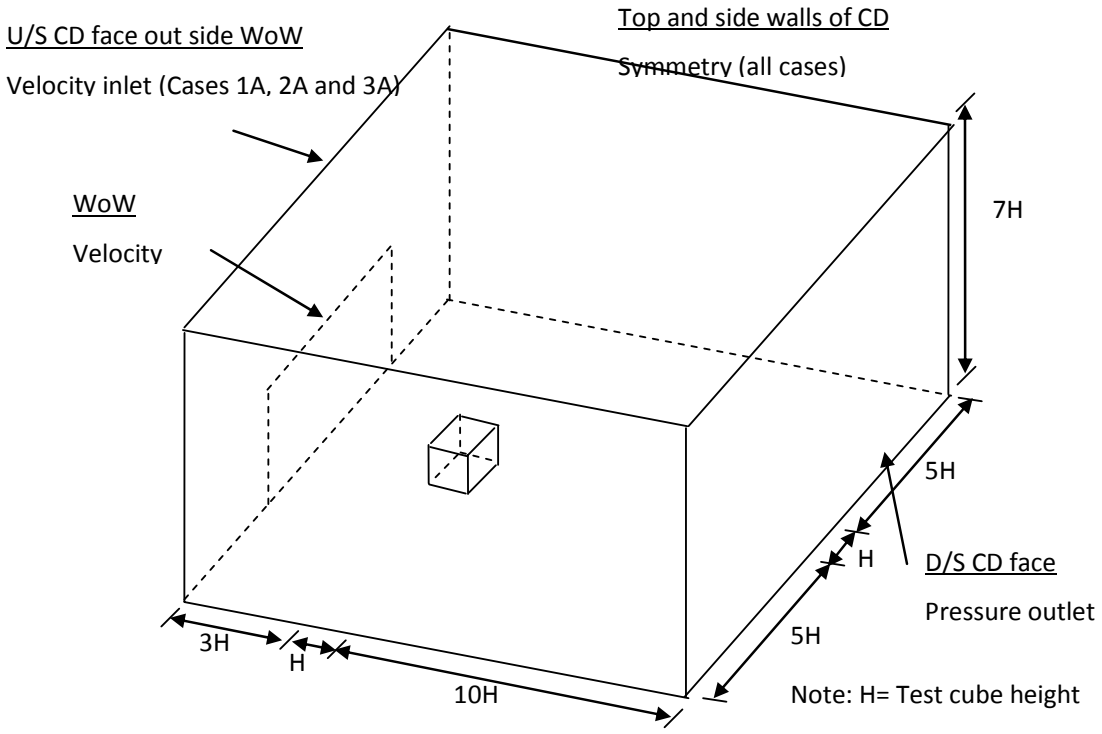

Figure 15: Computational Domain (CD) and Boundary Conditions as defined by FLUENT

buildings with windward faces located at H, 2H, 3H, 4H and 5H from the wind source (fans) were considered, as shown in Figure 17. For wall bounded flow, Fluent 6.2 provides two different approaches for modeling flows in the inner viscous layer, i.e. use of wall functions or near-wall modeling based on the non-dimensional wall units. The first grid point yp is placed at 0.01m from the surface of the test specimen and unstructured grids of hexagonal type were used for the CFD simulation. Considering the computational cost in resolving the inner layer, standard wall functions has been used in all present simulations by maintaining the wall unit y+ between 30 and 500. In addition, the inlet power law velocity profile with exponent α=0.25, a turbulence intensity TI = 12%, and a 10 m integral length scale were assumed. The latter is less than the typical accepted value for suburban terrain, owing to the need to limit to a minimum the computational domain (CD) size -- assumed to be three times the length scale -- to reduce computational time. These are reasonable assumptions considering the comparative nature of this

study. When simulating the ABL, the velocity inlet profile as described above was applied to the whole upstream face of the computational domain. However, when simulating the WoW flow, the application of the velocity inlet was limited to the 12 m x 9 m area of the U/S face of the CD representing the WoW type wind-field condition, as shown in Figure 15; on the remaining inlet area the atmospheric pressure condition was applied.

A segregated pressure-velocity solver has been used to all the discretization schemes. Pressure interpolation is standard and second order upwind and third order MUSCL schemes were used for convection and momentum terms respectively. The convergence criterion has been limited to 10^{-5}.

For blockage assessment studies, computational models mimicking the WoW and the ABL test model conditions were developed for the three cases shown below. It is to be noted that the blockage effect discussed in the present study is concerned with the size of the test specimen compared to the finite size of the wind field generated at the inlet (see Figure 16).

Case 1A - Base case for a 3x3x3 m (height x width x depth) cube placed in ABL wind-field condition (for this case $H=H_b=3m$);

Case 1B - Same as Case 1A but placed inside WoW wind-field condition;

Case 2A - A 4x4x3 m (height x width x depth) parallelepiped placed in ABL wind-field condition ($H=1.33H_b$);

Case 2B - Same as Case 2A but placed inside WoW wind-field condition;

Case 3A - A 5x5x3 m (height x width x depth) parallelepiped placed in ABL wind-field condition ($H=1.66H_b$);

Case 3B - Same as Case 3A but placed inside WoW wind-field condition.

For wind proximity effect studies, computational models mimicking the WoW and the ABL test model conditions for the 3x3x3 m base cube were developed for the following three cases:

Case 4A – Windward face of base cube located at distance H from the wind simulator and placed in ABL wind-field condition;

Case 4B - Same as Case 4A but placed inside WoW wind-field condition;

Case 5A - Windward face of base cube located at distance 2H from the wind simulator and placed in ABL wind-field condition;

Case 5B - Same as Case 5A but placed inside WoW wind-field condition;

Case 6A - Windward face of base cube located at distance 3H from the wind simulator and placed in ABL wind-field condition (note this case is the same as Case 1A);

Case 6B - Same as Case 6A but placed inside WoW wind-field condition (note this case is the same as Case 1B);

Case 7A - Windward face of base cube located at distance 4H from the wind simulator and placed in ABL wind-field condition;

Case 7B - Same as Case 7A but placed inside WoW wind-field condition;

Case 8A - Windward face of base cube located at distance 5H from the wind simulator and placed in ABL wind-field condition;

Case 8B - Same as Case 8A but placed inside WoW wind-field condition;

Figure 16 describes the relative size of the parallelepipeds relative to the WoW wind-field ($5H_b x 3H_b$) and the ABL wind-field (11H x 7H) for Cases 1 to 8, where H_b represents the height of the base cube (H_b= 3m) and H represents the height of the study building for each case. Note that the depth (along the wind flow direction) of all the parallelepipeds considered in the present study is 3 m. Figure 17 describes the distances from the windward face of the study base cube (3x3x3 m) from the wind simulator used for cases 4, 5, 6, 7 and 8. In all simulations the wind direction was perpendicular to the upwind face of the parallelepiped. Although the parallelepiped has simple geometry, it represents the complex bluff-body aerodynamic characteristics of a real building. In addition, several experimental studies and results are available for parallelepipeds, which allow the validation of results from the present study against values available in the

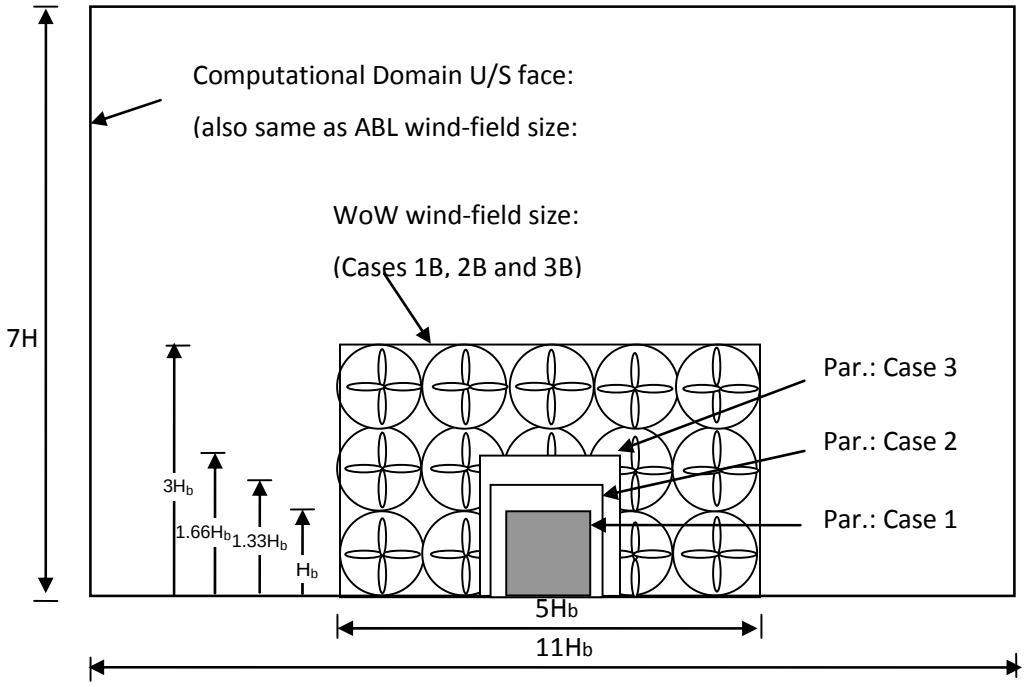

Figure 16: Sizes of test parallelepipeds and wind-fields at the inlet used for blockage assessment

literature.

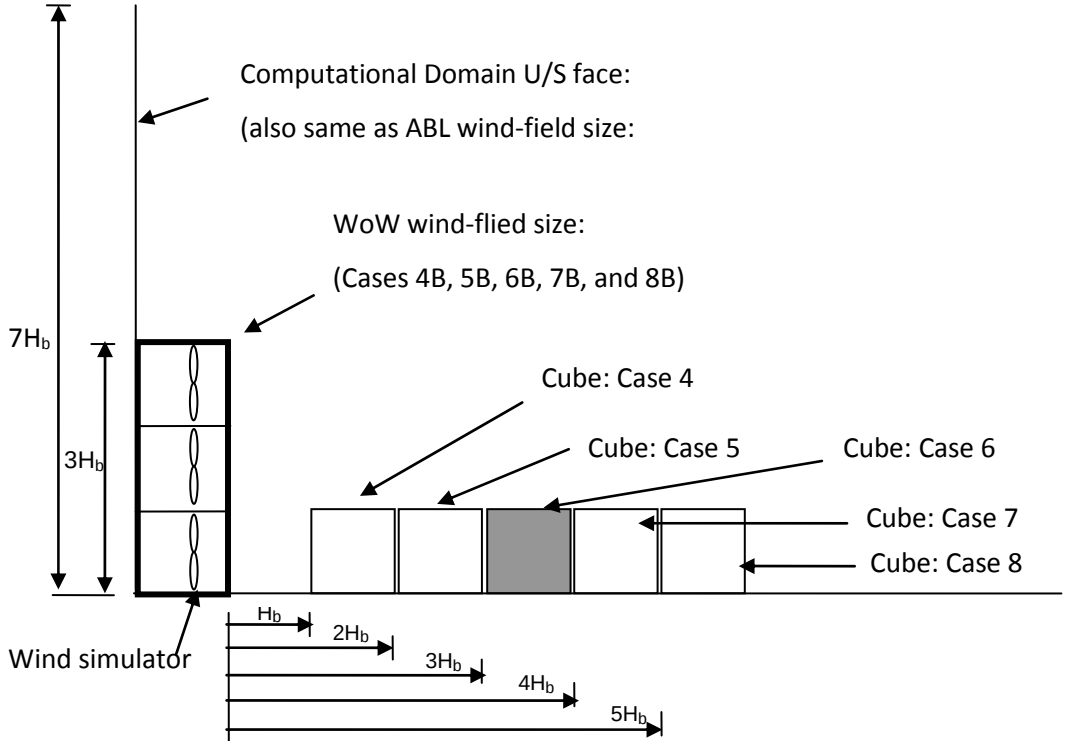

Figure 17: Test cube windward face distances from the wind simulator (fans) for different simulation cases (H_b, $2H_b$, $3H_b$, $4H_b$, and $5H_b$ for Cases 4, 5, 6, 7 and 8 respectively).

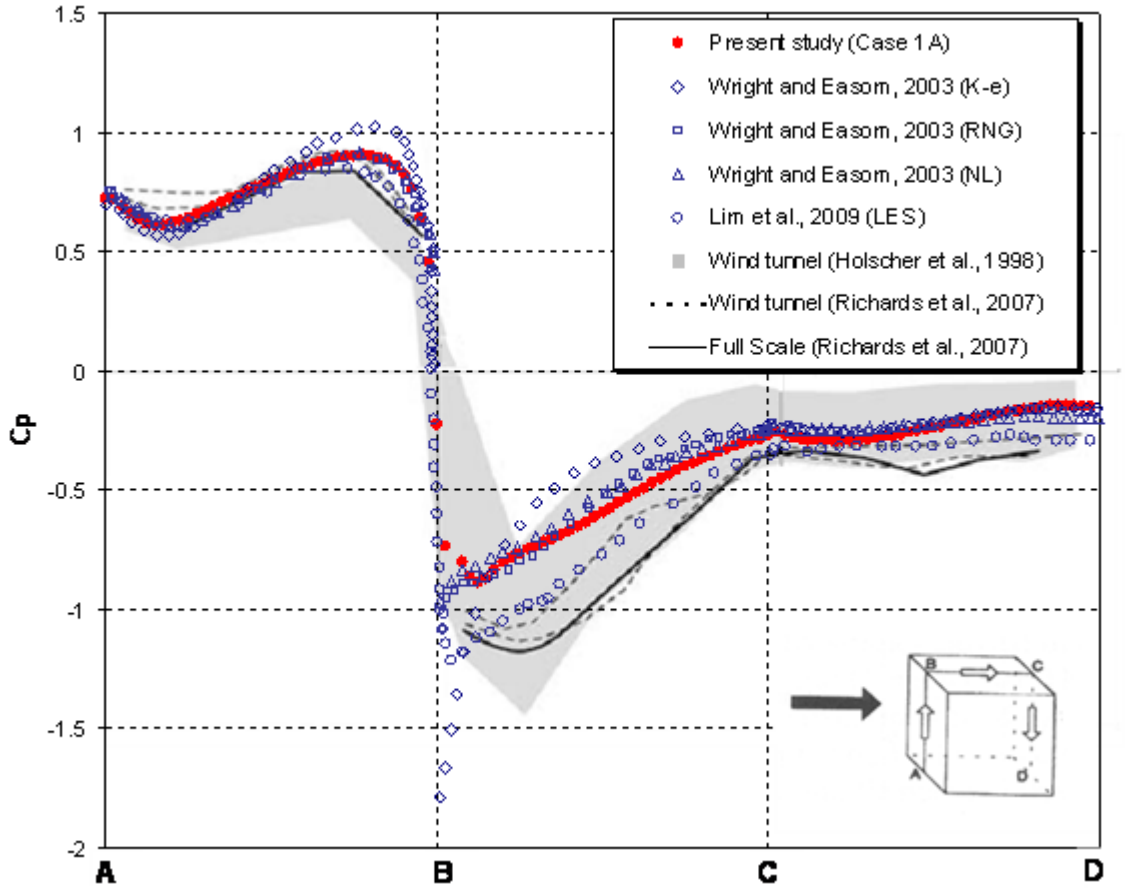

Figure 18: Comparison of mean wind pressure coefficients: Experimental measurements and numerical simulations by using several turbulence models. (Bitsuamlak et al. 2009)

2.4.2 Experimental assessment for blockage and proximity effect

2.4.2.1 Blockage assessment using small scale 1:8 WoW replica

To verify the numerical assessment of blockage, a small scale study was carried out to study the blockage and proximity effects experimentally using a small WoW (Figure 19) which is 1:8 scale replica of the full-scale WoW.

Three model cubes were fabricated using Plexiglas. Each model size was a direct replica of those cubes used in the full scale study (i.e., a 1:8 scale of 5ft. 7ft and 9.5ft cubes). In the experiment, 16 pressure taps of 0.39in long having 0.039in internal diameter tubes were inserted into the Plexiglas with one end of the tap being kept flush with the external envelope of the cube model. Pressure measurements were carried out by using Scanivalve having a 16 port pressure scanner.

with

2.4.2.2 Blockage assessment using full-scale WoW

In order to investigate the size and proximity effects on the aerodynamic data with certainty, three cubes (i) 5ft by 5 ft by 5 ft, (ii) 7ft by 7ft by 7ft, and (iii) 9ft by 9ft by 9ft were constructed and were instrumented with internal and external pressure transducers as shown in Figure 20.

model

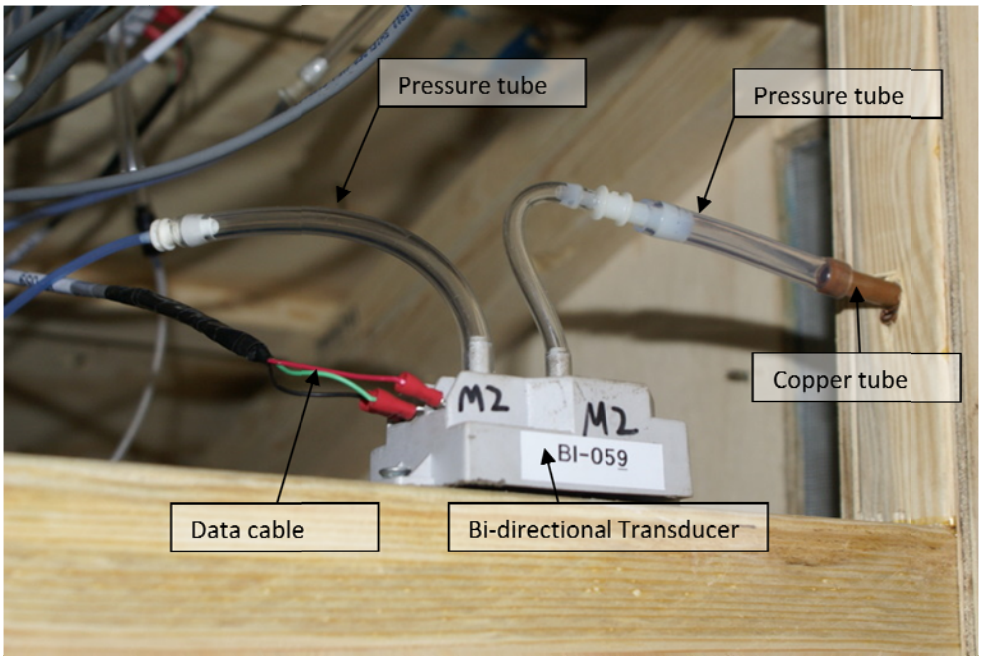

isition

The interaction of the building envelope with the wind generated is captured by pressure transducers located on both of the longitudinal and the transversal center lines of the building model. In analyzing the effect of the distance between the building and the WoW fans, each cube was placed at 12ft and 16ft away and rotated for a wind attack angles of 0°, 45°, and 90°. Pressure taps were constructed using copper tubes passing through specific locations of the

building envelope. Pressure signal captured at the spot of typical copper tube is transmitted pneumatically to the transducers through plastic tube (Figure 22). The length of the plastic tube that connects the transducer to the copper tube varies between 4in and 8in. A centrally located manhole is used to supply baseline pressure to each transducer (reference pressure). The manhole is located at a distance sufficiently far from the WoW flow field in order to prevent disturbances to the baseline pressure. The data is then transferred to a computer storage using a data acquisition system.

Each cube model is aerodynamically tested by placing it at a distance of 12ft and 16ft in front of the WoW . In order to capture the overall fluctuation of flow, separation and reattachment, each building is tested for 0°, 45° and 90° wind angle of attack. The building models were secured with hooks centrally so as to prevent the movement of the model during turbulent flow of wind. A total of 32 SETRA transducers were allocated over the center line of the envelope of each model. The pressure signals from all taps were low-pass filtered at 210Hz and sampled at a rate of 100Hz for 60seconds.

On the 7ft cube model, additional internal pressure study was carried out in the presence of dominant openings to determine the test duration and assess signal strength prior to the planned internal pressure tests for low-rise buildings with gable and hip roofs. A dominant door opening was provided on the windward side of the cube model and has a size of 13.5in x 54.8in making 10% of the windward wall area.

The entire model cubes were constructed to be air tight except for the minor porosities at connections, door and window frame openings that make up the natural background leakages.

In order to capture pressure data over the surfaces of the 7ft cube model, 68 transducers were uniformly placed as shown in the external and internal tap layout sketch, (Figure 23 & Figure 24). Pressure transducers were placed both longitudinally and transversally along the center line of the building to capture turbulent fluctuations, separation and reattachment of the external flow (Figure 23). Moreover, in order to estimate the pressure fluctuations at the entrance of the dominant openings, pressure taps were placed at the periphery of each opening so that the average area is considered for analysis. More pressure taps were also placed internally to capture the pressure fluctuations inside the building envelope.

External and internal pressures measured on the surfaces of the building model were used to assess the net design pressures on the envelopes. For this purpose, two representative cases of porosity were tested. These two cases are:

Case 1: Nominally sealed building wherein which the impact of background leakage from cracks, fractures and other construction openings in generating fluctuation in internal pressure is tested

Case 2: 10% door opening wherein which the impact of dominant opening is tested

Each of the above mentioned cases were tested for wind direction $0 \leq \theta \leq 90°$ at every 15° wind angle of attack

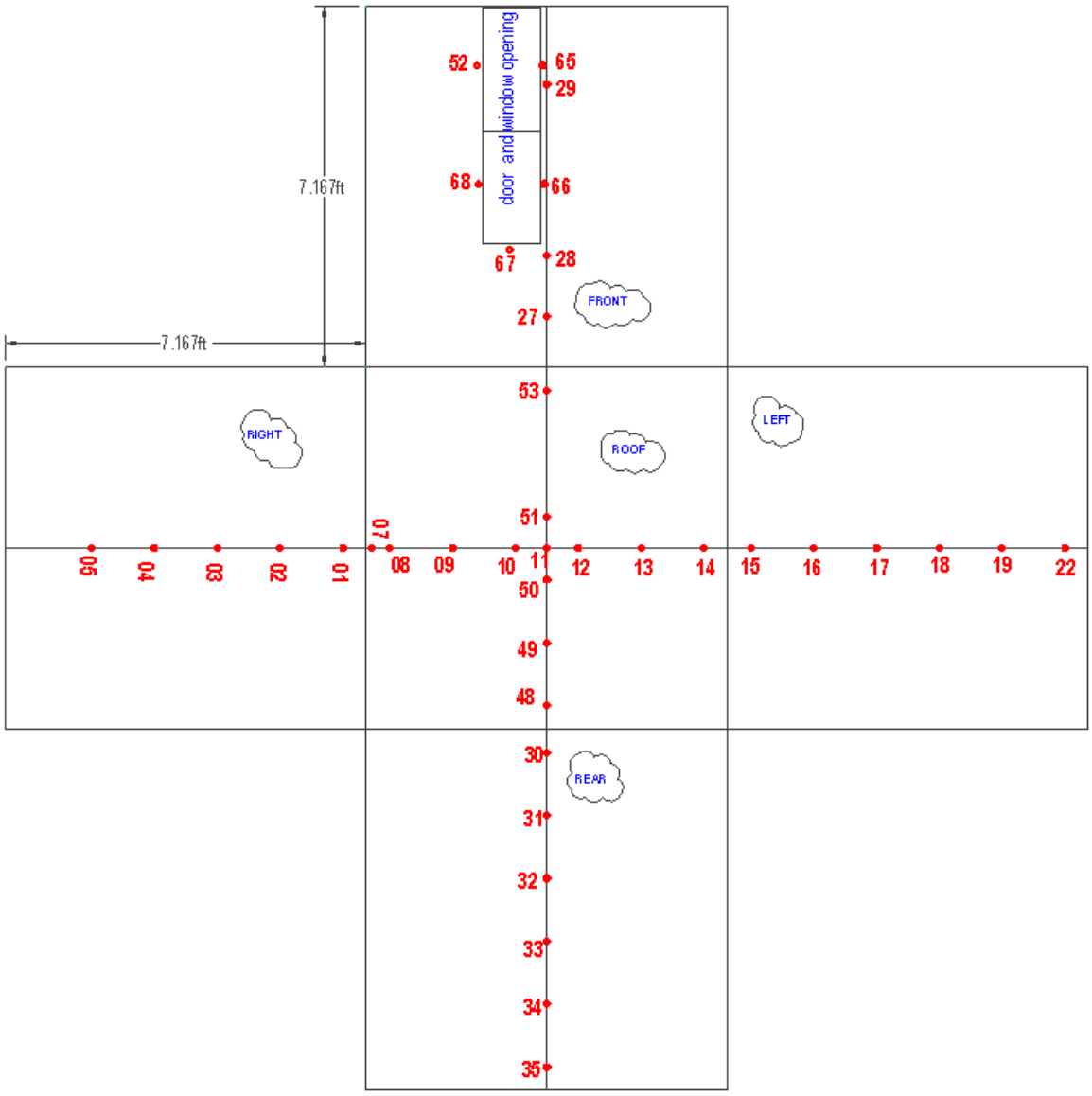

Figure 23: External pressure taps location

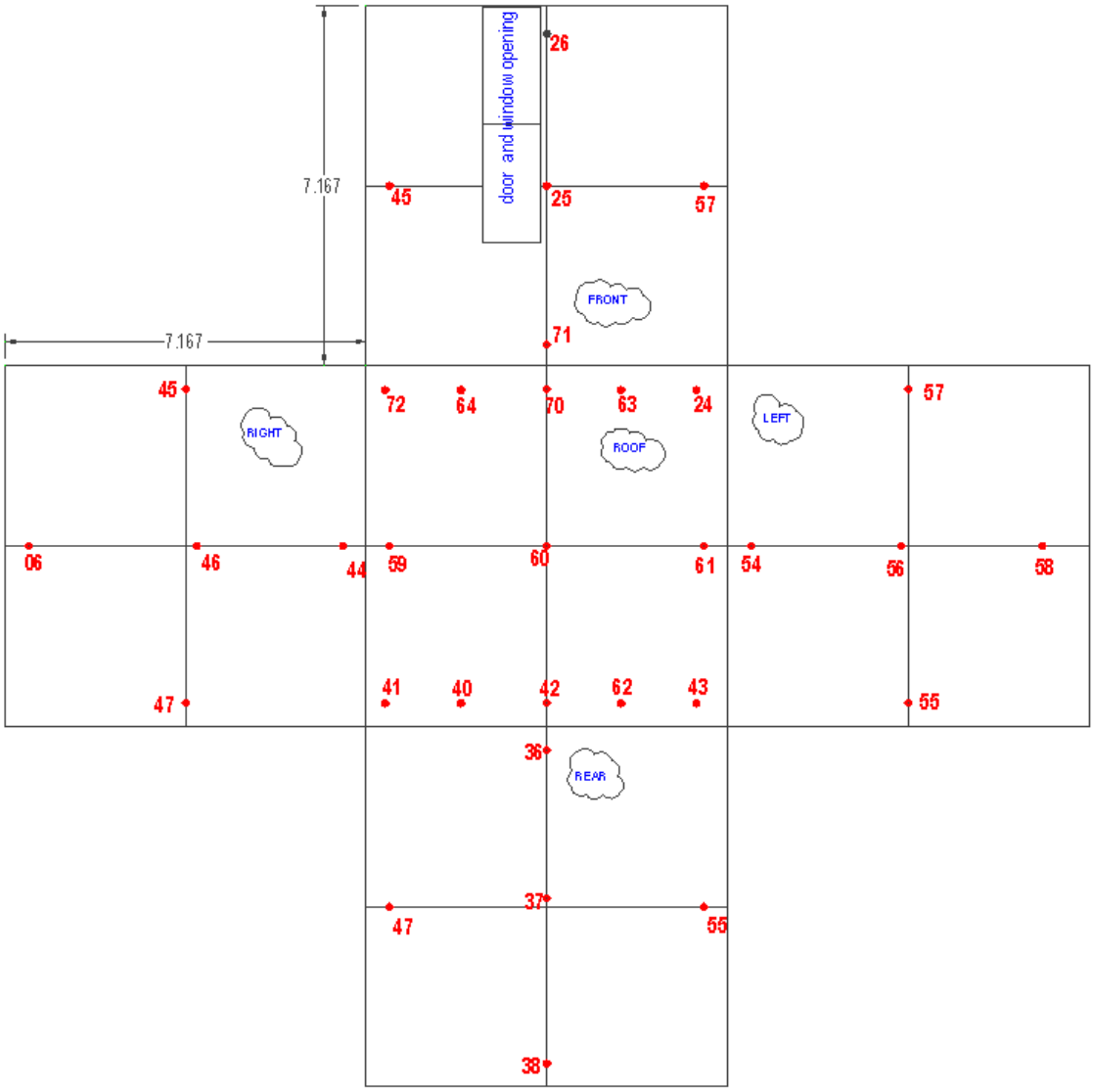

Figure 24: Internal pressure taps location

2.5 Internal and external pressure for Low-rise building with gable and hip roof

The main objective of the present study, the internal and external pressure investigation for gable and hip roof buildings, was performed using large low-rise building models as shown in Figures 9 to15. Design and fabrication details are discussed in Section 2.2. A low-rise building model of size 9ft W x 7ft L x 7ft H with interchangeable roof was placed at 12ft distance from the WoW front engines and secured with hooks centrally. The test model had gable and hip roof with a slope ratio of 4:12. The internal volume of the building is divided into two compartments (attic and living room) at ceiling level with a wood panel (7ft from the ground) and each compartment volume is treated separately in evaluating the internal pressure that develop in it.

The building has two dominant openings: a door with size 3.15ft by 1.50ft and a window with size 1.70ft by 1.40ft. These door and window openings make up 7.5% and 3.75% of the area of the windward wall, respectively. A hatch opening that connects the attic with the living room, a square hatch window, with size 1.5ft x 1.54ft was provided. The model was constructed in such a way that it represents a house with tight connections except for nominal porosities. Rubber pads were provided to all door and window jambs in order to reduce the leakage of air into the building premises.

2.5.1 Gable roof

In order to capture pressure data over the surfaces of the gable house model, 68 SETRA transducers were uniformly placed as shown in the external and internal tap layout sketch, Figure 25 & Figure 26 respectively. A total of 34 Pressure transducers were allocated both longitudinally and transversally along the center line of the building envelopes to capture external pressure fluctuations, separation and reattachment of flows externally (Figure 25).

Moreover, In order to evaluate the pressure fluctuations at the entrance of the dominant openings, pressure taps were placed at the periphery and center of each opening (a middle door and an upstream edge window with 7.5% and 3.75% porosity respectively) so as to have representative measurements for the respective area average analysis. A total of 31 pressure transducers were allocated internally throughout the inside of the building at the living room and the attic to capture the overall internal pressure fluctuations inside the building as shown in Figure 26. Generally, external and internal pressures measured on the surfaces of the building model were used to assess the net design pressures on the envelopes. The pressure signals from all taps were sampled at a rate of 100Hz for 180 seconds.

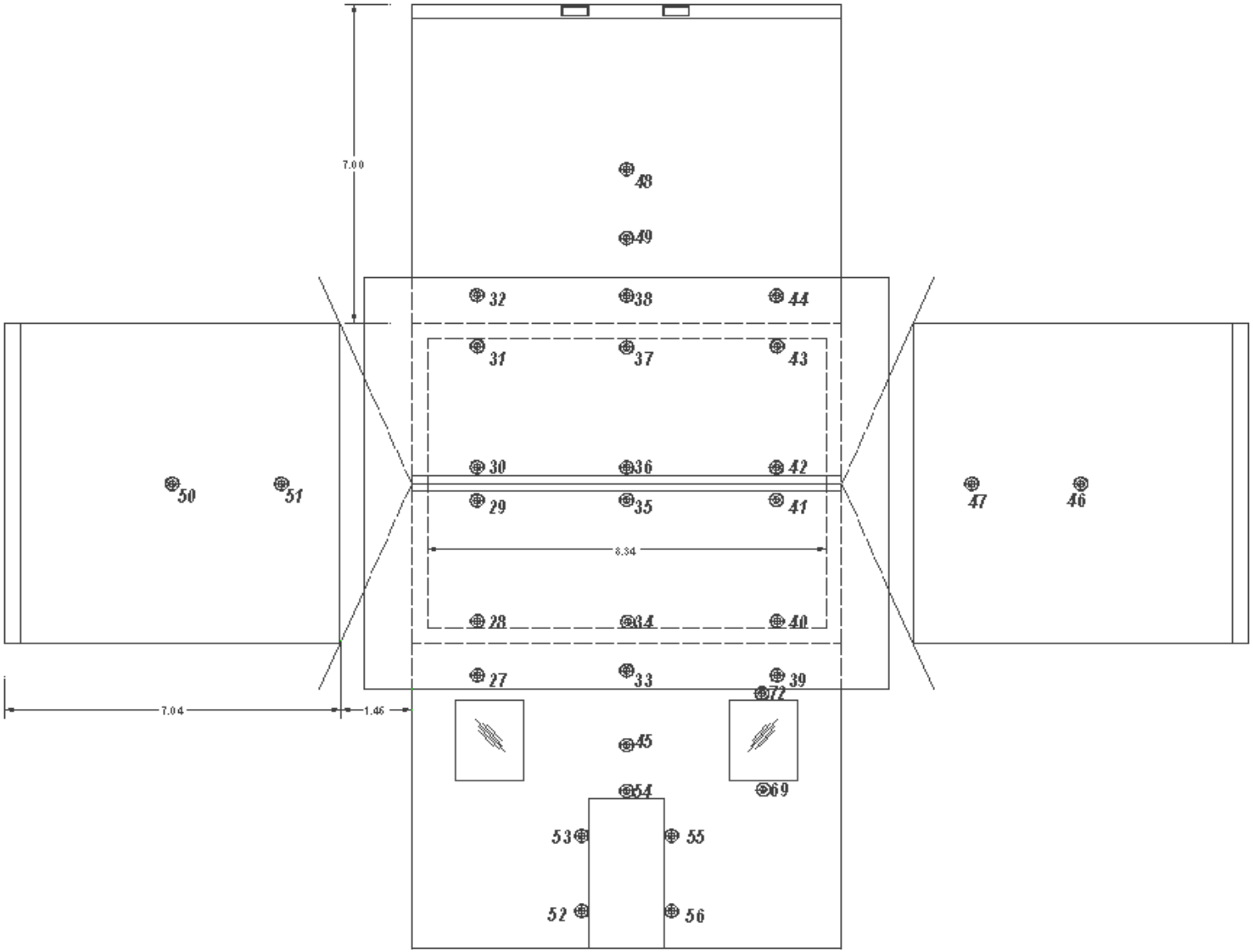

Figure 25: Exploded plan view of gable roof external pressure tap layout

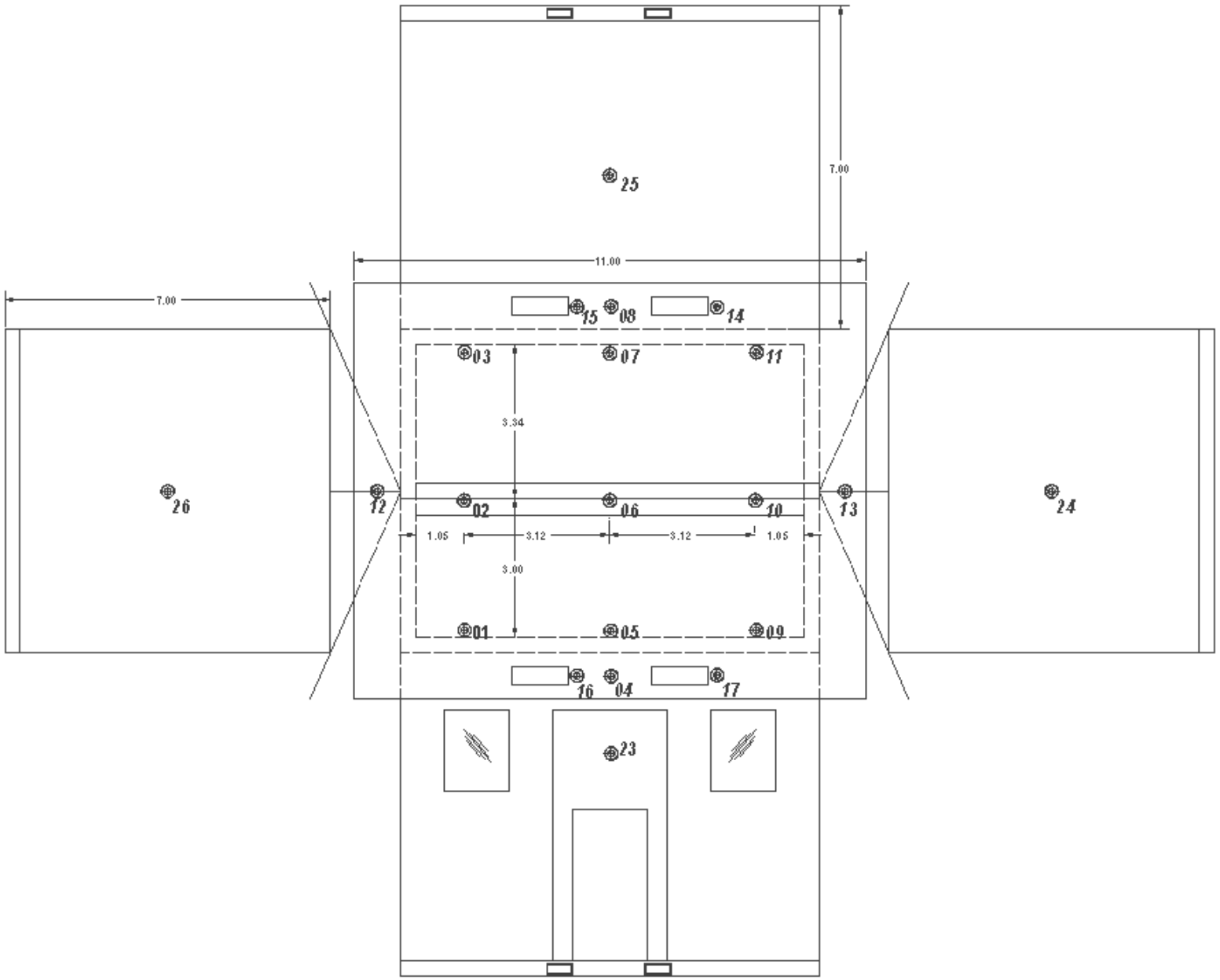

Figure 26: Exploded view of internal pressure tap layout

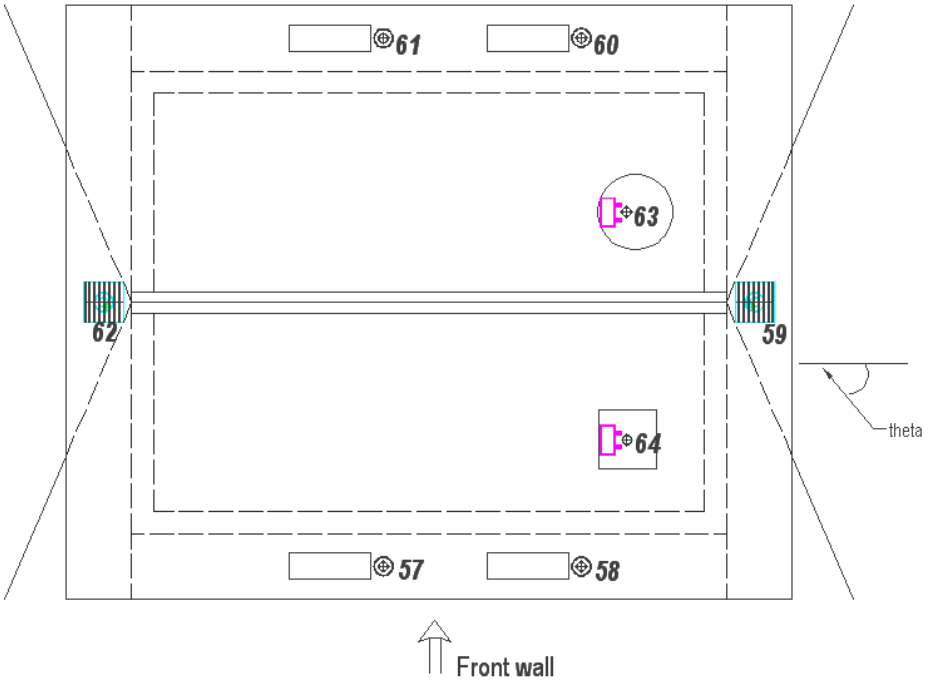

Figure 27: Gable roof ventilation system pressure tap layout

As shown in Figure 27, the pressure fluctuation, both internal and external, around the ventilation system was recorded by allocating transducers around each vent.

Regarding the configuration of the model geometry and transducer layout, the flow of wind is said to be at right angle when the wall, onto which the door and the windows are fixed, is facing the wind generated by the WoW. It is noteworthy to mention that the rotations of the models were performed in a counterclockwise sequence. The mean wind speed generated by the WoW at 12ft distance away and mean ridge height of 7.16ft is 45.61mph (i.e., 20.39m/s).

As a common practice, most buildings are equipped with ventilation systems in order to provide proper indoor air quality. Building performance guides such as Florida Building Code (FBC), ASHRAE, Canadian Mortgage and Housing Corporation (CMHC) require the provision of HVAC openings on the surface of roofing envelopes so as to effectively cross-ventilate attic space between ceiling joists and roof rafters. FBC R4409.13.3.2, for instance, entail the

Table 1: Different types of ventilation systems with respect to their opening size

S.N	Description	area [in^2]	ratio=vent opening to attic floor [%]
1	Ceiling area to be ventilated	11664.00	
2	Soffit opening	251.56	2.16
3	Gable end opening	180.00	1.54
4	Goose neck opening	38.00	0.33
5	Turbine opening	86.58	0.74
6	Ridge opening	144.00	1.23
	Total ventlation opening area (in^2)	**700.15**	
	Ceiling area to be ventilated (in2)	**11664.00**	
	Ratio of free ventilating opening to that of the ceiling floor	**0.0600**	

provision of approved mechanical ventilation systems having a total opening area of at least $1/150^{th}$ of that of the attic floor. To satisfy this requirement, the building model in our case was equipped with soffit, roof and gable-end ventilation scheme. The roof ventilation system consists of ridge, wind turbine and goose neck opening vents. The size of each ventilation opening and its respective porosity ratio is as shown in Table 1. Commercially available Miami Dade County approved ventilation systems (Goose neck, Turbine and Vent II-ridge) were used for the top roof openings. For the soffit openings, a bird/insect screen with mesh sizes of ¼'' were installed; two at each side of the eave of the wooden building.

In undertaking the differential pressure analysis of the gable roof building, five test configurations were setup as shown in Table 2 . Test case 1 is an arrangement of the model with all of the openings closed except for the natural leakage. It is basically a nominally sealed building scenario wherein which the impact of background leakage from cracks, fractures and other construction openings in generating fluctuation in internal pressure is tested. Test case 2 is a dominant door (D1) opened arrangement wherein which the door is located at the center of the

windward wall having a porosity of 7.5%. Test case 3, on the other hand, is a pattern in which case the dominant opening is a window (W1) instead of door. Unlike Test case 2, the W1 is located at the upstream edge of the windward wall and its center line at a level (2/3)h from the ground (apparently coinciding with the stagnation point). As shown in Table 2 , the porosity ratio of the window opening is 3.75% with respect to the windward wall. Test case 4 is basically a combination of windward door (D1) and hatch opening scenario. The hatch is located at the ceiling partition that connects the attic with the living room. Similarly, Test case 5 is a combination setup between windward window (W1) and hatch at the ceiling. The test cases and configuration setups are given in Table 3 for the gable roof and Table 4 for the hip roof model.

Table 2: Building opening position, size and porosity description

Description of opening		Dimensions (in)	Area (in^2)	Porosity (%)
Windward wall	Door D1, (7.5%)	18x37.8	680.40	7.50
	Window W1, (3.75%)	16.68x20.34	339.27	3.74
Attic floor	Ceiling hatch	18x18.5	333.00	2.85
	Soffit screen (4 pcs)	14.375x4.375	251.56	2.16
	Gable end opening (4 pcs)	9x5	180.00	1.54
Roof	Ridge vent (2 strips)	3/4*96	144.00	1.23
	Turbine opening (diam. 12'')	d=12	86.58	0.74
	Goose neck	4x9.5	38.00	0.33

Table 3: Summary of test cases for gable roof model

Part I-GABLE ROOF

0° 15° 45° 75° 90° 5 rotations per each test		Dominant opening	Background leakage			Ceiling hatch	Partition	Vents: ridge/soffit	Remark
			Wall	ceiling	roof				
Envelope opening combination	Test 1	-	✓	✓	✓	-	-	✓	+105° &120°
	Test 2	D1	✓	✓	✓	-	-	✓	
	Test 3	W1	✓	✓	✓	-	-	✓	+105° &120°
Dominant opening and ceiling compartment	Test 4	D1	✓	✓	✓	✓	-	✓	
	Test 5	W1	✓	✓	✓	✓	-	✓	+105° &120°

2.5.2 Hip roof

The full scale experiment on hip roof model was performed using the demountable building by removing the gable roof and changing it by hip roof as shown in Figure 29 and Figure 28. The overhang ratio (overhang length divided by eave height) of the building is 0.14 while the aspect ratio (eave height/base width) is 0.77 on one side and 1 on the other side since it is rectangular. A total of 69 SETRA transducers were used to capture both the internal and external pressure distributions as shown in Figure 30 and Figure 31. In order to simulate the impact of external opening area on internal pressure, two dominant openings (3% door and 7.5% window openings) were incorporated in the experiment along with background leakage. Measurements of Test 1 (background leakage case), Test 4(door and hatch opening case) and test 5(Window and hatch opening case) were obtained for five wind angle attack ranging from 0° to 90° at an increment of 15°. For Test 2(door opening case) and Test 3(window opening case), four more wind angles were added from 105° to 180° as shown in Table 4 Similar to Gable roof orientation, the wind direction is defined to be 90° when the wall of the building containing the dominant openings is normal to it.

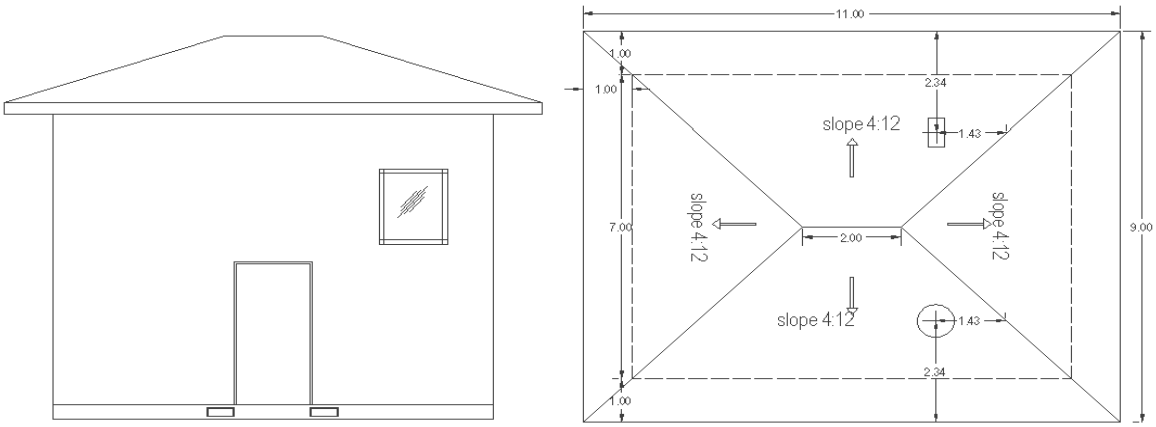

Figure 29: Hip roof front elevation and roof conceptual design detail

Table 4: Summary of test cases for hip roof model

Part II-HIP ROOF

0° 15° 45° 75° 90° 5 rotations per each test		Dominant opening	Background leakage			Ceiling hatch	Partition	Vents: ridge/soffit	Remark
			Wall	ceiling	roof				
Envelope opening combination	Test 1	-	√	√	√	-	-	√	
	Test 2	D1	√	√	√	-	-	√	+105°,120°,150° &180°
	Test 3	W1	√	√	√	-	-	√	+105°,120°,150° &180°
Dominant opening and ceiling compartment	Test 4	D1	√	√	√	√	-	√	
	Test 5	W1	√	√	√	√	-	√	
	Test 6	W1	√	√	√	-	-	-	
	Test 7	W1	√	√	√	√	√	√	

Figure 28: Wooden hip roof model in front of Wall of Wind

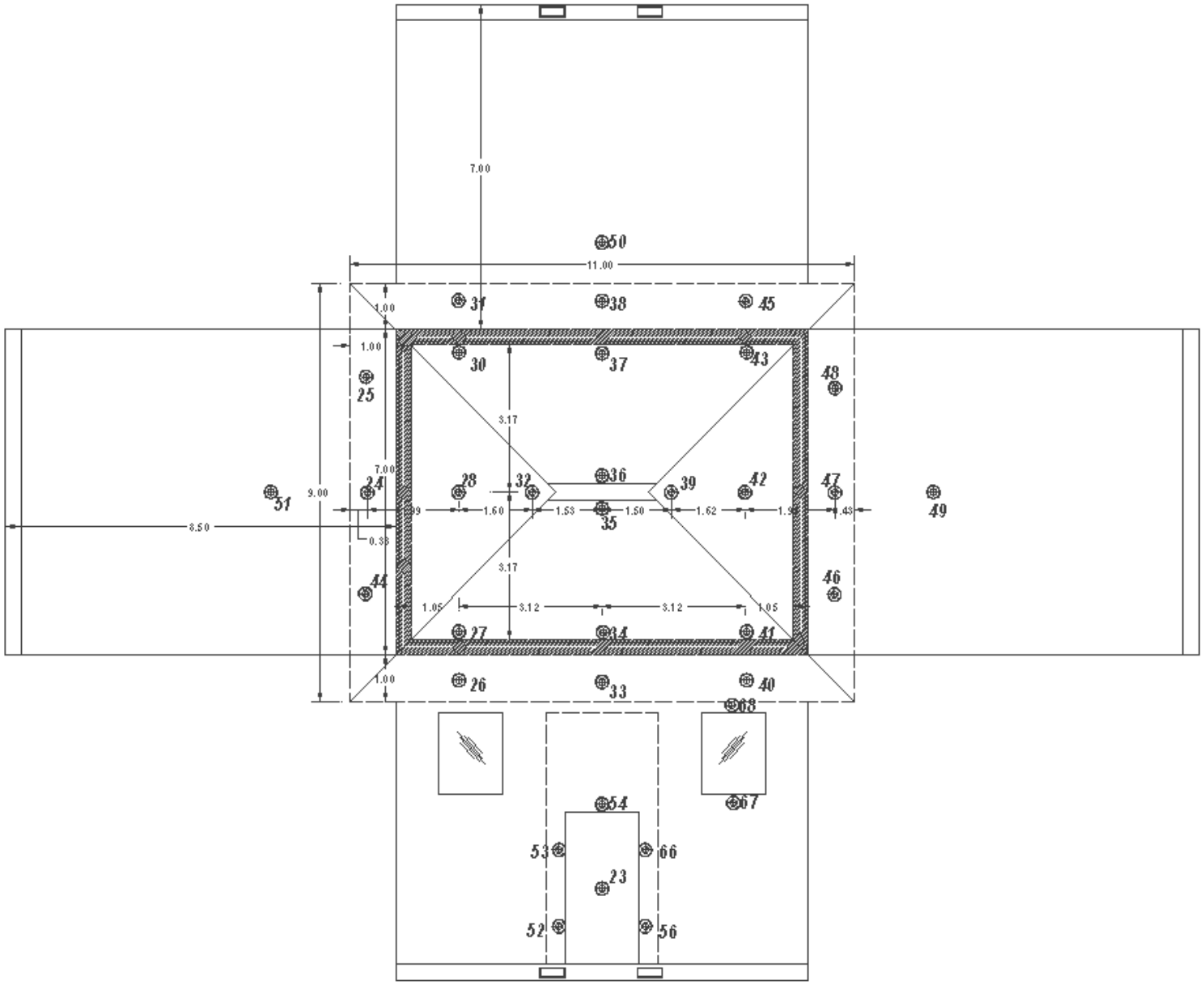

Figure 30: Exploded view of hip roof external pressure tap layout

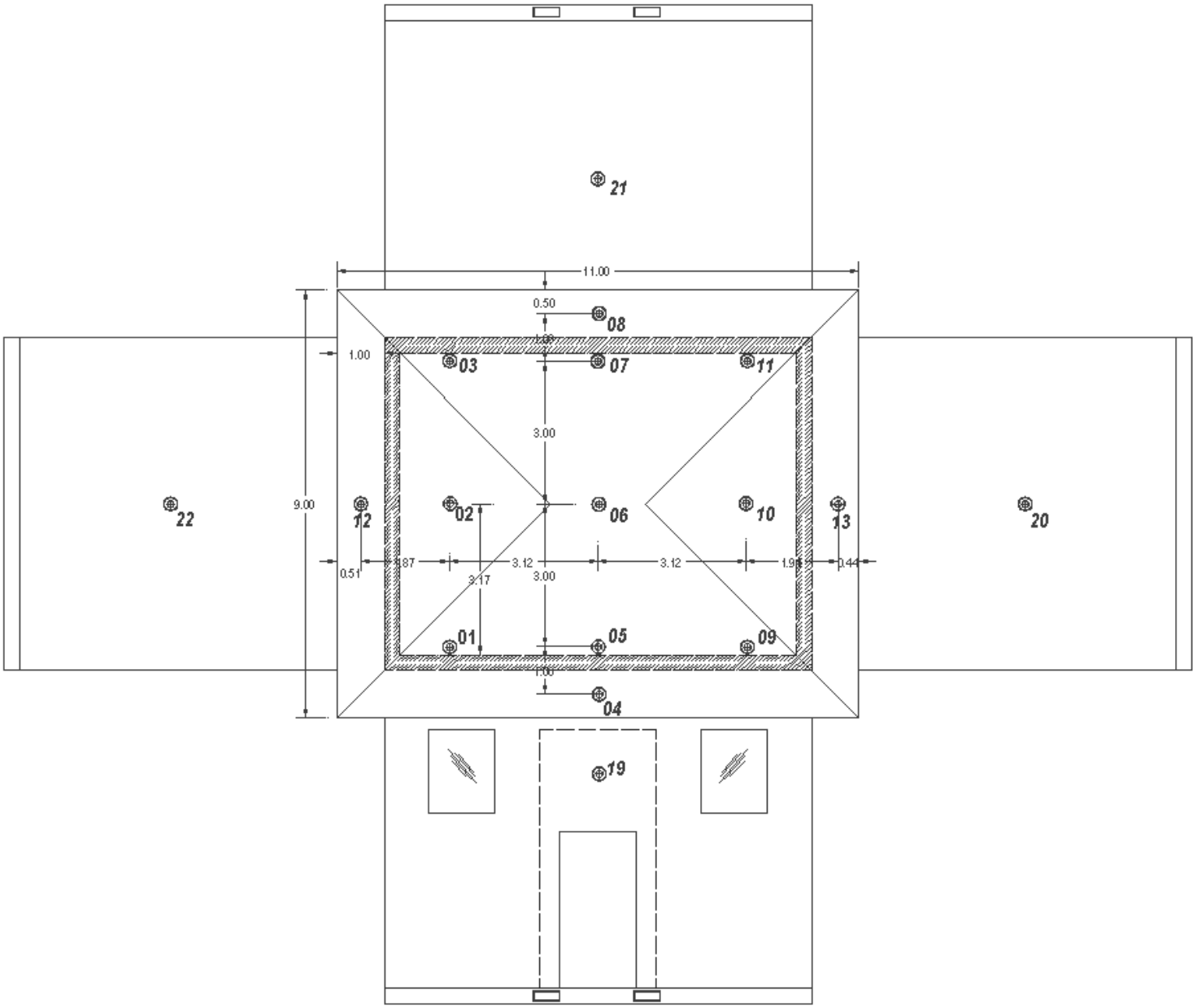

Figure 31: Exploded plan view of hip roof internal pressure tap layout

3. Results and discussions

3.1 Blockage and proximity effects

3.1.1 Preliminary numerical assessment of blockage and proximity effects

Following the comparisons of the numerical simulations with results from the literature to validate the accuracy of the numerical approach (as discussed in section 2.4.2.1), the blockage assessments were pursued. The velocity contours for Case 1 are shown in Figure 32 a and Figure 33 b shows the contours on a horizontal plane at mid-height of the cube. Similarly, 33 (a) and 31(b) shows the contours on a vertical plane passing through the center of the cube. Figure 34 shows the path-lines for the recirculation zones for Case 1. Qualitatively, there is a general good agreement in terms of size of recirculation length behind the parallelepipeds. Quantitatively, Figure 36 shows mean pressure coefficient comparisons for Cases 1A (ABL) and 1B (WoW). As can be seen from the figure, there is a very good agreement between the two cases. This confirms the viability of using a proper wind-jet flows generated using the WoW system with proper turbulence and boundary layer generation schemes representing the ABL conditions. Figure 35 and Figure 37 show similar results for Cases 2 and 3, respectively. Slight differences in mean pressure coefficients (Cp values) were observed for Cases 2 and Case 3 at the roof and the leeward wall. These differences could be due to blockage or inadequacy of the basic type of turbulence model used in the present study. Finally, the wind simulator proximity assessments were pursued. Similar to the blockage assessments, mean Cp values extracted from the center vertical lines at U/S and D/S faces of the parallelepiped (i.e., AB and CD) and the center horizontal line of the roof (i.e., BC) were used for comparison purposes. The mean Cp values for Cases 4, 5, 6, 7, and 8 were compared with the wind tunnel data obtained from the literature as

shown in Figure 38. There is a general good agreement between the CFD and the wind tunnel data for Cases 5, 6, 7, and 8. For Case 4, however, the comparison reveals exaggerated Cp values in the windward wall. This means that the pressure coefficients at the windward wall were created by higher wind speed than the wind speed used to obtain the pressure coefficients. It is to be recalled that the wind speed measured at H ft from ground (H= cube height) before placing the cube in the testing position has been used to obtain the pressure coefficients. This is believed to be due to the close proximity of the test cube to the wind simulator blocking the flow before it expands upwards and to the sides. Because of this, a higher velocity created the pressure system compared to the velocity used for obtaining the pressure coefficients. Compared to windward wall, the roof Cp values were less sensitive to test building proximity to the wind simulator as can be seen in Figure 38. The insensitivity of the roof pressures to the proximity of the wind simulator is believed to be due to localized flow effects such as flow separation at the roof level, which is less independent of the proximity parameter. For Cases 5, 6, 7, and 8, where the test cube was placed at >2H distance from the wind simulator, the exaggerated positive pressure disappeared. Thus, it may be concluded that in order to obtain a good quality aerodynamic data on walls, the models needs to be placed at a distance of more than 2H from the wind simulator or conduct detail blockage correction factor studies. However, for roof or roof top equipment tests the aerodynamic data are less sensitive to the proximity of the test-specimen to the wind simulator.

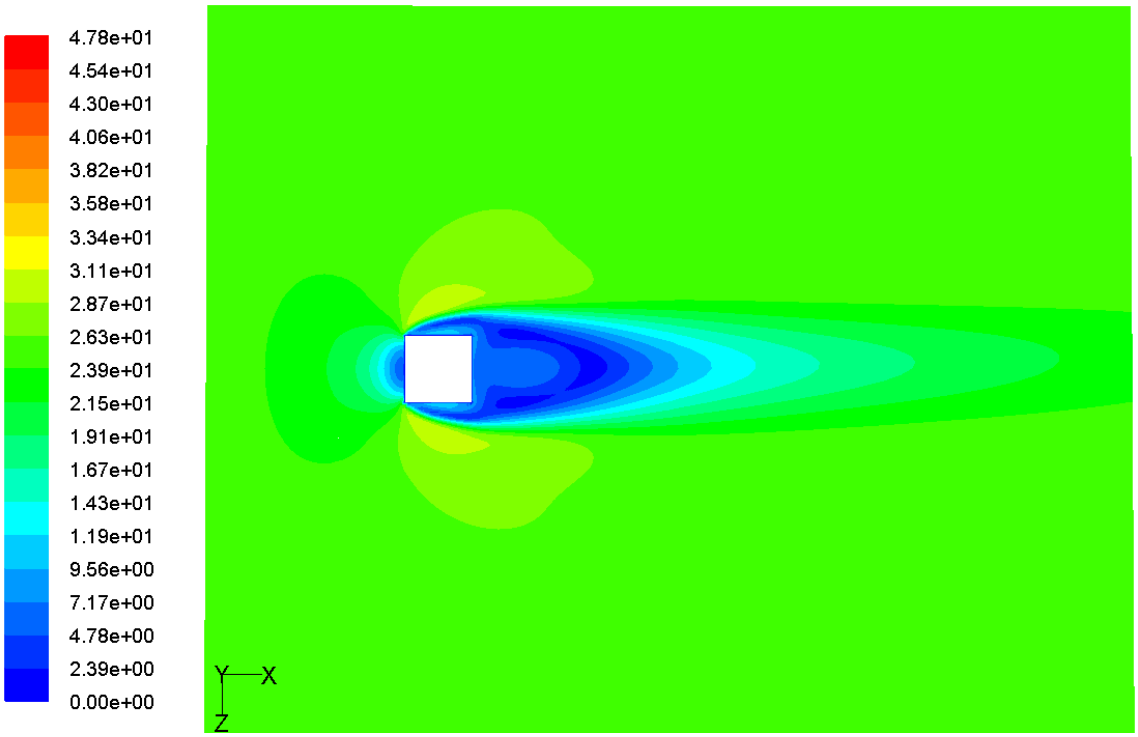

(a) Case 1A (ABL) – Horizontal plane at mid-height of the parallelepiped.

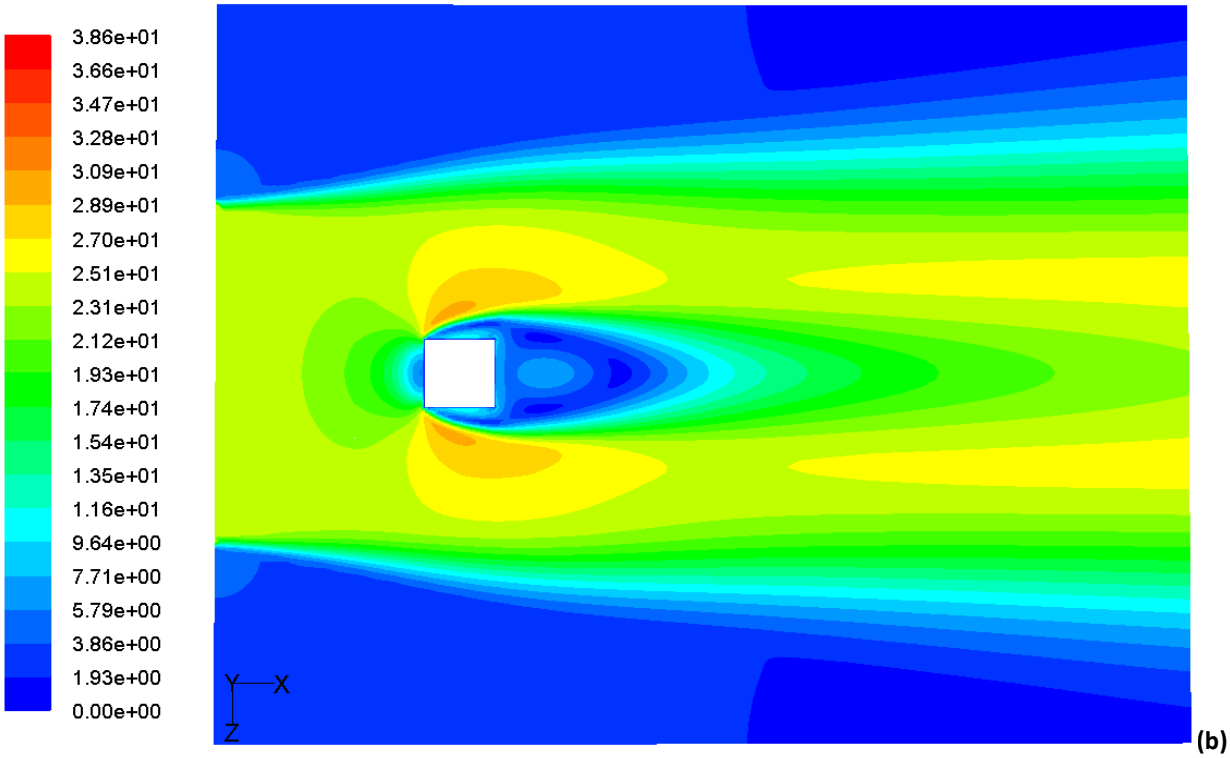

(b) Case 1B (WoW) – Horizontal plane at mid-height of the parallelepiped.

Figure 32 Wind velocity contour plots for ABL and WoW simulation (continued).

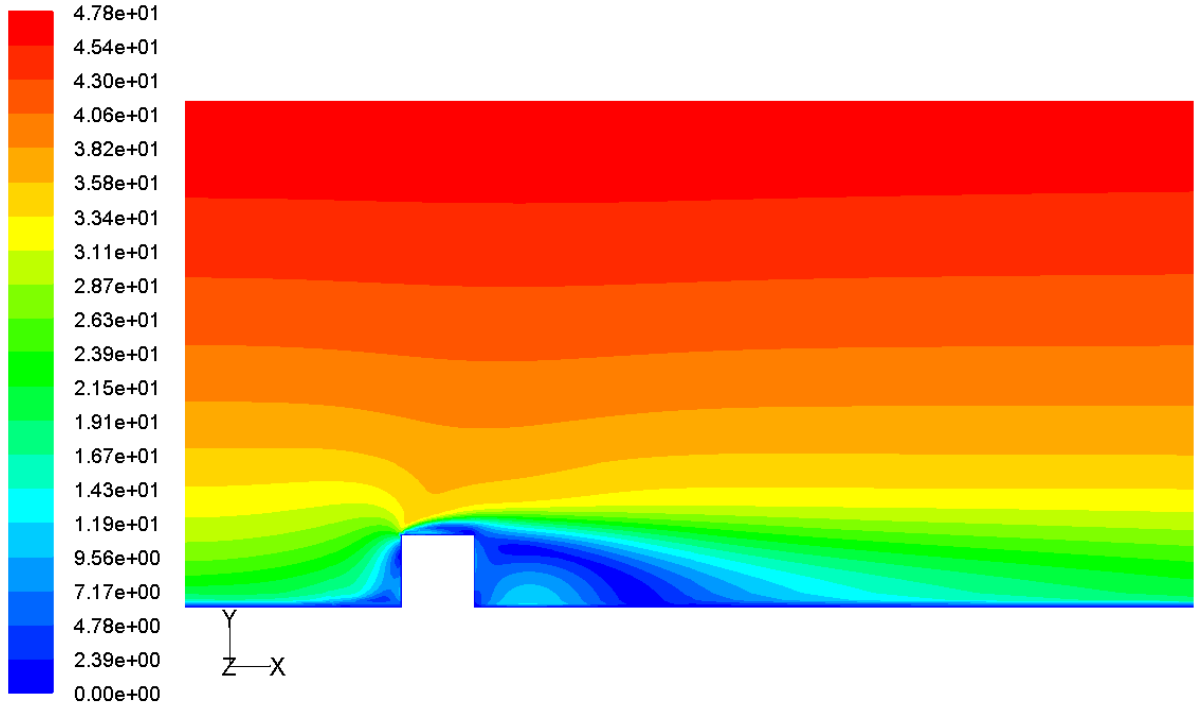

(c) Case 1A (ABL) – Vertical plane at the center of the parallelepiped.

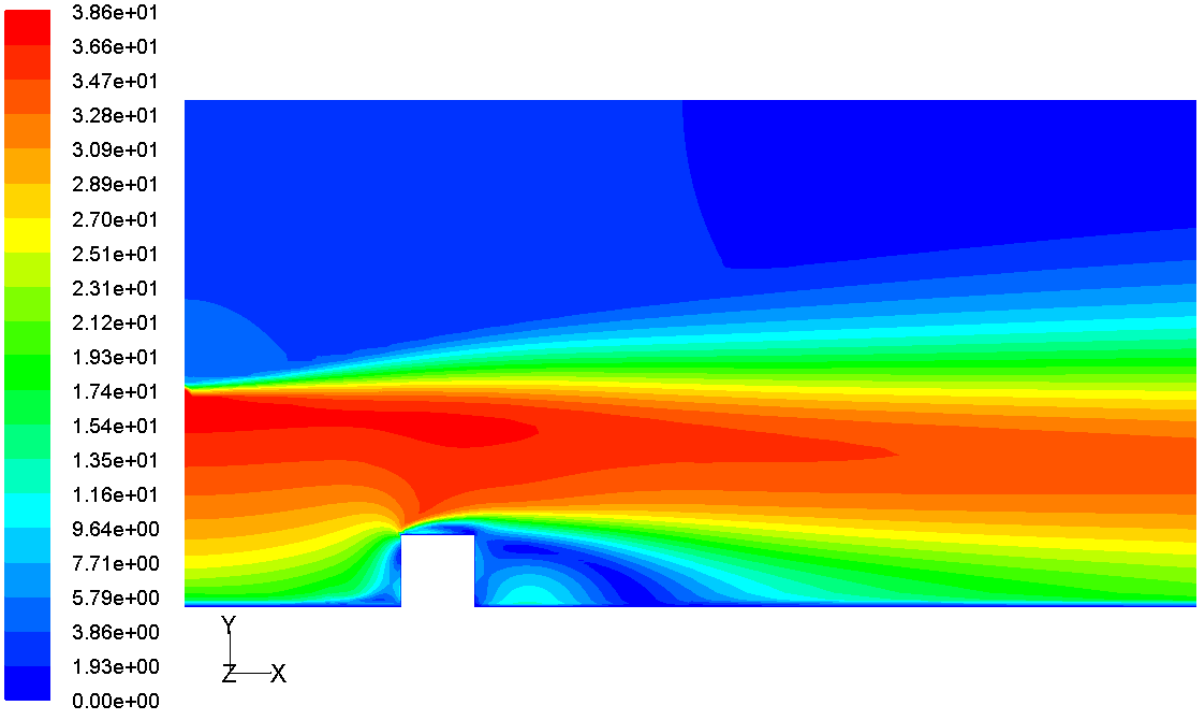

(d) Case 1B (WoW) – Vertical plane at the center of the parallelepiped

Figure 33 Wind velocity contour plots for ABL and WoW simulation.

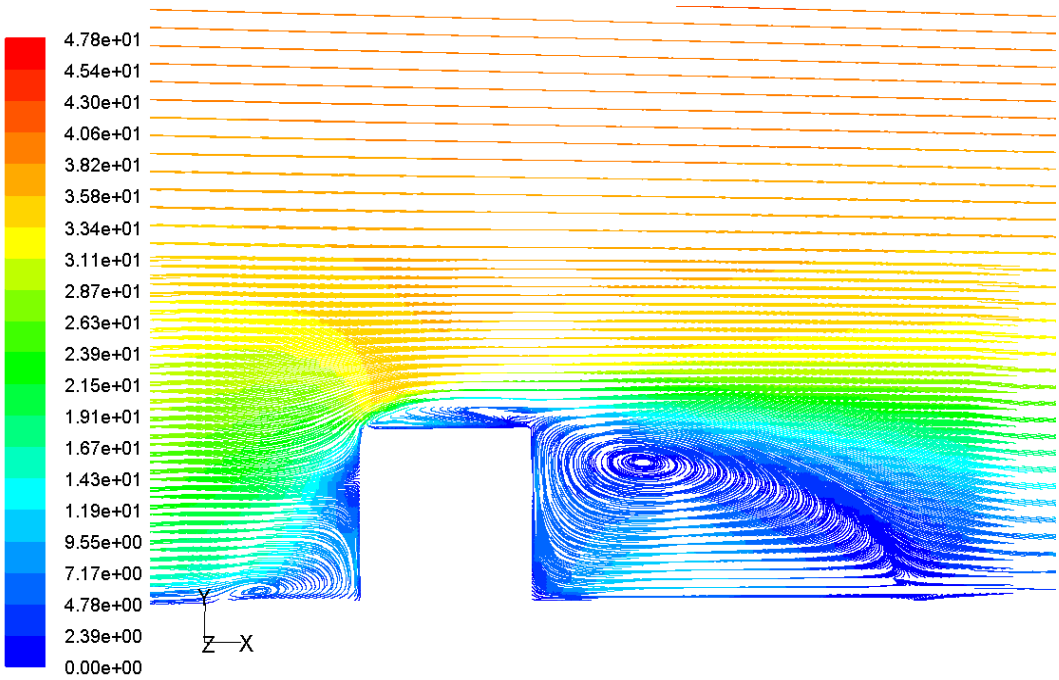

Case 1A (ABL)

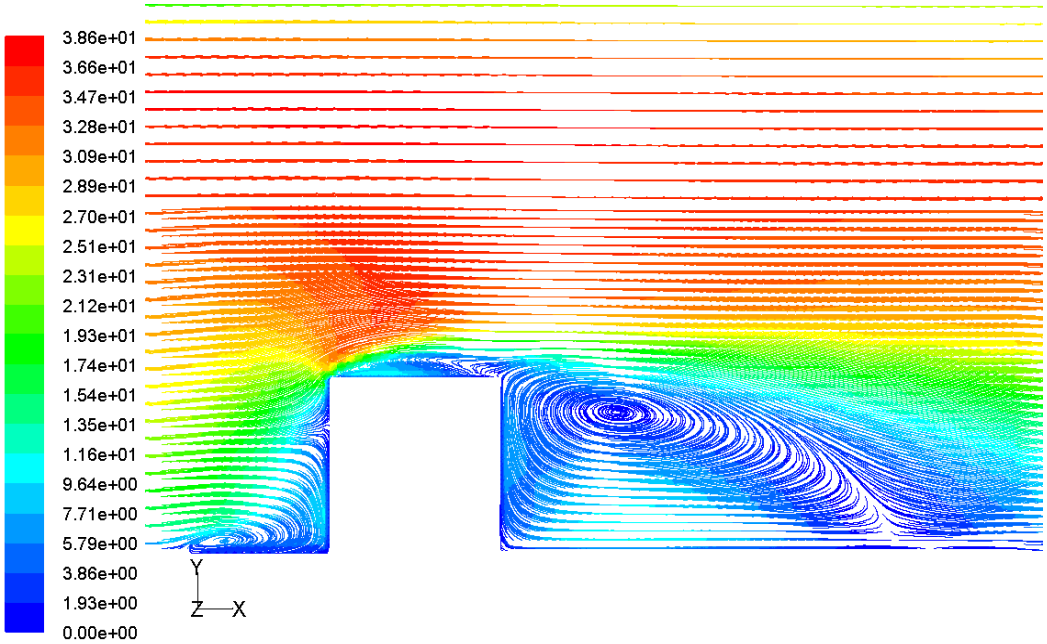

Case 1B (WoW)

Figure 34 Wind velocity path-lines and recirculation zones.

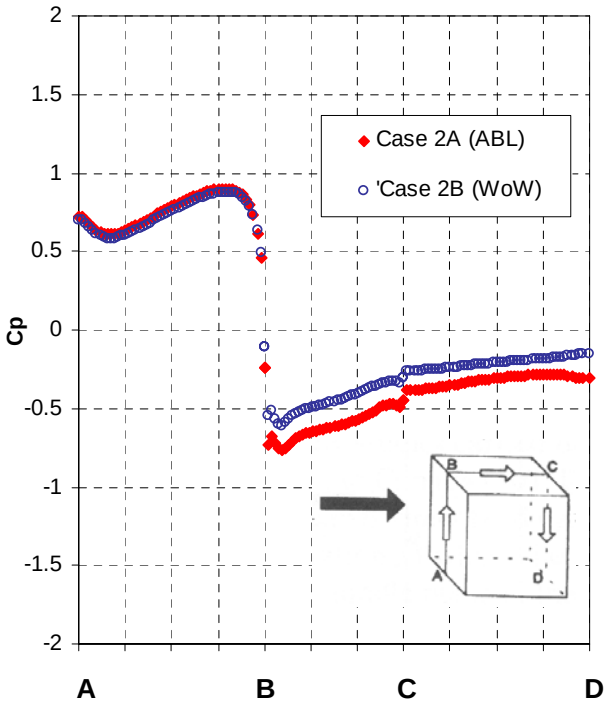

Figure 35 ABL and WoW mean Cp comparisons for Case 2 (4x4x3 m parallelepiped)

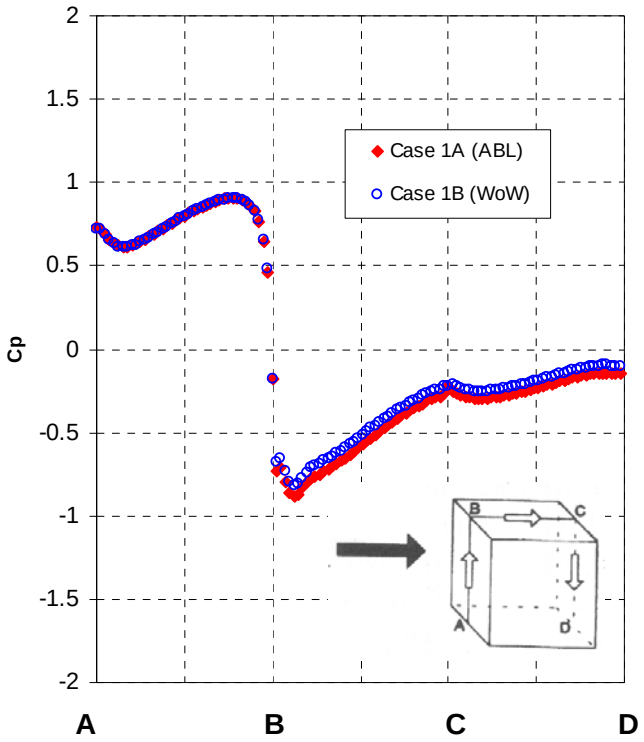

Figure 36 ABL and WoW mean pressure coefficient comparisons for Case 1 (3x3x3 m cube)

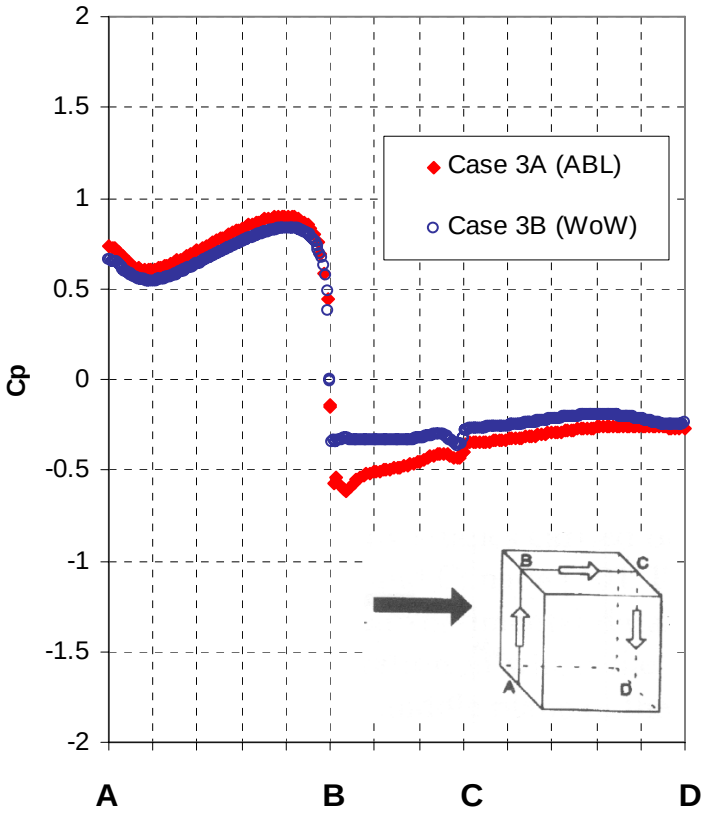

Figure 37 ABL and WoW mean Cp comparisons for Case 3 (5x5x3 m parallelepiped)

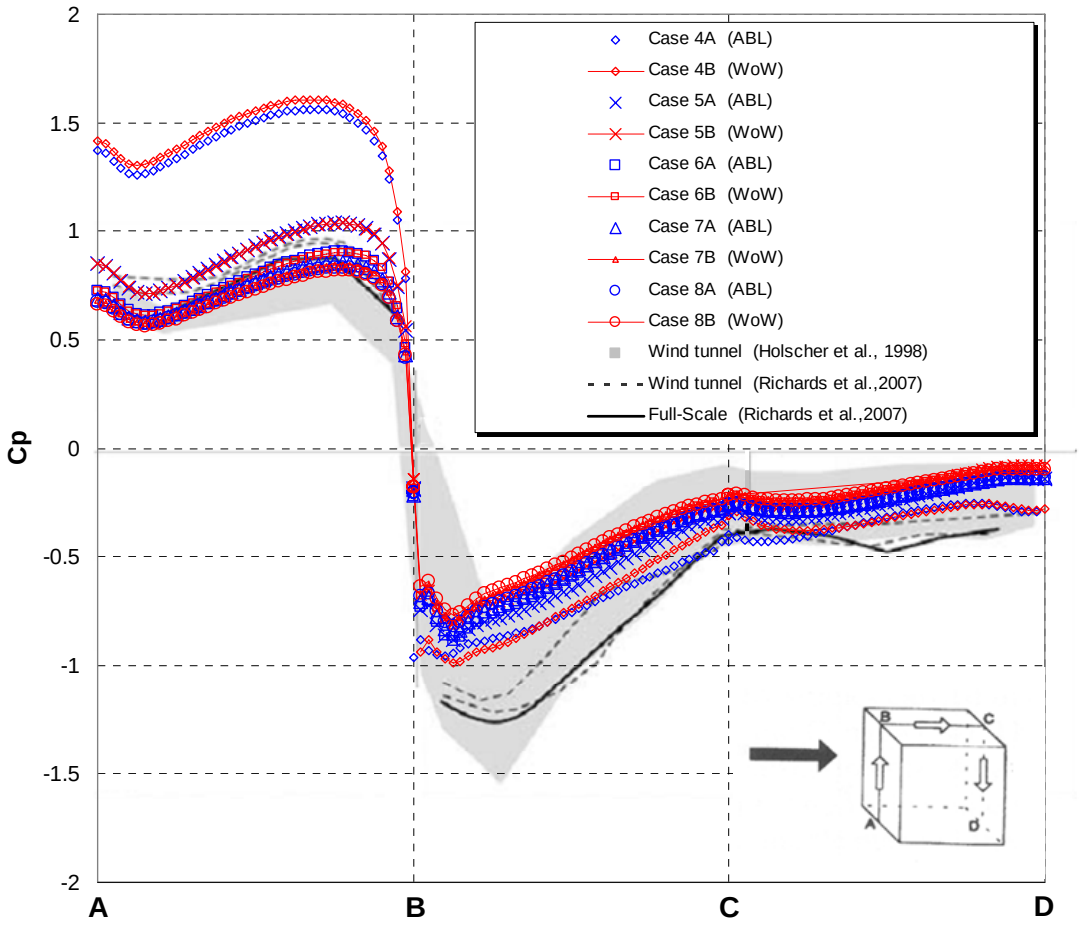

Figure 38 ABL and WoW mean Cp comparisons for Cases 4, 5, 6, 7 and 8 with wind tunnel data from literature.

Outcomes of the numerical proximity and blockage assessment studies:

- WoW flows can replicate atmospheric boundary flows.
- For large test models, i.e. for cases where the height of the test model is larger than one third of the wind field height, carrying out proper blockage assessments is necessary.
- Test buildings shall be preferably located at least 2H from the wind source (fans). If the model is placed closer than 2H, the quality of the aerodynamic data particularly in the windward wall can be compromised and appropriate correction needs to be applied. The roof aerodynamic data appears less sensitive compared to the windward wall.

3.1.2 Small-scale WoW (1:8) blockage

Based on the observations from the numerical simulation a blockage assessment using the small-scale WoW (1:8 scale) was pursued to experimentally assess and ascertain the blockage effects. The mean external pressure distribution obtained along the center line of the small scale models, i.e. 1:8 scaled models of the corresponding full-scale WoW models is shown Figure 39. The comparison of results among (i) SILSOE Cube test from literature (Richards et al. 2007), (ii) the present small-scale WoW tests (i.e. 1:8 scale replica of a 5ft, a 7ft, and 9.5 ft cubes), and (iii) full-scale WoW tests (i.e. for 5ft, a 7ft, and 9.5 ft cubes) shown in Figure 39 indicate the following: the overall mean external pressure distribution along the center line of the cube model is similar to that of the full scale WoW data; of the three models tested, the 7ft and 5ft cube models show the same pattern of flow field in both the small and full scale WoW experiment; and the 9.5 ft cube results deviates both from the other cubes as well as the SILSOE cube results.

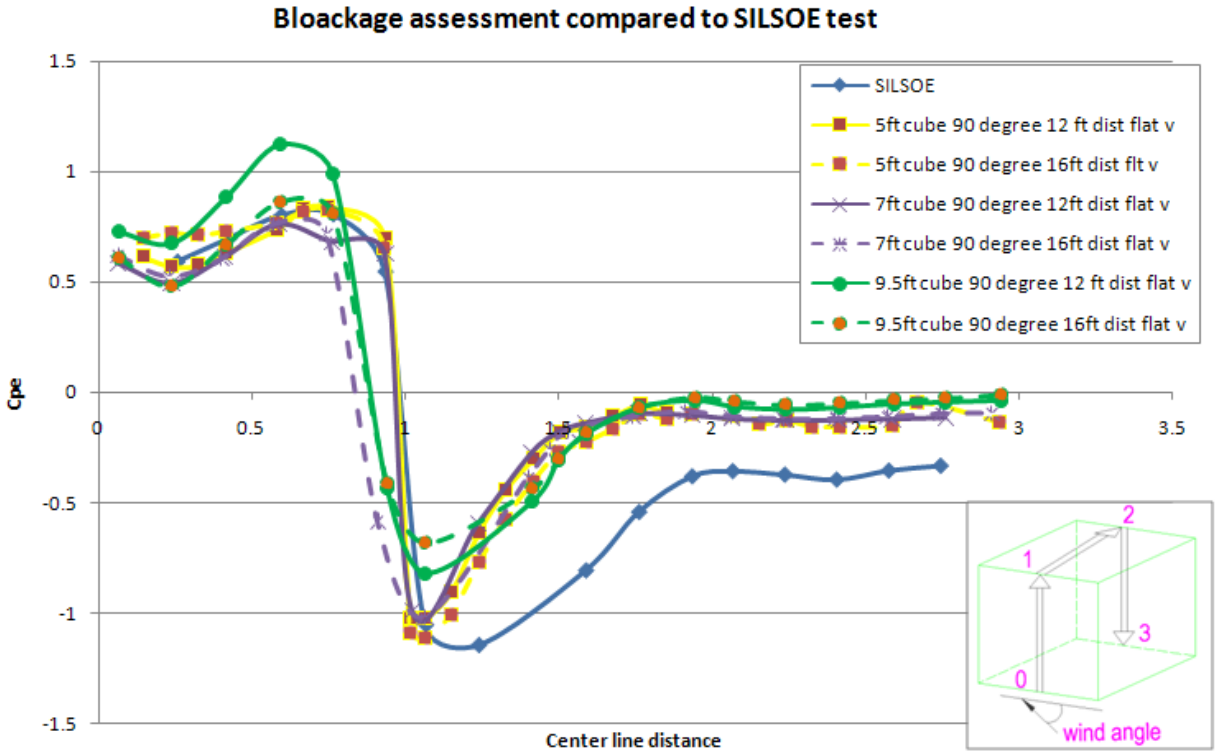

Figure 39: Comparison between small and full scale WoW tests for the 5ft, 7ft, and 9.5ft cubes along with data from SILSOE

Outcomes of the small-scale WoW (1:8 scale) and blockage assessment studies:

- Experimental (at low Reynolds number) and numerical simulation results consistently indicated the need to carefully select the size of the test specimen
- The 7ft cube model was identified to be a good size for further study using the current 6-fan WoW.

3.1.3 Full-scale WoW assessment of blockage and proximity effects

In this section blockage and proximity effect results obtained experimentally by using the full-scale WoW is presented. The objective of this experiment is determining the appropriate size (with less blockage effects) of the test specimen and the distance of the test specimen form the wall of wind (with less proximity effects) to be used for the proposed internal and external pressure investigation. The external pressure data obtained for each of the 5ft, 7ft, and 9.5ft cubes were compared among each other and with the results obtained from SILSOE full-scale measurements (Richards et al 2007). Figure 40 shows the mean external pressure distribution comparisons along the center line of each of the cubes when the wind angle of attack is 90°. It is observed that the external pressure on the windward wall is equivalent to that of the SILSOE data particularly for the 5ft and 7ft cubes at 12ft distance while the results for the 9.5 ft cube

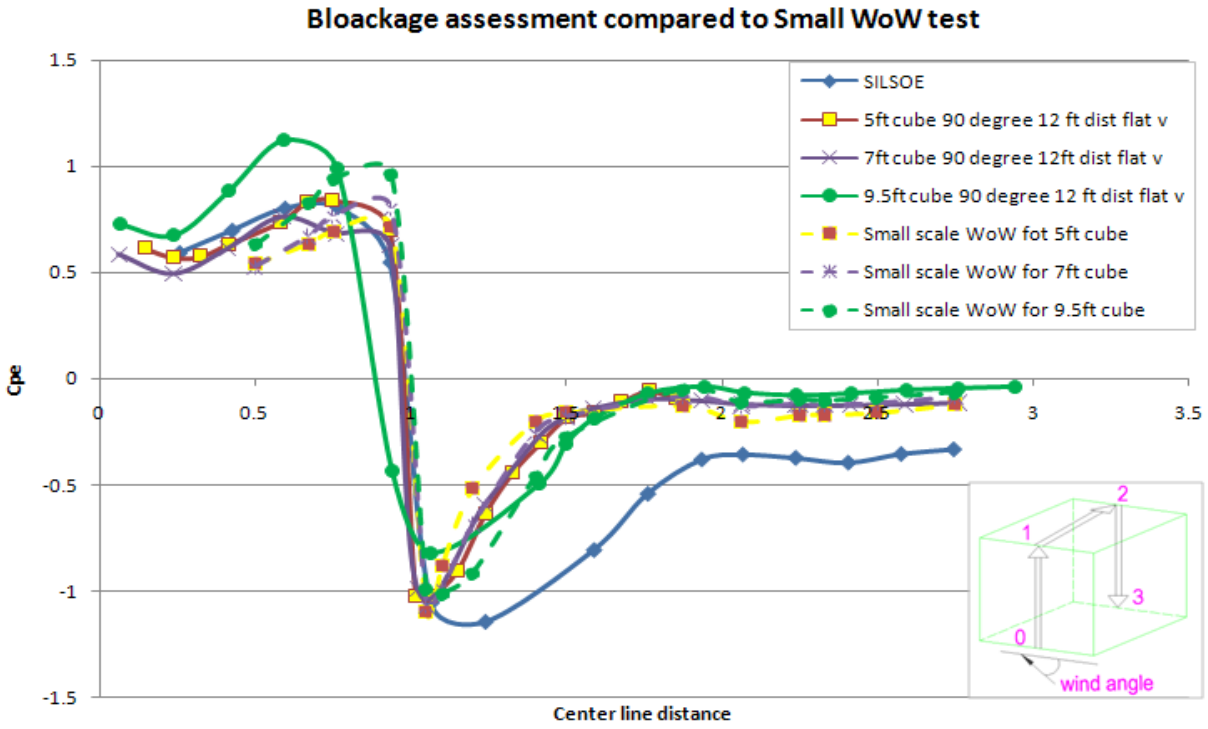

Figure 40: Mean pressure coefficients at the vertical center line of 5ft, 7ft and 9.5ft cube models along with

deviated from SILSOE. On the roof and leeward side, however, the mean external pressure on the cubes undergoes early reattachment as compared to that of SILSOE test. This difference might be due to the higher turbulence use for the case of the flow field of the cube models compared to the SILSOE model which is located in open field. It is also noteworthy to mention that SILSOE measurements provide higher Cp values on the lee-ward walls compared to literature values such as those observed from Texas Tech full-scale measurements (Levitan et al. 1991).

Outcomes of the full-scale WoW blockage and proximity effect studies:

- A model size with a representative *7ft dimension* located at *12 ft from the WoW* is finally selected for the internal and external pressure study.
- More specifically a low-rise building model of size 9ft W x 7ft L x 7ft H with interchangeable gable and hip roofs placed at 12ft distance from the WoW was identified to be an optimum size that for further study using the current 6-fan WoW.

3.2 Internal and external pressure study

3.2.1 Gable roof

Internal pressure in the living room: The internal pressure study inside the living room of the gable building model were carried out by using multiple transducers (a total of ten) uniformly distributed inside the interior of the building. As shown in Table 4, a total of 5 test cases were performed. All of the five cases were tested for wind attack angles of 0°, 15°, 45°, 75°, and 90°. In addition, test cases 1, 3, and 5 were tested for two more additional attack angles (105° and 120°) included mainly due to the window's (W1) off-center location. The results from the test

(Figure 41) show that the coefficient of internal pressure (C_{pi}) reaches peak value when the wider face of the building is almost normal to the direction of the wind flow.

Internal pressure coefficients for test case 1, where all of the dominant openings are closed and the coefficient of internal pressure fluctuation developed only due to background leakage, are relatively small compared to all other cases studied. Since most of the nominal background leakage took place through the wall that contains the door and windows (inside the living room), considerable internal *suction* pressure develops when this wall is parallel with the direction of wind(wall with door and windows is arranged as side wall for an angle of attack of 0°). Moreover, increased positive internal pressure coefficient is observed as the building is rotated to 90° location (i.e. the wall with a door and windows on windward side) and this is mainly due to the fact that background infiltration in the windward wall coupled with literally no exfiltration in the leeward side of the building envelope which leads to some positive pressurization inside the building. The impact of the background leakage alone on internal pressure relatively is not significant.

It is observed that the peak values of the coefficients of internal pressure occur when the dominant openings of the building face the WoW for a wind attack angle of about 75°. It was observed that the maximum internal pressure coefficient for open door case is in the order of 500% higher compared to the closed case (i.e. only with background leakage). This explains the importance of proper covering doors and windows with shutters (or other means) during storms is not only to protect the doors and windows themselves but also to avoid a potential failure the property due to high internal pressure developments.

Comparing the various test cases among each other, test case 3 (3.5% window opening) produced the highest *positive* and *suction* (i.e. negative) internal pressure fluctuations as shown in Figure 41 (a) and (d) respectively. Even though the door opening with a higher porosity of 7.5% (test Case 2) was expected to result in a peak C_{pi} value compared to the window case, the measured data show comparatively lower value for all of the analyses. This is believed to be due to the location of the two openings on the wall. The following observation is made with regard to the increased positive pressure, The door is located at a lower elevation while the window, although the size is smaller (3.5% versus 7.5%), is located at higher level coinciding with the point of stagnation where the maximum external pressure develops, and the internal pressure responds to this peak fluctuations almost instantaneously as shown in Figure 26. This was also deduced by examining the coefficient of external pressure that develops over the periphery of the window and the door as shown in Figure 42. In order to properly capture representative external pressure data from the dominant openings, the area-averaged pressure was adopted by installing six pressure transducers at the periphery of the door and two pressure transducers for the window. Beyond the 90° rotation, the positive internal pressure coefficient for window opening decreased compared to that of the door opening. The following observation is made with regard to the increased suction (i.e. negative pressure) due to the distance of these two dominant openings from the upstream wall corner when the wall containing the door and the window is tested as a side wall (i.e. 0° angle of attack). The window is closer to the upstream edge of the windward wall (0.95 ft from upwind wall corner) and this is aerodynamically higher suction zone compared to the location of the door which is 3.7 ft away from the edge.

Another observation is the decrease of the internal pressure inside the living room as the hatch is opened along with the door (test case 4) or the window (test case 5). When the partition that

separates the living room from the attic is removed (i.e., opening the hatch), the volume of the living room increases. The size of the dominant door or window opening, however, is kept the same for all cases. With the blockade of the ceiling partition, the volume of the living room is V_l = 609126.91 in^3 while the attic floor accounts for a volume of approximately V_a = 95992 in^3. This represents a 15.75 % volume increase when the ceiling hatch is opened. The major impact from the additional attic volume is the increase in damping effect inside the living room as compared to that of the closed hatch cases. The results obtained from the experiments reflect the effect of partitioning with respect to different types of openings as shown in Figure 41 (a-d). For example the maximum internal pressure coefficient in the living room for open door case with open ceiling hatch case is 26% lower compared to a similar case but with a closed ceiling hatch.

It is also noteworthy to mention that the instantaneous response of the *internal* pressure to the area averaged *external* pressure over the dominant openings (door and window) is closely correlated as expected, as shown in Figure 42. As depicted in Figure 42 the correlation between the internal and external pressures as a result of the door opening (7.5%) is lower than that of the window opening (3.5%).

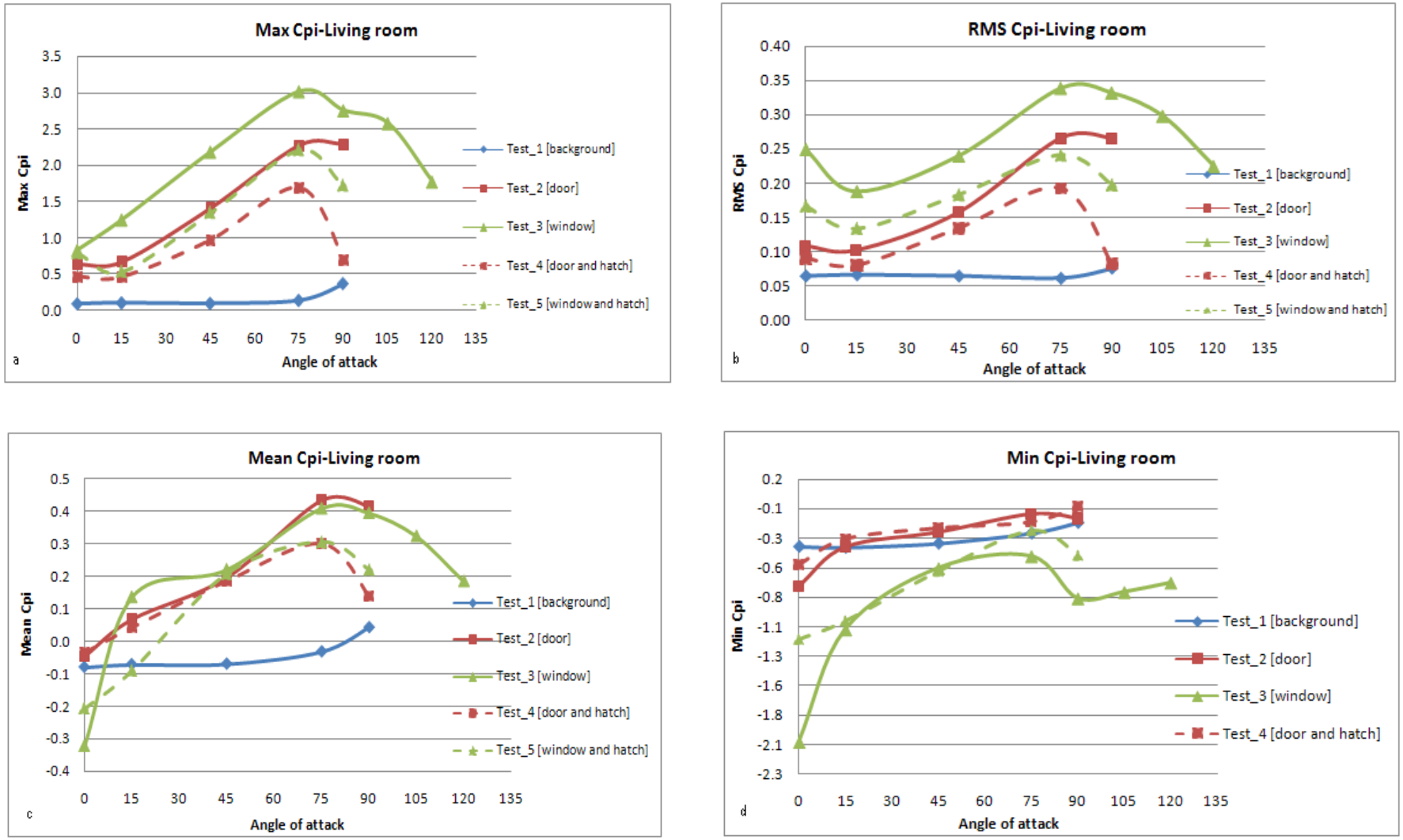

Figure 41: Internal pressure fluctuations inside living room: (a) Maximum, (b) RMS, (c) Mean and (d) Minimum Cp values for test cases 1-5

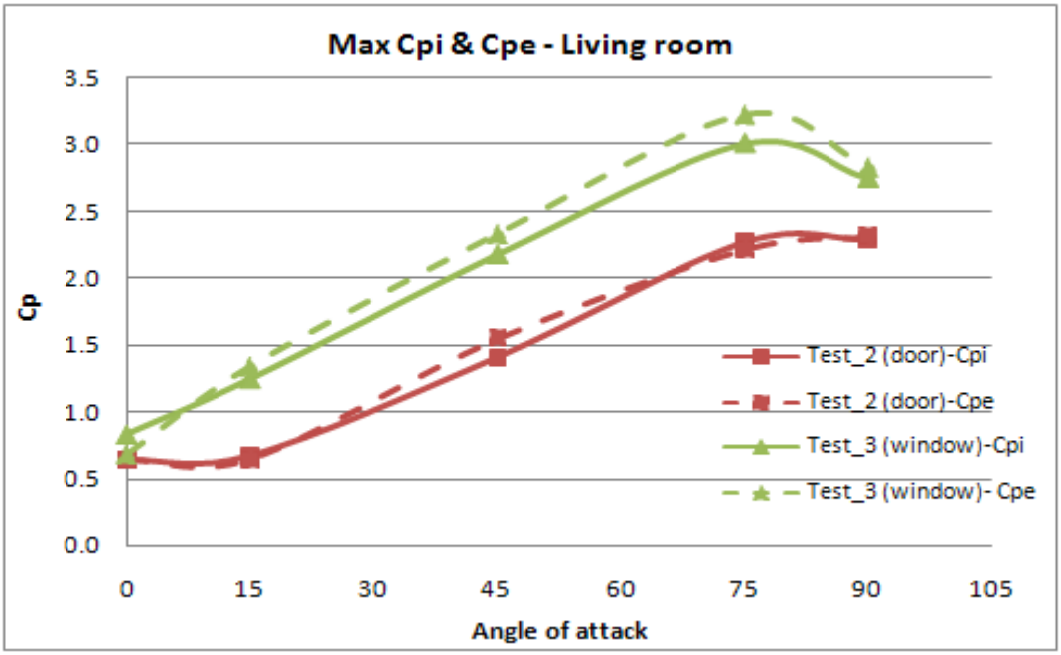
Max Cpi & Cpe - Living room
Cp
3.5
3.0
2.5
2.0
1.5
1.0
0.5
0.0
0
15
30
45
60
75
90
105
Angle of attack
Test_2 (door)-Cpi
Test_2 (door)-Cpe
Test_3 (window)-Cpi
Test_3 (window)- Cpe

e


Turbine
Goose neck
Gable end
FLORIDA INTERNATIONAL UNIVERSITY
a


soffit
b

Attic floor: Unlike the internal pressure fluctuations inside the living room, the pressure distribution inside the attic is composed of two peak points. As shown in Figure 45(a-d). The peak positive internal pressure coefficient occurs at about 45° angle of attack when only door or window is opened (i.e., test cases 2 & 3). The occurrence of the peak value shifts to 75° angle of attack when both the door and ceiling hatch or window and ceiling hatch are opened at the same time (i.e., test cases 4 and 5, respectively). The results obtained clearly show the impact of compartmentalization on both positive and negative internal pressures inside attic floor. The internal pressure in the attic floor is affected by ventilation openings (such as gable end, turbine, goose neck and soffit vents) and the ceiling hatch as shown in Figure 43 coupled with the different wind angles of attack. For test case 2 (where only door is opened) and test case 3 (where only window is opened), the internal pressure generated inside the attic floor is governed by the infiltration of air through the front and rear soffit, right and left side gable end ventilation system, and the background leakage through the ceiling partition. The contribution of the right side Gable end ventilation system is significant when the building model is at 0° angle of attack (i.e. wind is perpendicular to the vent opening). However, as the wind changes to other oblique directions, its impact reduces gradually as shown in Figure 45. At the same time, the contribution of the front soffit begins to build up (Figure 46) as the model is rotated in which case the wall containing the dominant openings and the front soffit vent faces the WoW. On the other hand, the magnitude of the suction inside the living room as a consequence of the external pressure averaged over the dominant openings (either door or window) is significantly higher at 0° angle of attack a C_{pi} of -1.5 for test case 2 (open door) and -2.2 for test case 3 (open window). The magnitude decreases to a C_{pi} of -0.75 when the building is rotated to 45° and it peaks up for wind angles of attack beyond the 45°, forming a bell shaped curve as shown in Figure 47

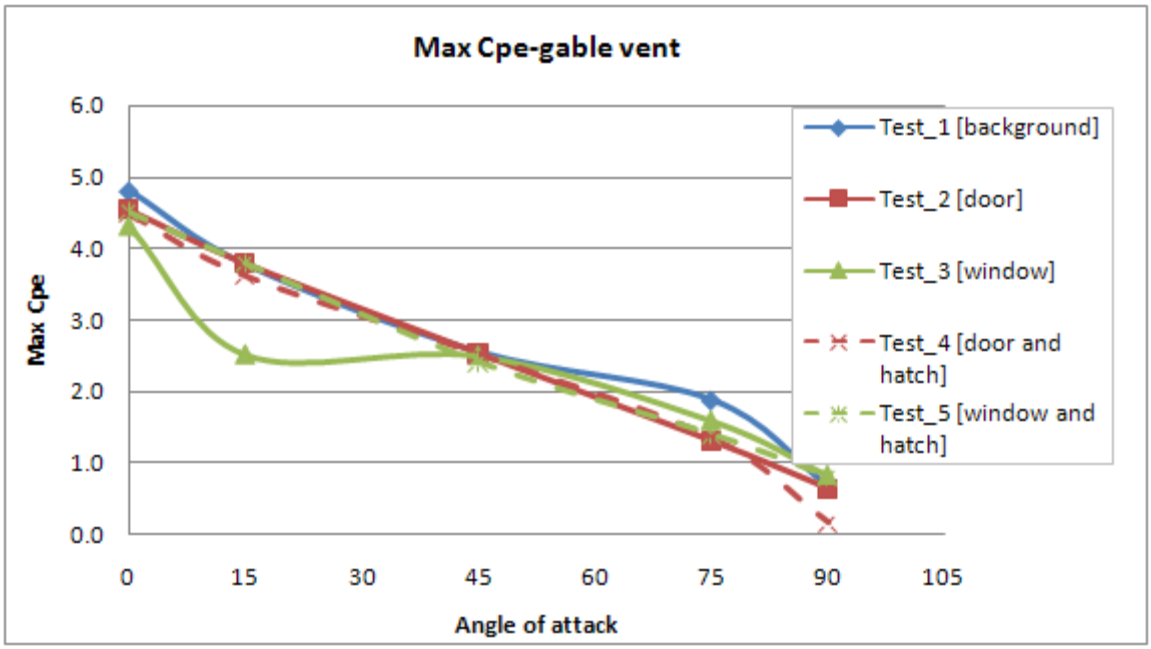

Figure 44: External Pressure Variation for: (a) Right side gable vent

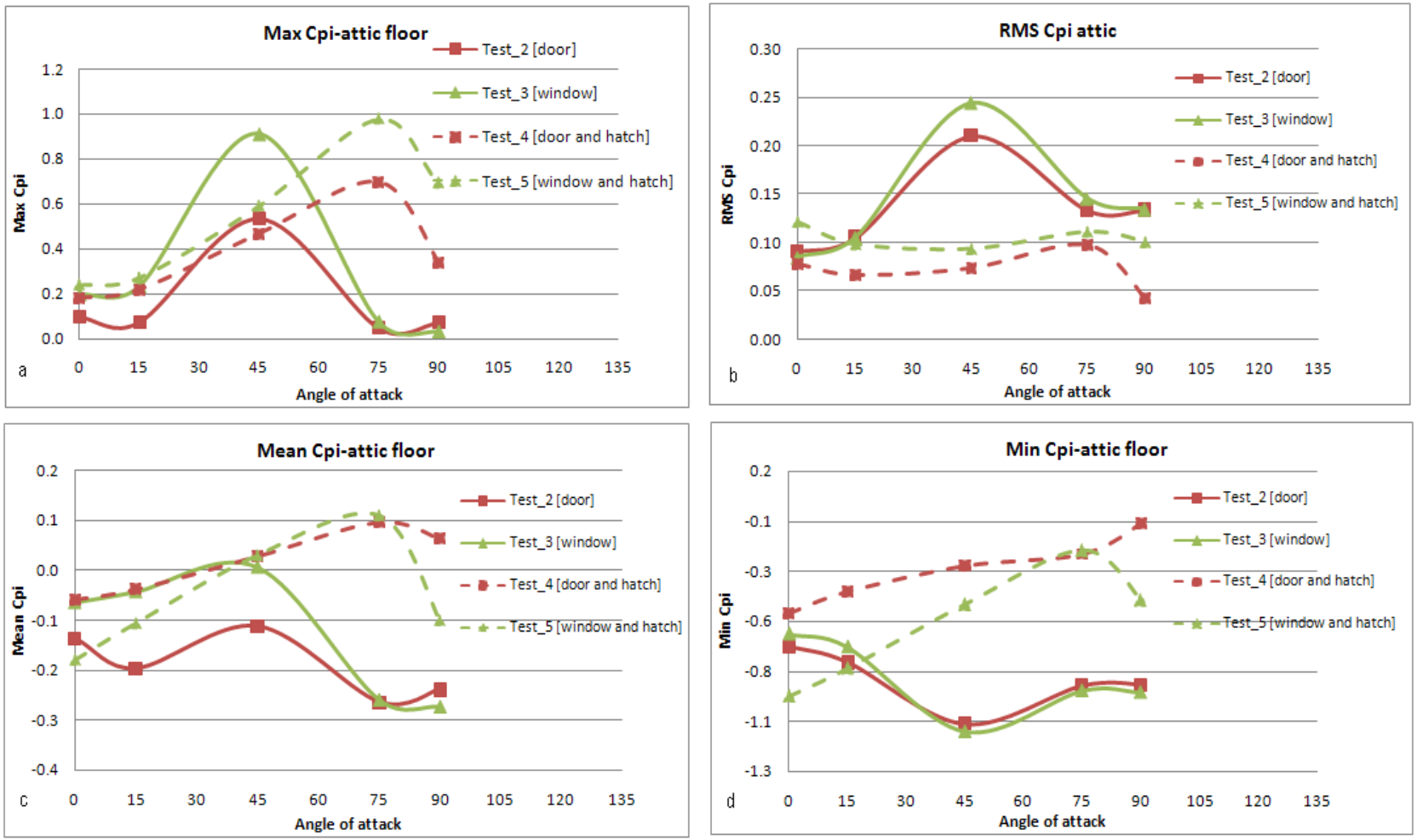

Figure 45: Internal pressure fluctuations inside attic floor: (a) Maximum, (b) RMS, (c) Mean and (d) Minimum Cp values for Test Cases 1-5

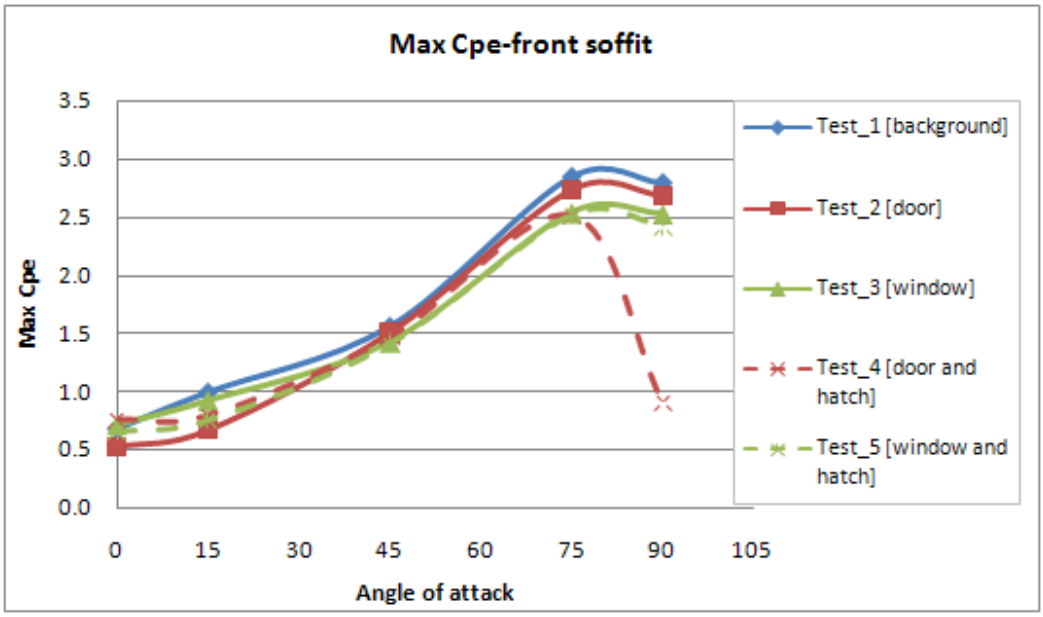

Figure 46: External Pressure Variation for: front soffit vents

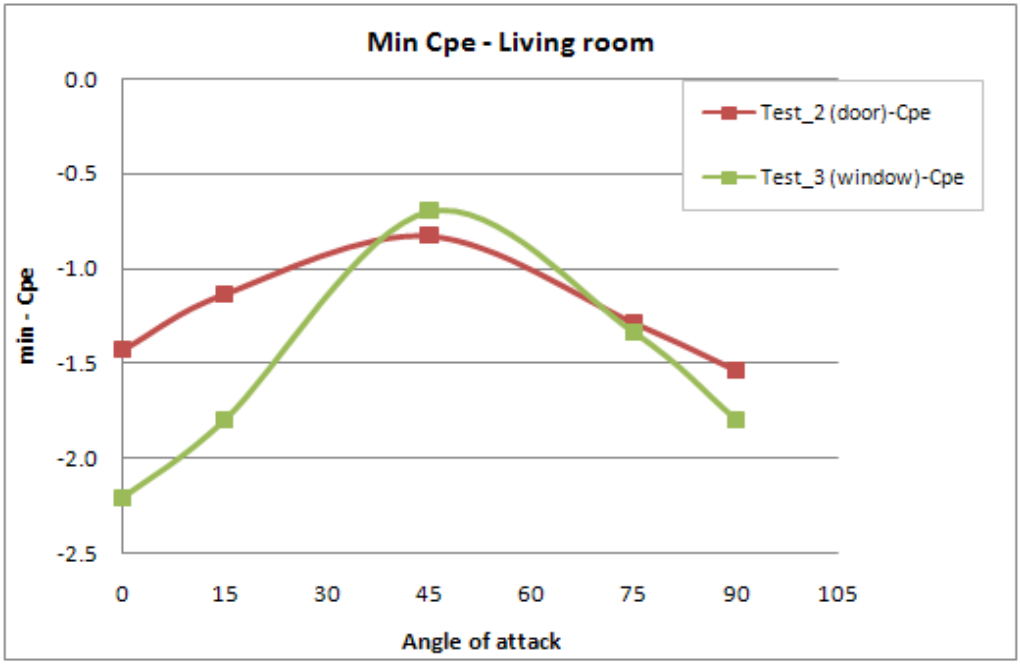

Figure 47: External pressure coefficient at the openings of the living room)Averaged

The pattern of positive internal pressure test i.e. test cases 2 (open door) and 3 (open window) inside the attic are related to the suction pressure inside the living room, when the attic positive pressure surges as the suction pressure weaken.

For test cases 4 (open door and open hatch) and 5 (open window with open hatch), the trend of attic internal pressure differs from that of test cases 2 (open door only) and 3 (open window only) due to the opening of the ceiling hatch. While the opening of the ceiling hatch results in dampening of the internal pressure in the living room due to the increase in the volume, however, inside the attic the internal pressure increases since the fluctuation in external pressure around the dominant openings is propagated into the attic through the open ceiling hatch. Since the peak external pressure at the windward wall occurs at a 75^0 angle of attack the attic internal pressure also follows the same trend and reaches its peak value at the same wind angle of attack.

The peak value of positive internal pressure inside the attic is comparatively less when the hatch is closed. In this case the internal pressure development is mainly due the ventilation systems (gable end, goose neck, turbine, soffit vents) and other nominal background leakages. The hatch opening causes the propagation of the pressure from the living room to the attic resulting in a higher internal pressure in the attic while dampening the internal pressure in the living room. The dampening of internal pressure inside the living room is shown in Figure 41 a, where opening of the door and ceiling hatch or window and ceiling hatch leads to a reduction of peak C_{pi} from 3.0 to 2.25 and from 2.4 to 1.6 respectively. For the attic floor, however, similar conditions cause an increase in C_{pi} from 0.5 to 0.75 for the opening of the door and ceiling hatch case and from 0.9 to 1.0 for the window and ceiling hatch case as shown in Figure 45 a.

From net design wind load (i.e. combined external and internal pressure) point of view, the magnitude of the internal pressure that develops inside the attic roof is significant as it might lead to an increased peak wind load on roof sheathing. Thus, it is preferable to seal ceiling hatch during strong storms. For example, the opening of the window together with ceiling hatch led to 45%increason the net wind load on the windward side of the gable roof. This reinforces the need for keeping doors and windows covered with shutters during strong storms.

Helmholtz resonance: Computing the Helmholtz resonance using the numerical equation given in eqn. (3) also presented here for completeness:

$$f_H = \frac{1}{2\pi}\sqrt{\frac{\gamma A P_o}{\rho L_e V_{ie}}}$$

The values of the parameters for the Gable roof low-rise building considered in this section are as follows:

γ = 1.4 ratio of specific heat for air (adiabatic condition is considered)

A = 0.439 m^2 for door and 0.219 m^2 for window

P_o = 101284.6 Pa in Miami area

ρ = 1.25 Kg/m3, air density

$L_e = L_o + 0.89\sqrt{A}$ = 0.6913 m (door) and 0.5181 m (window)

V_{ie} = 9.982 m^3 (living room only)

Therefore, the measured Helmholtz frequency is

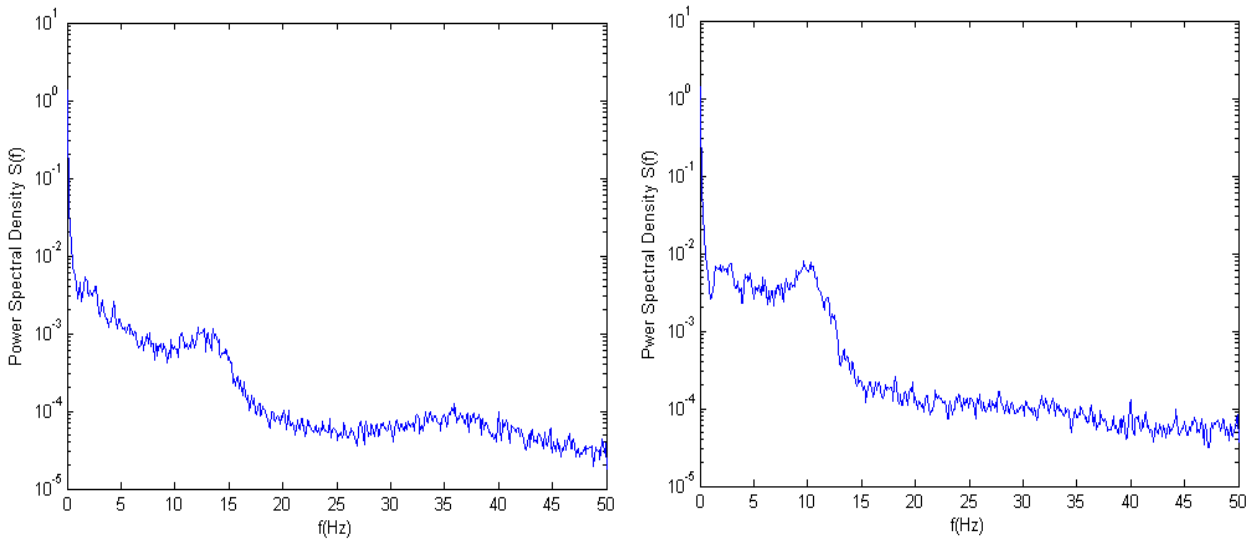

Figure 48: Power Spectra of Internal pressure for door opening (left) and window opening (right)

a) Dominant opening door case (i.e. A=0.439 m^2 and L_e = 0.6913m)

$$f_H = \frac{1}{2\pi}\sqrt{\frac{\gamma A P_o}{\rho L_e V_{ie}}} = 14.29\text{Hz}$$

b) Dominant opening window case (A = 0.219 m^2 and L_e = 0.5181 m)

$$f_H = \frac{1}{2\pi}\sqrt{\frac{\gamma A P_o}{\rho L_e V_{ie}}} == \sqrt{\frac{\gamma A P_o}{\rho L_e V_{ie}}} = 11.03\text{Hz}$$

As shown in Figure 48, the measured frequency for both the door and window opening case is in good agreement with those analytically predicted values by using eqn. (3).

The significance of Helmholtz resonance on internal pressure excitation is determined by considering the ratio of the RMS of coefficient of internal to external pressure. When the RMS (C_{pi}/C_{pe}) > 1, the Helmholtz resonance is said to be significant (Holmes 1993, Liu 1983 and Sharma 2007). In this project, the peak RMS C_p ratio was obtained to be 1.05 for a window

opening case at 90° wind angle of attack. This shows that, for the above specified living and attic volume and the area of the dominant openings, the Helmholtz resonance is barely significant to cause internal pressure amplification.

Outcomes of internal and external pressure study for the gable roof:

- Peak positive internal pressure occurs when a dominant opening of the building faces the incoming wind flow.
- Peak negative internal pressure occurs when a dominant opening of the building are in parallel to the incoming wind flow.
- Dominant openings resulted in an increase internal pressure. For example, the opening of the window together with ceiling hatch led to 45%increason the net wind load on the windward side of the gable roof. This reinforces the need for keeping doors and windows covered with shutters during strong storms.
- Opening of a hatch along with the window and door causes an increase in the internal pressure of the attic roof which reveals the importance of sealing ceiling hatches during strong storms to protect the roof and the building.

3.2.2 Hip roof building

Internal pressure in the living room: The internal pressure study inside the living room of the hip roof low-rise building model were carried out, similar to the gable roof, by using multiple transducers (a total of ten) uniformly distributed inside the interior of the building. As shown in Table 5, a total of 5 test cases were performed. The test cases applied to the hip roof building are similar to those explained in section 3.2.1 for gable roof. In Figure 49, the mean, RMS, maximum, and minimum coefficients of internal pressures are plotted for all test cases for multiple wind angle of attack. As shown in Figure 49 a and c, the mean and maximum positive internal pressure coefficients (C_{pi}) both for test cases 2 (door opening) and 3 (window opening) reach their peak values when the incoming wind is perpendicular to the opening. Unlike the gable roof building, the internal pressure inside the living room is comparatively higher for opened door case compared with open window case for wind angle of attack ranging between 0° and 90°. Beyond 90° angle of attack (i.e. the windows and doors becomes parallel to the wind and negative pressure –suction-- develops inside the building), the living room C_{pi} for open window case becomes larger over that of the door. This is believed to be due to wind flow separation closer to the leading edge of the wall where the windows are located. As depicted in Figure 50 a, for instance, the opened window (right side) is located at upstream corner of the building compared to the door and the separation of the flow that develops over this region can easily be observed. Beyond the 90° wind angle of attack, the right side window becomes part of the flow reattachment region as compared to the door. The same pattern of flow condition was observed for external pressure captured at the periphery of the door and window (Figure 51). For the external pressure at the dominant door, a total of six pressure taps (five at the periphery and one at center) was used to determine the area averaged external pressure at the door. The

external pressure data at the center of the door was obtained while undertaking closed door cases. For the window opening case, area averaged external pressure is obtained by allocating two pressure taps at the periphery as shown in Figure 30.

Another observation is that the peak positive internal pressure tends to occur at about 45° and 105° angle of attack for the door opened case and at about 15° and 135° angle of attack for the window opened case (Figure 51). For all of the simulations undertaken, the minimum mean internal pressure (C_{pi}) and area averaged external pressure (C_{pe}) is measured at about 75° angle of attack for test case 3 (for opened window only) and at about 90° angle of attack for test case 5 (window and hatch), as shown in Figure 49.

Table 5: Ventilation openings size and porosity ratio

S.N	Description	area [in^2]	ratio=vent opening to attic floor [%]
1	Attic area to be ventilated (9x11 in)	14256.00	
2	Soffit opening (8 pcs, 4.375 x 14.375 in)	503.13	3.53
4	Goose neck opening (4 x 9.5 in	38.00	0.27
5	Turbine opening (dia. 10.5 in)	86.58	0.61
6	Ridge opening (2 pcs, 1 x 14 in)	28.00	0.20
	Total ventlation opening area (in^2)	**655.71**	
	Ceiling area to be ventilated (in2)	**14256.00**	
	Ratio of free ventilating opening to that of the ceiling floor	**0.0460**	

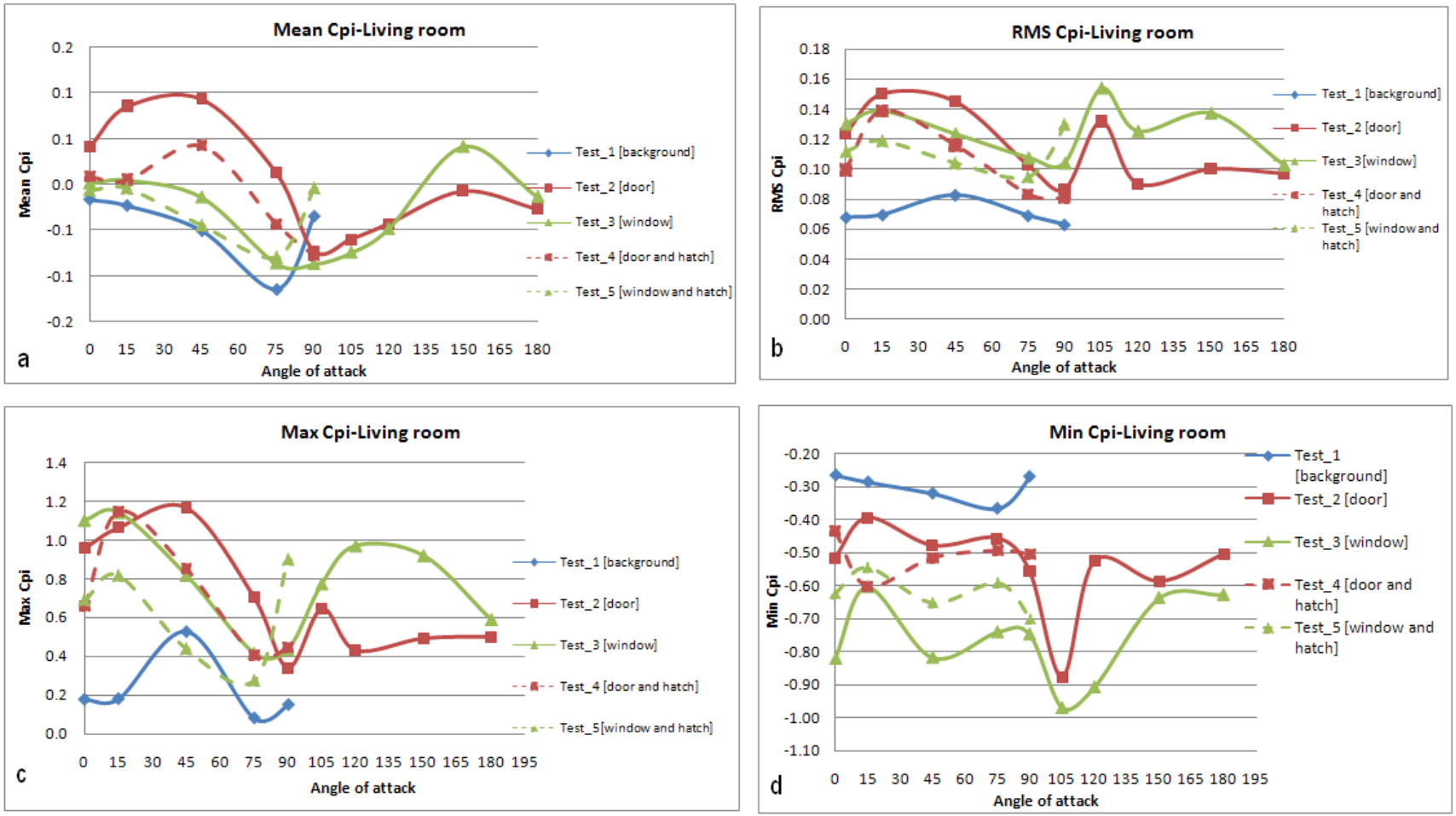

Figure 49: Hip roof living room coefficient of internal pressure: a) Mean, b) RMS, c) Maximum, and d) Minimum values.

Figure 50: Hip roof model for Test case 3: a) at 15° and b) at 120° wind angle of attack (only right side window open)

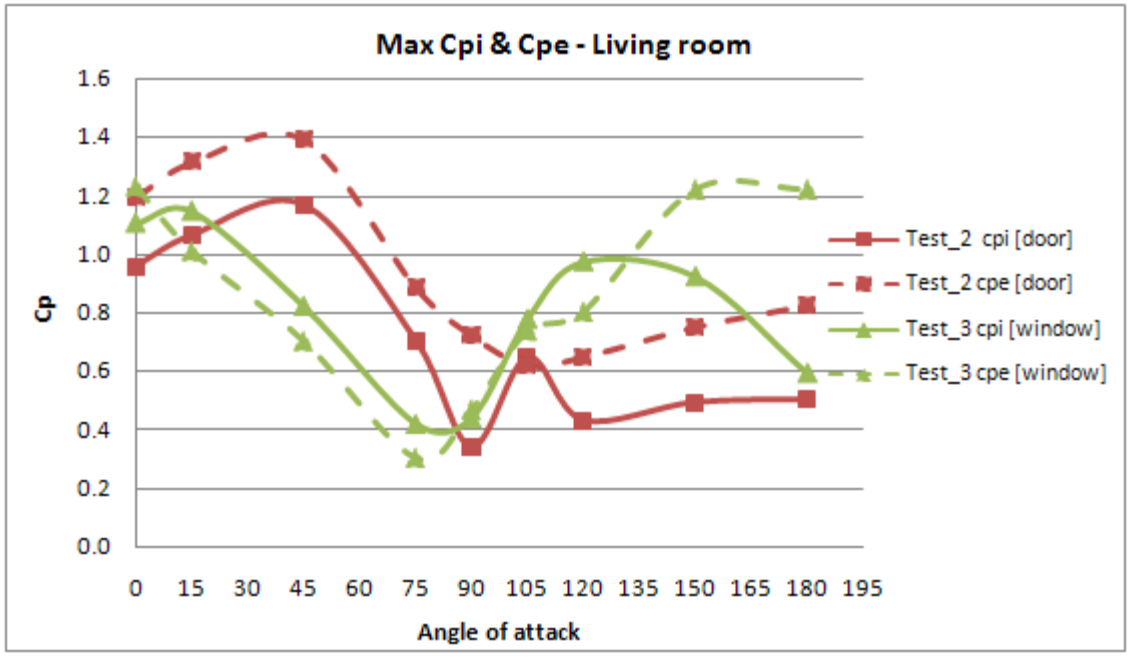

Figure 51: Maximum internal and external pressure distribution for test cases 2 and 3

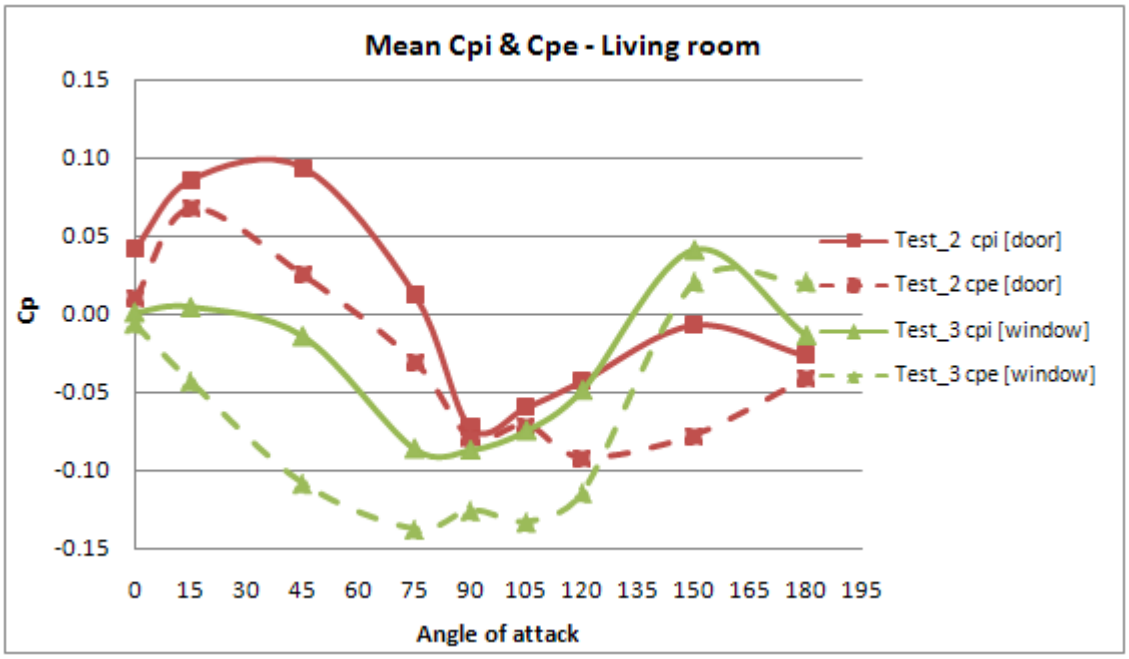

Figure 52: Mean Internal and external pressure coefficient for test 2 cases and 3

Attic floor internal pressure

Similar to the gable roof building described in section 3.2.1, the hip roof building is compartmentalized by separating the living room from the attic using a ceiling partition. A ceiling hatch of size (18 in by 18.5 in) is also provided. The effect of the load transfer to the attic floor is twofold. In one hand, it allowed the internal pressure to propagate the internal pressure to from the living room to the attic floor resulting in high internal pressure inside the attic. On the other hand the internal pressure inside the living room decreases due to the dampening effect of the increased volume created due to the opening of the ceiling hatch (livening room volume + attic volume). The reduction in internal pressure fluctuation that results from opening of a hatch is governed by the volume of the attic floor and the opening area of the hatch itself. However

since roofs are the most vulnerable component of residential buildings, the increase in internal pressure is more critical and needs to be avoided by closing the ceiling hatches during strong storms.

Attic floor internal pressure distribution analysis was performed by taking the average pressure obtained from the three center line transducers along the length of the building located underneath the roof sheathing (i.e., taps number 02, 06, and 10 as shown in Figure 31). As described previously, the attic floor contains ventilation systems (i.e., soffit, ridge, turbine, and goose neck vents). The presence of these ventilation openings have significant influence on the level of internal pressure that generate inside the attic floor depending on the location of the vents and the direction of the wind. Figure 53 depicts the effect of the internal pressure inside the attic floor. Generally, it is observed 45° angle of attack generates peak positive coefficient of internal pressure (0.43) for both door and window opened case with ceiling hatch. The mean internal pressure inside the attic floor is below zero for all of the wind angles of attack simulated and goes to lowest minimum value (suction) when the building is positioned at a 75° wind angle of attack. For test cases 2 (open door only) and 3(open widow only), the peak positive internal pressure fluctuation ranges between 0.25 and 0.35 as shown in Figure 53a. Figure 53 b shows the negative internal pressure inside the attic is significant for the door or window opened case without hatch and goes to lowest a minimum value of -0.56 between 15° and -45° wind angles of attack.

The peak attic internal pressure measured at oblique 45° angle of attack is due to the result of the wide surface area of the wind sees for hip roof building at this orientation coupled with the positive pressure contribution that the roof gains from the four soffit vents (No.1,2,3, and 4) as shown in Figure 54 and Figure 55. The same pattern of flow condition is observed when the

building is positioned at about 135° where the soffit vents (No. 1, 2, 7, and 8) play a significant role in generating positive pressure fluctuations inside the attic floor.

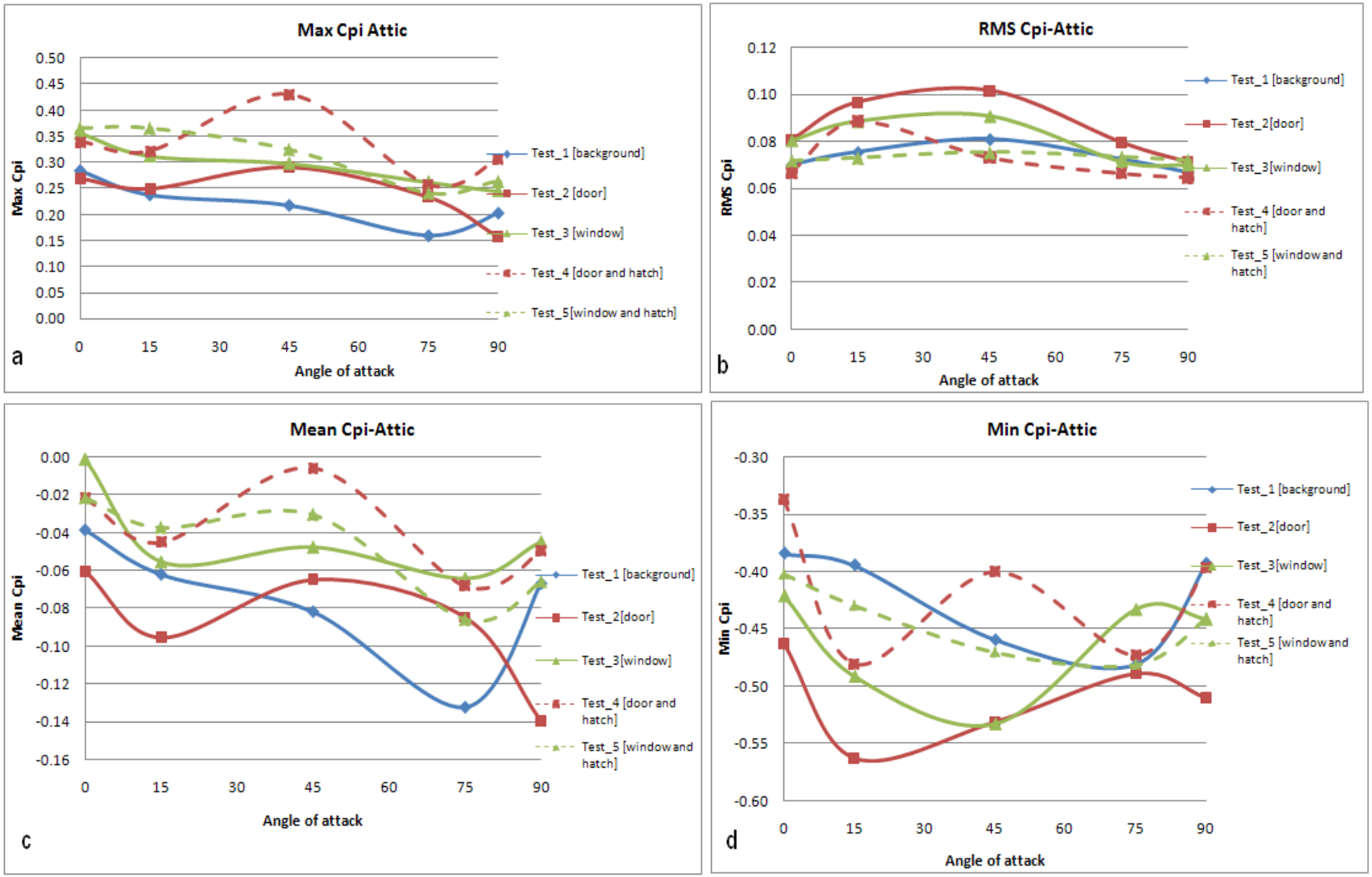

Figure 53: Attic floor coefficient of internal pressure: a) Maximum, b) RMS, c) Mean, and d) Minimum values.

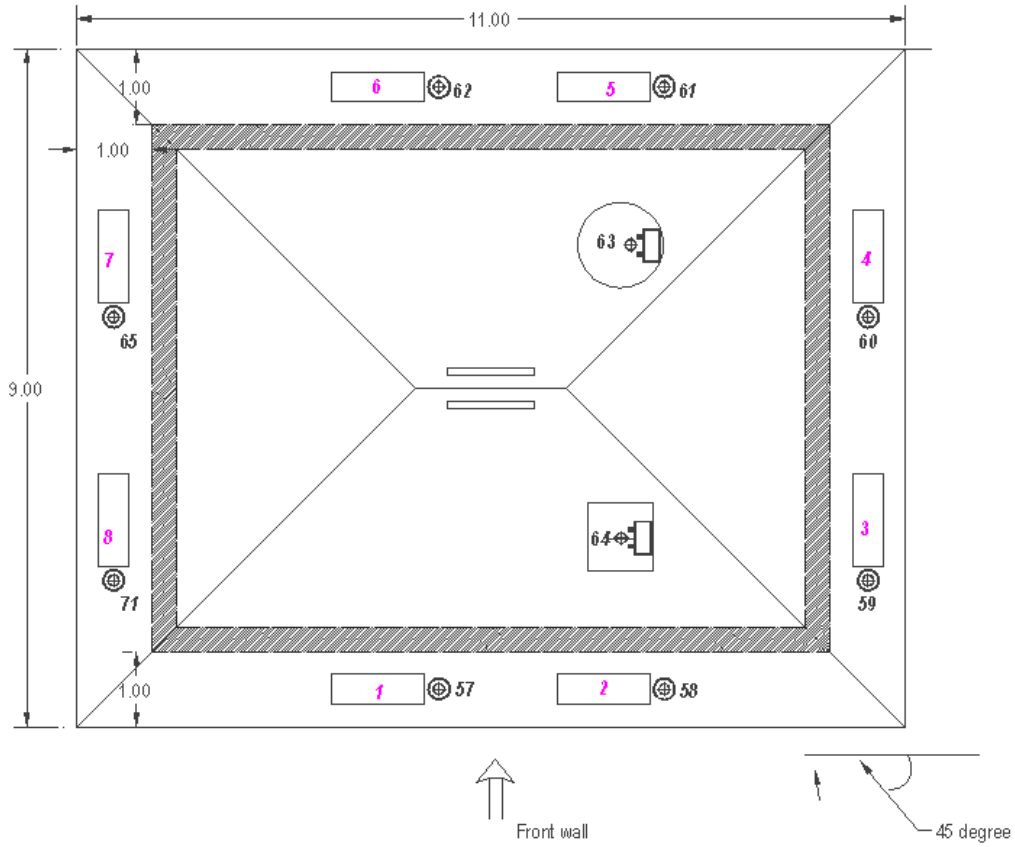

Figure 54: Ventilation openings number and location at 45 degree rotation

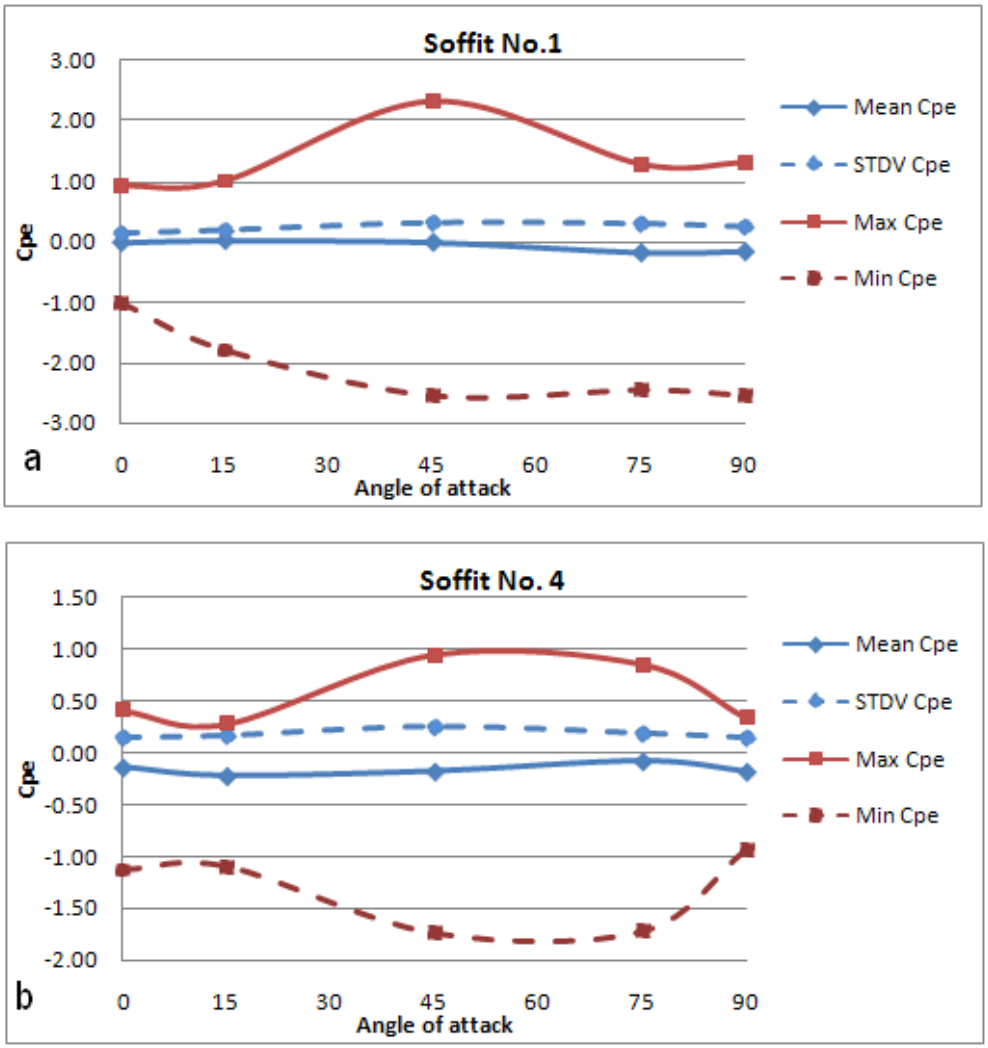

Figure 55: External pressure contribution of soffits: a) soffit No.1 & b) soffit No.2

3.2.3 Effect of ventilation openings on attic internal pressure

Most low-rise buildings are equipped with ventilation systems for the purpose of keeping the attic floor cool and dry. A properly installed venting system provides comfort to the ventilated rooms and improves the durability of the structural members. Improperly fixed vent systems also become a cause for the accumulation of moisture and wind driven rain entry point that can eventually lead to the formation of molds and other health hazards. In this project, the effect of the ventilation openings on the attic internal pressure is studied by undertaking two separate tests on the hip roof building model: one with complete ventilation system (ridge vent, soffit, turbine and goose neck) and the other with blocked vent openings. A companion study by Chowdhury et al. (2009), funded by FL DEM, has investigated the water intrusion through the vents. Detail discussion on the application of WoW for water intrusion study is presented by Bitsuamlak et al. 2009.

As shown in Table 5, the soffit porosity ratio is comparatively larger than the other vents on the roof surface. Two rectangular openings with size 4.375 in by 14.375 in were used in each overhang (total eight) as shown in Figure 56. As shown in Figure 57, the presence of the ventilation slightly increased the positive internal pressure that develops inside the attic floor and significant increase on the negative pressure. Due to the location of the vents which is mostly on the part of the buildings that sees significant negative external pressure explains why the vents caused relatively higher negative internal pressure compared to their effect on the positive pressure.

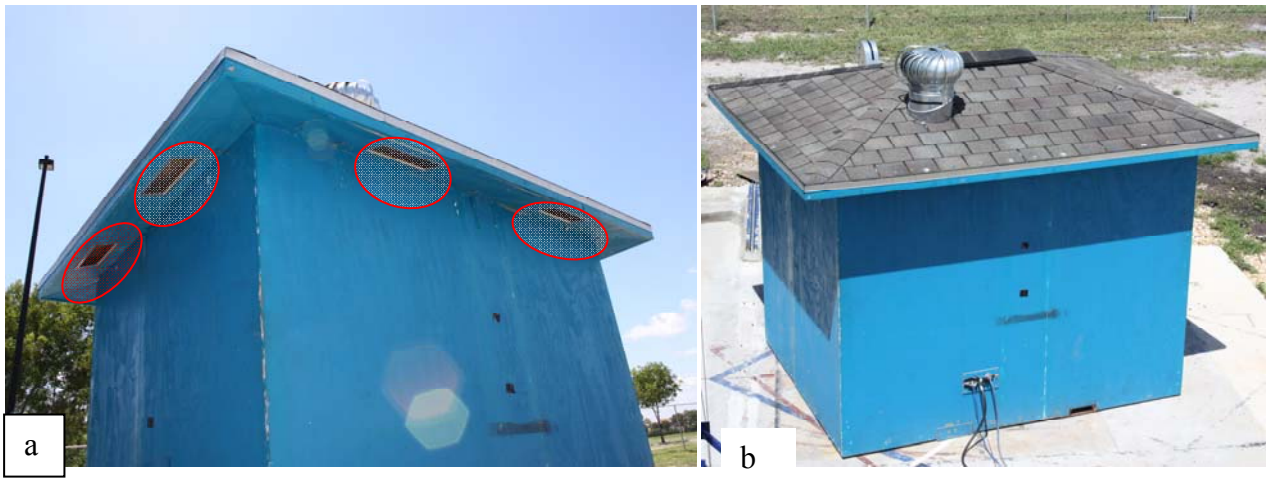

Figure 56: Ventilation openings; a) two sides' view of soffit mesh & b) top view of turbine, gooseneck and ridge vent

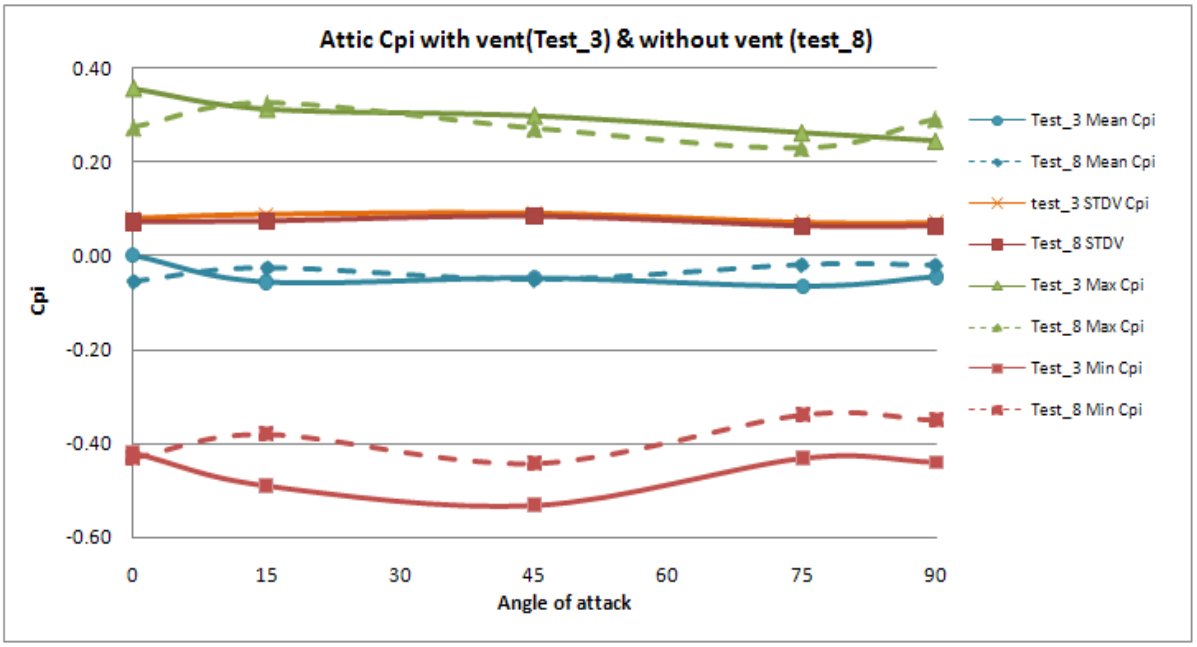

Figure 57: Attic internal pressure with and without ventilation opening

3.2.4 Net pressure analysis for wind load design

The relationship between the peak internal and external pressures is necessary in the assessment of design wind loads for buildings. The combined effect of the external and internal wind pressure acting in the same direction simultaneously may cause overloading of the envelopes and hence could initiate failure under strong storms.

3.2.4.1 Net Pressure on the ceiling compartment

The net pressure on hip roof produces resulting from the simultaneous pressure fluctuation inside the attic and the living room causing stress over the ceiling surface. When positive and suction pressures occur concurrently on the ceiling member that separates the attic from the living room, critical pressure combination may develop over the ceiling compartment as indicated by Figure 58 a & b. During the construction of low-rise buildings, it is a common practice to build ceiling partitions from aluminum frames or metal strips and loose box panels hooked to roof members. This practice would facilitate the malfunctioning of the ceiling compartment in the presence of net critical coupled pressure. The net pressure can be used as design wind load, should the designer decided to make firm ceilings. It is also worth noting during the present study (see Figure 53), the presence of ceiling hatch (18 in x18.5 in) has caused a surge in attic internal pressure which needs to be avoided to decrease the total net pressure on the roof sheathing.

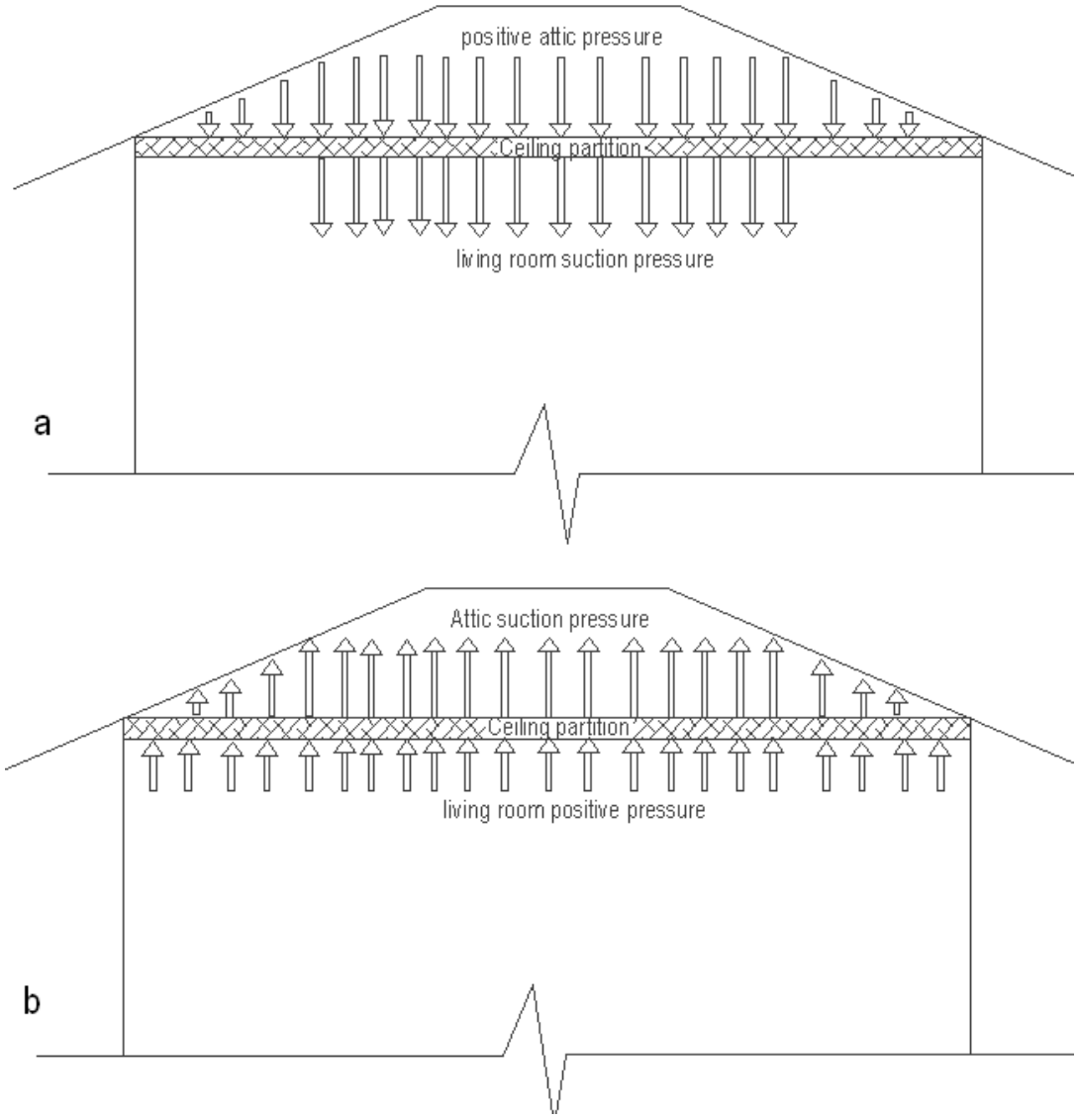

Figure 58: Net ceiling internal pressure; a) Suction pressure & b) positive pressure on ceiling compartment

In order to investigate the probable peak pressure that develops on the ceiling compartment due to the net effect of pressure inside the attic floor and living room (ceiling), net internal pressure computation is performed as follows

$$Peak\ suction\ C_{pi} = Living\ room\ C_{pi-min} - Attic\ floor\ C_{pi-max} \qquad [7.a]$$

$$Peak\ positive\ C_{pi} = Living\ room\ C_{pi-max} - Attic\ floor\ C_{pi-min} \qquad [7.b]$$

Equation 7 a represents the downward force exerted onto the ceiling partition as shown in Figure 58 a while equation 7b represents an upward force as shown in 58 b.

Table 6 depicts the results of the net internal pressure computation for each test case simulated with its respective angle of attack. Since the analysis is based on the coupling of critical peak internal pressures, the advantage of the computation is twofold. It helps to evaluate which simulation scenario (i.e., tests with various dominant openings) leads to severe the net loading and at the same time it gives an indication to which angle of attack will be critical for the peak net wind loading. Figure 59 (a) shows the net suction internal pressure over the ceiling partition. It is observed that the peak suction pressure for test case 8 (window opening with all roof vents blocked) is critical at 0° angle of attack

Table 6: Peak suction and positive pressure on the ceiling compartment

Average		Angle of rotation				
		0	15	45	75	90
Test_1 (background leakage)	Peak suction Cpi	-0.55	-0.52	-0.54	-0.53	-0.47
	Peak Positive Cpi	0.56	0.58	0.99	0.56	0.54
Test_2 (7.75% door opened)	Peak suction Cpi	-0.78	-0.64	-0.77	-0.69	-0.72
	Peak Positive Cpi	1.42	1.63	1.70	1.19	0.85
Test_3 (3% window opened)	Peak suction Cpi	-1.18	-0.92	-1.11	-1.00	-0.99
	Peak Positive Cpi	1.52	1.64	1.35	0.85	0.88
Test_4 (7.75% door and hatch opened)	Peak suction Cpi	-0.77	-0.93	-0.95	-0.75	-0.81
	Peak Positive Cpi	1.00	1.63	1.25	0.88	0.84
Test_5 (3% window and hatch opened)	Peak suction Cpi	-0.99	-0.91	-0.97	-0.83	-0.96
	Peak Positive Cpi	1.09	1.25	0.91	0.76	1.34
Test_8 (3% window open, vent closed)	Peak suction Cpi	-1.00	-0.98	-1.02	-0.90	-0.91
	Peak Positive Cpi	1.38	1.24	1.23	0.70	0.79

N.B., Peak Suction Cpi= Living room min Cpi - Attic floor max Cpi
N.B., Peak positive Cpi= Living room max Cpi - Attic floor min Cpi

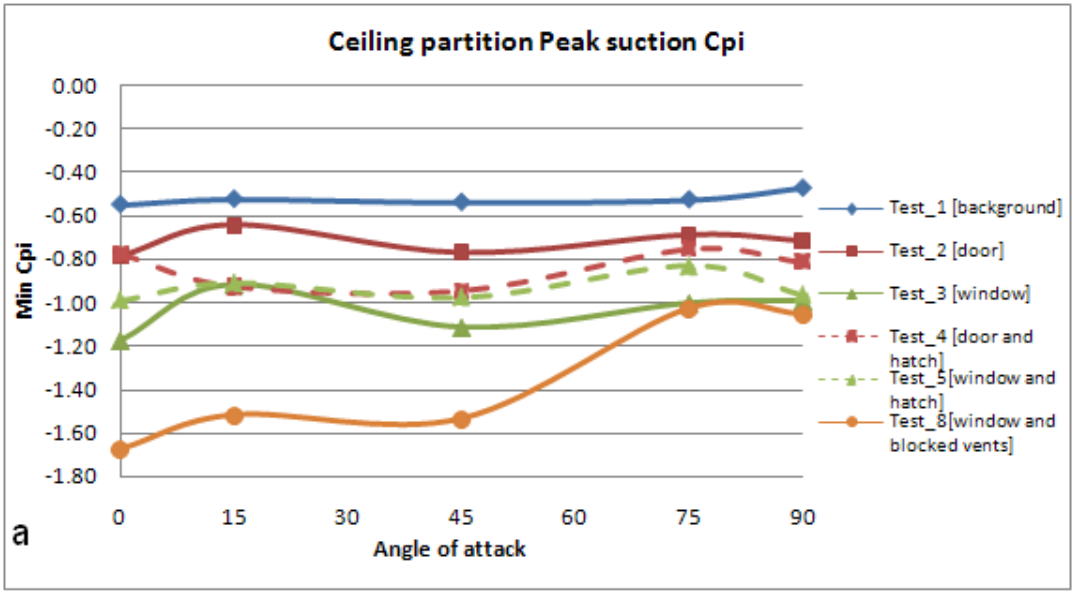

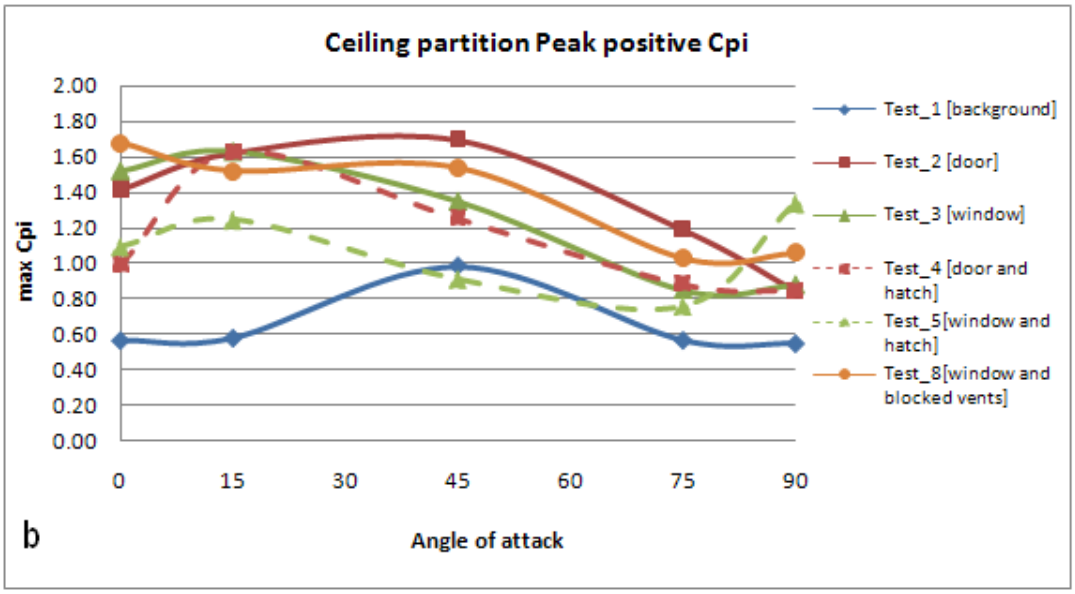

Figure 59: Peak Cpi at ceiling partition a) Peak suction Cpi, and b) Peak positive Cpi

3.2.4.2 Net pressure on roof sheathing

Similar to the net pressure that develop over the ceiling compartment, the external pressure that builds up over the roof envelope coupled with the positive internal pressure that acts in the same direction as that of the external (Figure 60) pressure generates a worst net pressure that can undermine the strength of the roof components. The dominant factors that govern the uplift force over the surface of low rise buildings are wind velocity, degree of inclination of the roof, the wind angle of attack, turbulence intensity, roof shape and location of the structure.

Common experience and post hurricane observations (FEMA 2005 &2006) have shown that the severe local suction pressure that develops at the top corner of roof perimeter when coupled with positive internal pressure on the same surface leads to excessive pressure fluctuations that instigate extraordinary high uplift pressure. According to post hurricane studies undertaken by

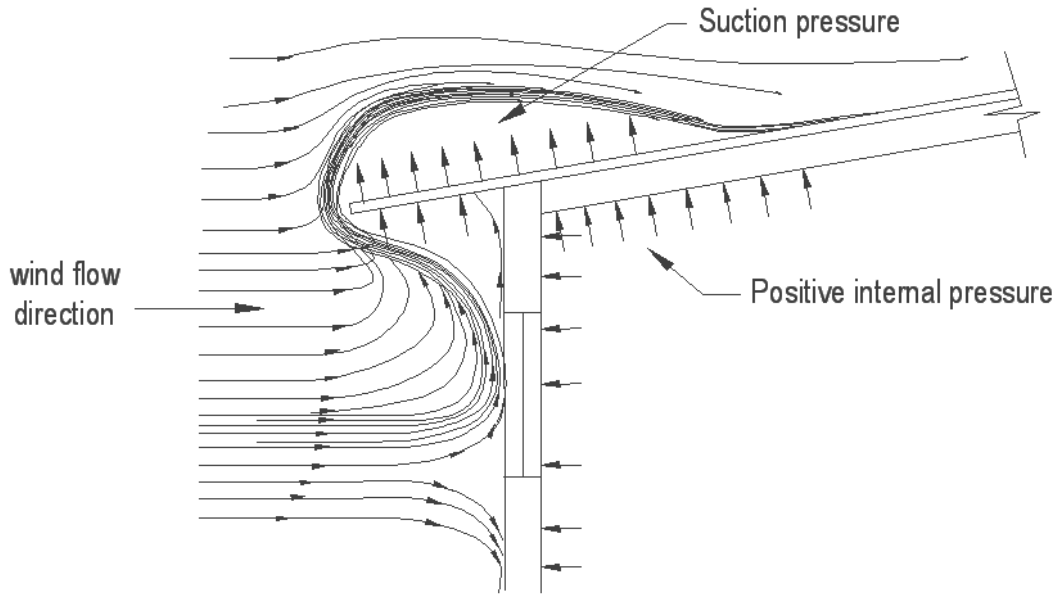

Figure 60: Net pressure at roof corners causing severe uplift pressure

FEMA 2005 &2006, the removal of roof sheathings is considered to be the primary failure mechanism. Moreover, the failure of roof sheathings due to excessive net pressure generally exacerbates the progressive failure of the roof structures such as trusses and walls. This kind of failure would allow the intrusion of wind driven rain into the interior of the building which consequently damages the building and the internal contents. In this project, the investigation of net pressure coefficient on the hip roof envelope was performed by analyzing the peak external suction roof pressure synchronized with the peak attic positive internal pressure. Internal and external pressure taps allocated along the center of the roof longitudinally and transversally were used to compute the pressure values. As stated above, wind angle of attack is one of the governing factors in the study of critical net pressure and in order to address this issue wind angles of attack (0°, 45° and 90°) were considered in analyzing the internal and external pressure coefficients as shown in Figure 51-61. Even though various combination of peak internal and external pressure can be observed, the most critical one is the uplift pressure that results from the combination of external suction and internal positive pressure. Figure 61 depicts the statistical external pressure variation along the longitudinal length of the hip roof for wind angle of attack between 0°, 45° and 90°. The worst wind direction that caused the instigation of peak suction pressure coefficient is 45°. A peak value of -2.71 is measured at the left corner of the gable ridge which is the downwind side of the gable with respect to the wind flow. The wind flow condition for the 45° wind angle of attack being diagonal, it initiates the formation of strong vortices along the windward edges. The diagonal wind flowing across the roof eventually generates severe uplift force at the corner overhangs. The external suction pressure excited along the transversal direction (across the gable roof) was observed to be critical when the wind flow position is

diagonal (i.e., 45°) to the building which is as shown in Figure 61(c), the peak suction pressure coefficient is estimated to be about -2.0 and occurs on the downwind side of the gable ridge.

As a general observation of the results of external pressure analysis (Figure 61 and Figure 62), each wind angle of attack produces peak external suction pressure and this peak pressure consistently happens to occur just behind the windward hip ridge or roof ridge depending on the direction of the wind with respect to the position of the roof. This is basically related to the formation of separation bubble right after the windward ridges creating high suction pressure and the intensity depends on the degree of inclination of the roof under consideration.

Considering the internal pressure inside the attic floor, it is the positive pressure coefficient that contributes towards exacerbating the uplift force is shown in Figure 60. Unlike the external suction pressure, the positive internal pressure doesn't show local crests. Generally the positive internal pressure coefficients are distributed in the range of 0.4 and 0.6 as depicted in Figure 63 and Figure 64.

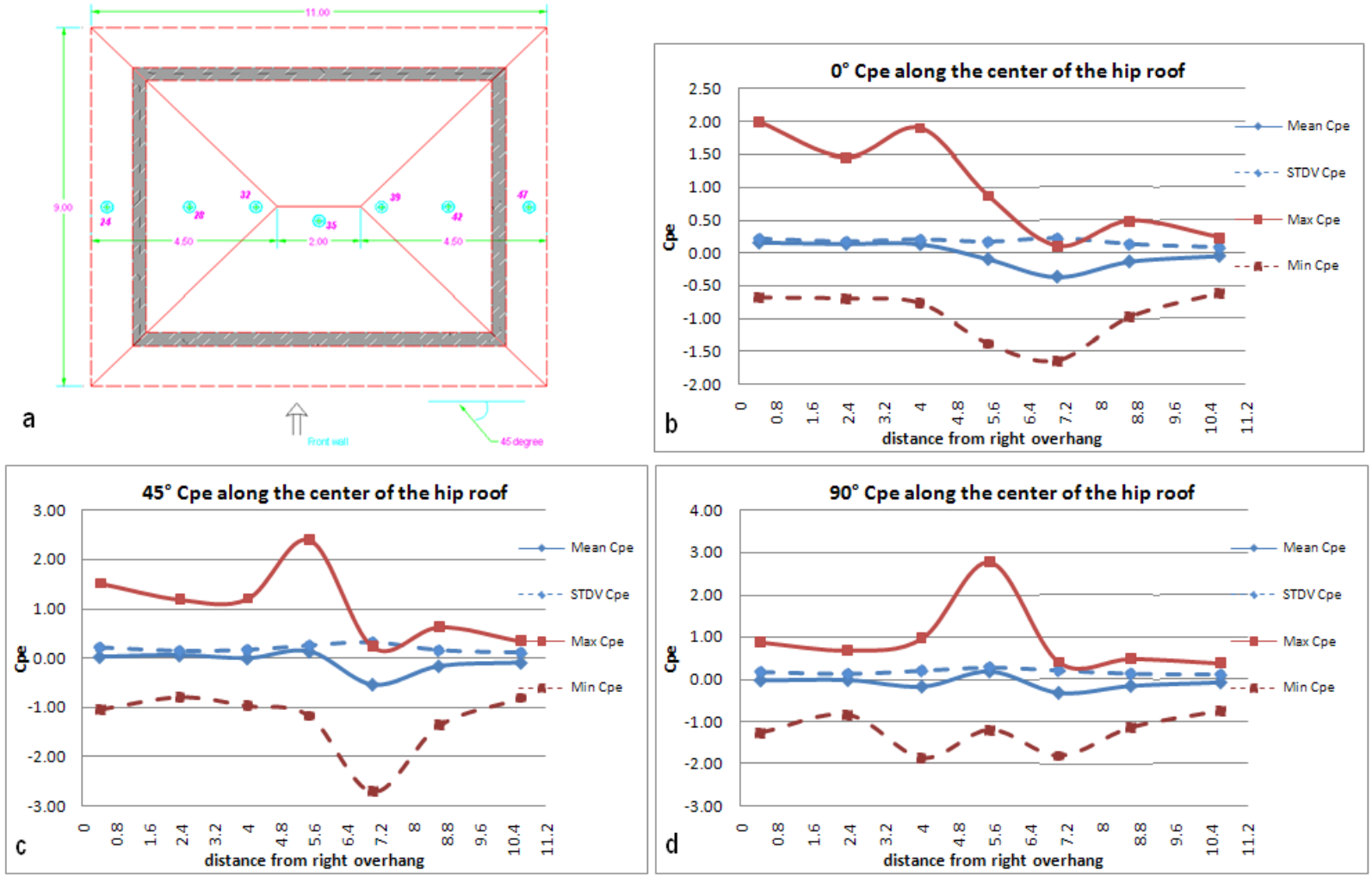

Figure 61: Roof external pressure along the center length of the hip; a) tap location along center of hip, b) 0 ° c) 45° & d) 90° wind angle of attack

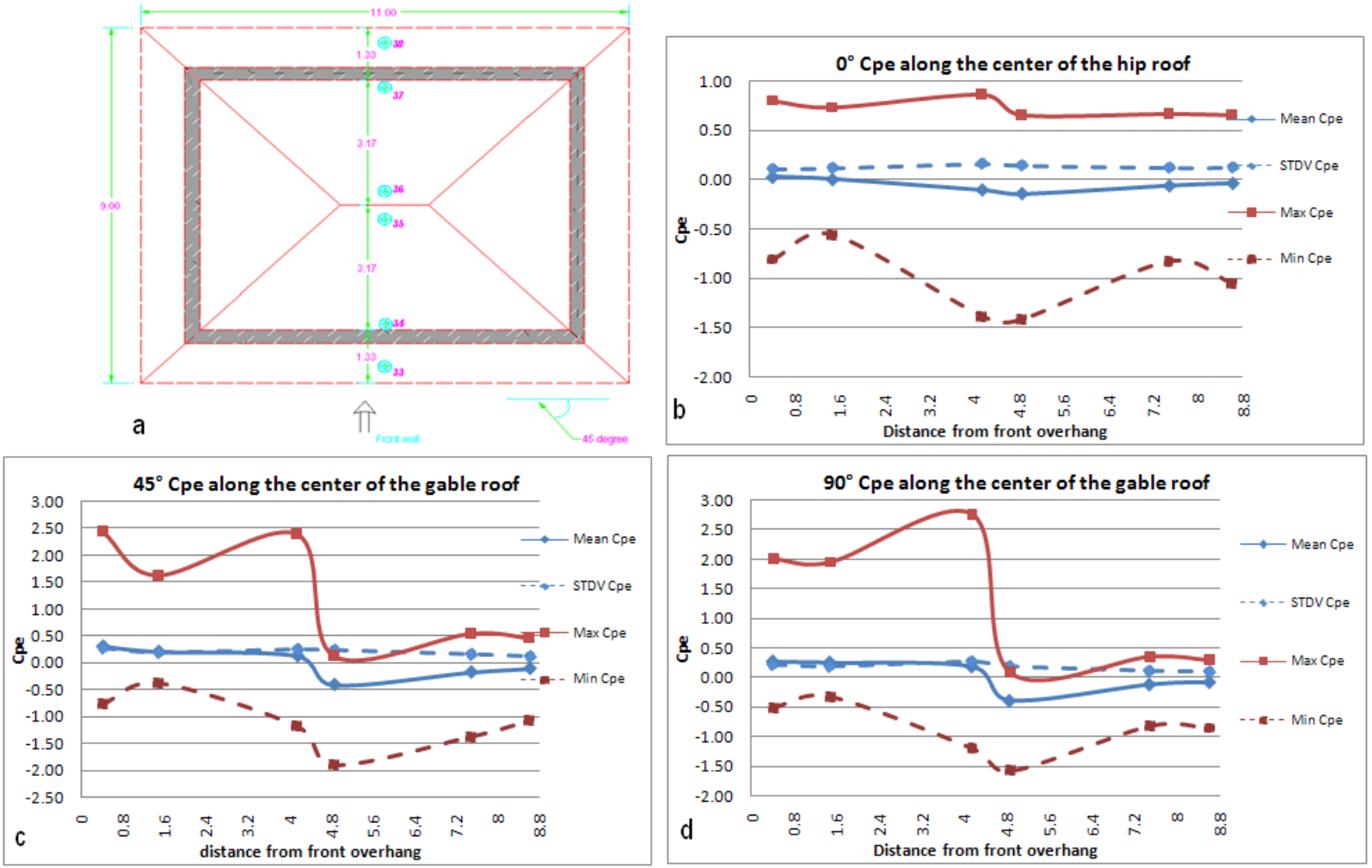

Figure 62: Roof external pressure along the center length of gable; a) tap location along center of gable, b) 0 ° c) 45° & d) 90° wind angle of attack

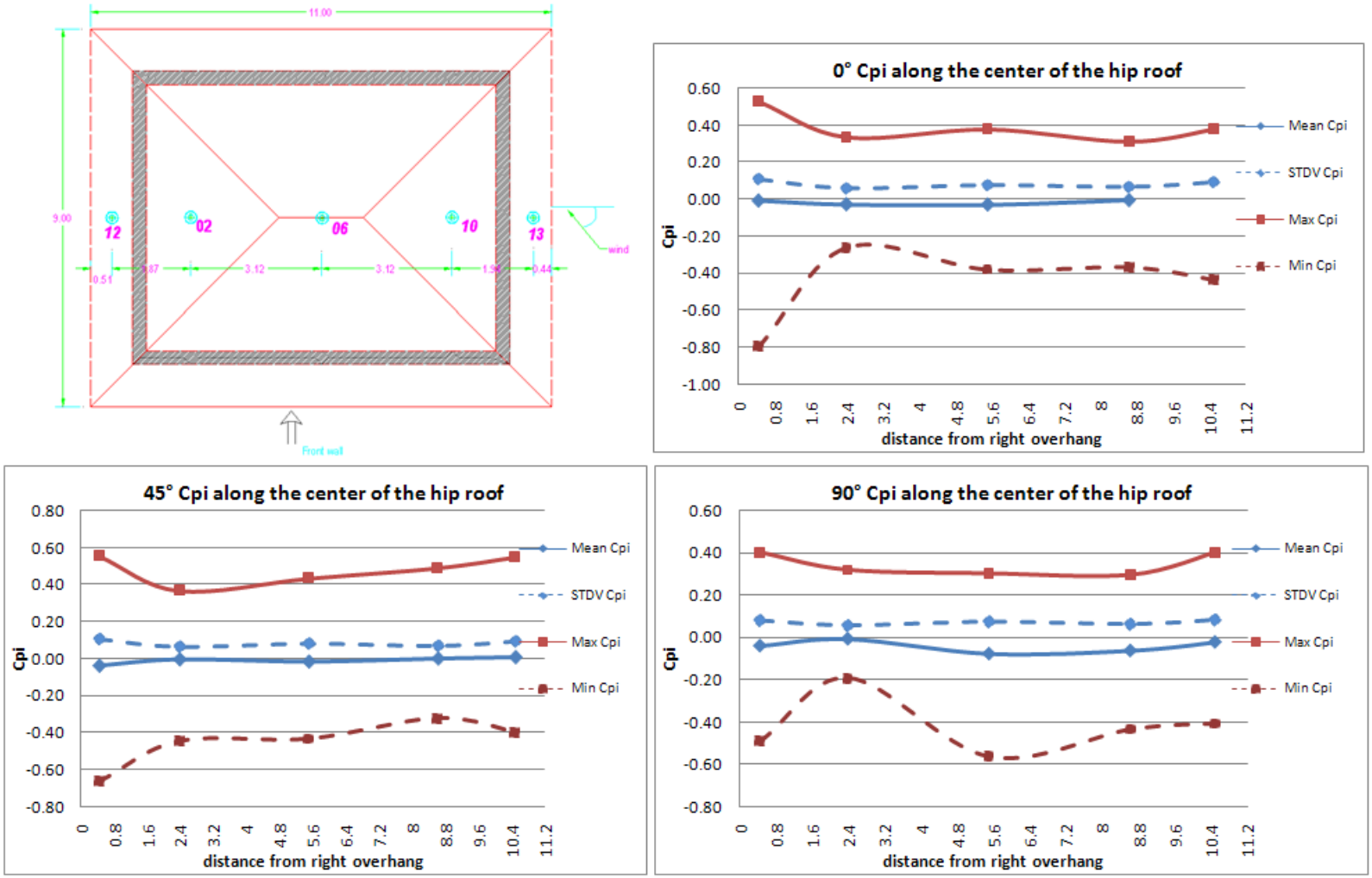

Figure 63: Roof internal pressure along the center length of hip; a) tap location along center of hip, b) 0 ° c) 45° & d) 90° wind angle of attack

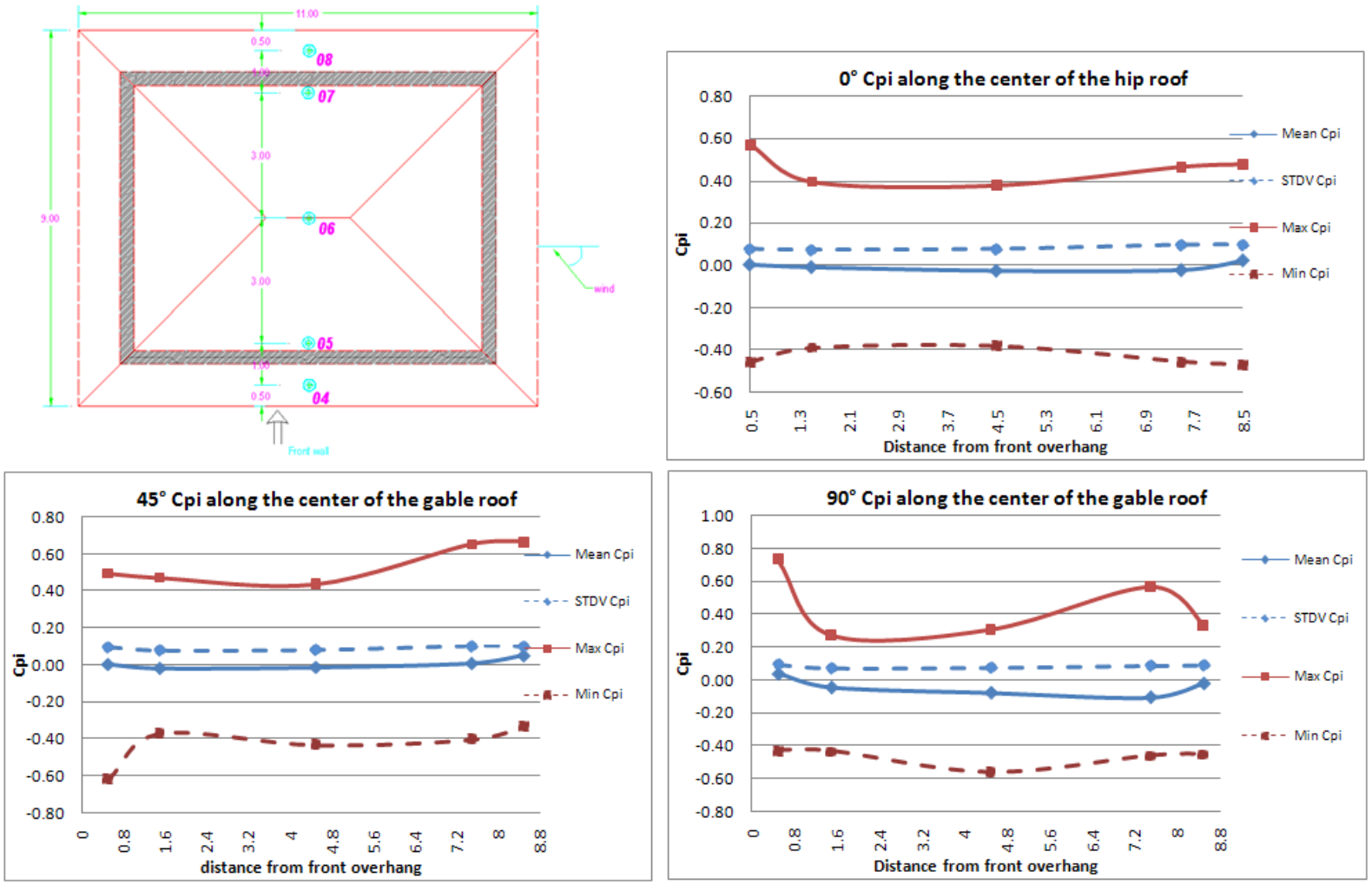

Figure 64: Roof internal pressure along the center length of gable; a) tap location along center of gable, b) 0 ° c) 45° & d) 90° wind angle of attack

In order to have better visualization on the critical uplift forces, the net pressure that develops on the roof envelop when the building is at 45° to the wind flow direction is organized as shown in Figure 65 a and b. Computing the critical uplift pressure for each case:

Critical uplift pressure across gable $= Attic\ floor\ C_{pi-max} - Roof\ surface\ C_{pe-min}$

$= 0.433-(-1.89)$

$= 2.323$

Critical uplift pressure along hip center$= Attic\ floor\ C_{pi-max} - Roof\ surface\ C_{pe-min}$

$= 0.433-(-2.71)$

$= 3.143$

It is observed that the critical uplift pressure occurs immediately behind the windward ridge. In our case, since the positive internal pressure was more or less uniform, the suction pressure that develops on the downwind side of the roof ridge or hip is dominant and plays crucial role towards generating critical uplift force.

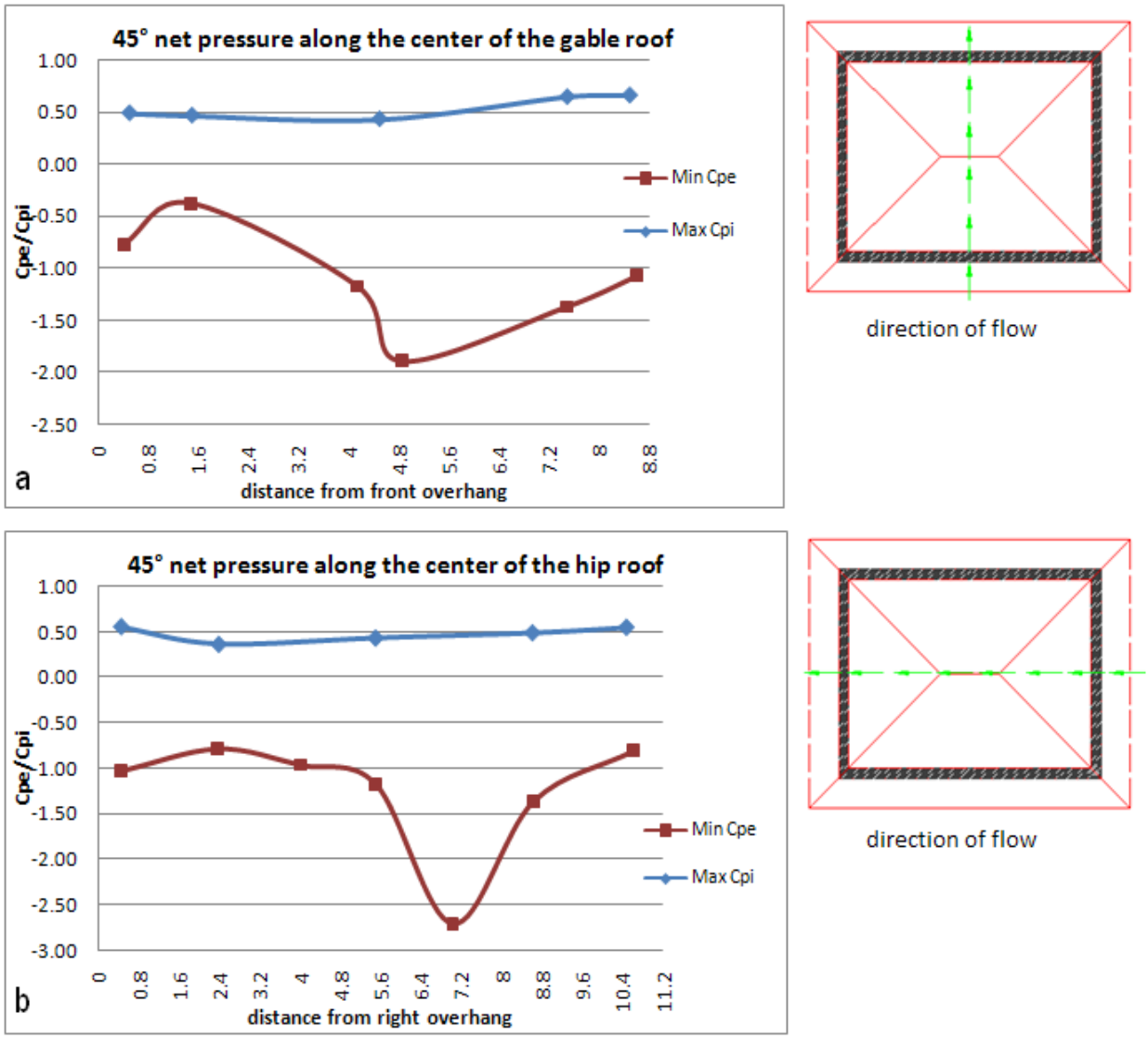

Figure 65: Uplift force due to net pressure along: a) the center of the gable, b) the center of the hip roof

<u>Outcomes of internal and external pressure study for the hip roof:</u>

- Peak positive internal pressure occurs when a dominant opening of the building faces the incoming wind flow.

- Peak negative internal pressure occurs when a dominant opening of the building are in parallel to the incoming wind flow.
- Dominant openings resulted in an increase internal pressure. For example, the opening of the window together with ceiling hatch led to 20% increase on the net wind load on the windward side of the hip roof. This reinforces the need for keeping doors and windows covered with shutters during strong storms.
- Opening of a hatch along with the window and door causes an increase in the internal pressure of the attic roof which reveals the importance of sealing ceiling hatches during strong storms to protect the roof and the building.
- Relative increase both in the negative and positive pressure has been observed due to the presence of vents (gable end, ridge, turbine, goose neck and soffits).
- Similar to literature values lower external pressure values for hip roof were observed compared to the gable roof.

4. **Conclusions**

An optimal size of the full-scale building specimen and its respective location from the wind generator WoW without compromising the aerodynamic data collected is identified by performing numerical computation and small scale model analysis which was later confirmed with detail full-scale WoW study.

The current study considered actual opening and porosities that are found in typical low rise buildings and used high wind speeds that resulted in accurate assessment of internal pressures circumventing the shortcomings in traditional wind tunnel tests.

The internal pressure that develops inside the building is shown to have a significant effect on the overall design wind loading.

The intensity of internal pressure is directly related to the size of dominant openings and their location with respect to the direction of wind angle of attack. Moreover, the intensity of internal pressure is highly dependent on compartmentalization and the presence of opening on the partitioning wall.

- Peak positive internal pressure occurs when a dominant opening of the building faces the incoming wind flow.
- Peak negative internal pressure occurs when a dominant opening of the building are in parallel to the incoming wind flow.
- Dominant openings resulted in an increase internal pressure. For example, the opening of the window together with ceiling hatch led to 45% increase on the net wind load on the windward side of the gable roof and 20 % increase for hip roofs. This reinforces the need for keeping doors and windows covered with shutters during strong storms.
- Relative increase both in the negative and positive pressure has been observed due to the presence of vents (gable end, ridge, turbine, goose neck and soffits).
- Similar to literature values lower external pressure values for hip roof were observed compared to the gable roof.
- Opening of a hatch along with the window and door causes an increase in the internal pressure of the attic roof which reveals the importance of sealing ceiling hatches during strong storms to protect the roof and the building.

5. **Acknowledgments**

The financial support from Florida Department of Emergency Management (FDEM) is gratefully acknowledged. We acknowledge the help received from FIU graduate students – Agerneh Dagnew, Huma Khan and Dhawal Sambare, Tuan-Chun Fu, Workamaw Warisdo, Ruilong Li and the following FIU under graduate students Francis Bian, Zak Lata, Alvaro A. Quinonez, and to our WoW lab manger Walter Conklin and WoW Research Scientists James Erwin, Roy Liu and Ali Masoud.

6. References

1. Bitsuamlak, G.T., Dagnew, A., and Chowdhury, A., (2009) "Computational assessment of blockage and wind simulator proximity effects for a new full-scale testing facility", Wind and Structure, In Press.

2. Bitsuamlak, G.T., Gan Chowdhury, A., Sambare, D. (2009), "Application of a Full-Scale Testing Facility for Assessing Wind-Driven-Rain Intrusion," Building and Environment, 44 (12), pp. 2430-2441.

3. Chowdhury, A.G., Kawade, P. and Fu, T.H., (2009), "Roof and Wall Vents Study under Simulated Hurricane Winds," Report submitted to IHRC, Research Project funded by The State of Florida Department of Community Affairs.

4. Davenport, A.G., Surry, D., Stathopoulos, T. (1978). Wind loads on low rise buildings: Final report of phase I and II. Boundary Layer Wind Tunnel Report BLWT-SS4, University of Western Ontario, Canada.

5. FEMA (2005a). Mitigation, Assessment, Team. Hurricane Ivan in Alabama and Florida: Observations, Recommendations and Technical Guidance.

6. FEMA (2005b) Mitigation, Assessment, Team. Mitigation Assessment Team Report: Hurricane Charley in Florida.

7. FEMA (2006). Mitigation, Assessment, Team. Hurricane Katrina in the Gulf Coast: Mitigation Assessment Team Report, Building Performance Observations, Recommendations, and Technical Guidance.

8. FEMA (2007a). Debris Management Guide. FEMA Publication 325. 06 June 2008. <http://www.fema.gov/government/grant/pa/demagde.shtm>.

9. Holscher, N., Niemann, H.J. (1998), "Towards quality assurance for wind tunnel tests: A comparative testing program of the Windtechnologische Gesellschaft", Jnl. of Wind Eng. Ind. Aerod., 74, 599-608.

10. Holmes, J.D. (1979). "Mean and fluctuating internal pressures induced by wind," Proc. 5th Int. Conf. on wind engineering. Vol.1, Colorado, USA, pp. 435-450.

11. Holmes, J.D. (1993). "Wind loads on low rise buildings-a review," CRISO. Division of Building Research. Highett, Victoria, Australia.

12. Holmes, J.D. (2001). Wind Loading of Structures. Spon Press, Chapter 6: p128-138.

13. Lim, C.H., Thomas, T.G., Castro, I.P. (2009), "Flow around a cube in a turbulent boundary layer: LES and experiment", Jnl. of Wind Eng. Ind. Aerod., 97, 96-109.

14. Levitan, M.L., J.D. Holmes, K.C. Mehta and W.P. Vann, Field measurements of pressures on the Texas Tech building. J. Wind Eng. Ind. Aerodyn. 38 (1991), pp. 227–234

15. Liu, H. (1990). Wind Engineering: A Handbook for Structural Engineers. Prentice Hall, USA.

16. Liu, H., Rhee, K.H. (1986) Helmholtz oscillation in building models. J. Wind Eng. Ind. Aerodyn. 24, 95-115.

17. Liu, H., Saathoff, P.J. (1982). "Internal pressure and building safety," J.Struct. Div., ASCE, 108(10), 2223-2234

18. Liu, H., Saathoff, P.J., (1983) "Internal pressure of multi-room buildings," ASCE J. Engineering Mechanics Division, Vol. 109, No. EM3, p908-919.

19. Karava, P. (2008), "Airflow Prediction in Buildings for Natural Ventilation Design: Wind Tunnel Measurements and Simulation", PhD. Thesis, Concordia University, Montreal, Canada.

20. Okajima, A., Yi, D., Sakuda, A., Nakano, T. (1997), "Numerical study of blockage effects on aerodynamic characteristics of an oscillating rectangular cylinder", J. Wind Eng. Ind. Aerodyn. 67&68, 91-102

21. Richards, P.J., Hoxey, R.P., Connell, B.D., Lander, D. P. (2007), "Wind-tunnel modelling of the Silsoe Cube", Jnl. of Wind Eng. Ind. Aerod., 95, 1384–1399.

22. Sharma, R.N. (2007). "Internal and net envelope pressures in a building having quasi-static flexibility and a dominant opening," J. Wind Eng. Ind. Aerodyn. 91, 807-828.

23. Sharma, R.N., Richards, P.J. (2003). "The influence of Helmholtz resonance on internal pressures in a low-rise building," J. Wind Eng. Ind. Aerodyn. 91, 807-828.

24. Sharma, R.N., Richards, P.J. (2005). "Net pressure on the roof of a low-rise building with wall openings." J. Wind Eng. Ind. Aerodyn. 93, 267-291.

25. Sharma, R.N., Richards; P.J. (1997). "The effect of roof flexibility on internal pressure fluctuations," J. Wind Eng. Ind. Aerodyn. 72, 175-186.

26. Vickery, B.J. (1986). "Gust factors for internal pressures in a low rise buildings," J. Wind Eng. Ind. Aerodyn. 23, 259-271.

27. Vickery, B.J., Bloxham, C. (1992). "Internal pressure dynamics with a dominant opening," J. Wind Eng. Ind. Aerodyn. 41, 193-204.

28. Vickery, B.J., (1986). "Gust factors for internal pressures in low-rise buildings," J. Wind Engineering and Industrial Aerodynamics, Vol. 23: p259-271.

29. Vickery, B.J. (1994). “Internal pressures and interactions with building envelope,” J. Wind Eng. Ind. Aerodyn. 53, 125-144.

30. Wright, N.G., Easom, G.J. (2003), “Non-linear k–ε turbulence model results for flow over a building at full-scale”, Applied Mathematical Modeling, 27(12), 1013-1033.